Dissertation zur Erlangung des Doktorgrades

der Fakultät für Chemie und Pharmazie

der Ludwig-Maximilians-Universität München

Self-interaction and targeted engineering of monoclonal antibodies

Martin Domnowski

aus

Leinefelde, Deutschland

2020

Erklärung

Diese Dissertation wurde im Sinne von §7 der Promotionsordnung vom 28. November 2011 von Herrn Prof. Dr. Wolfgang Frieß betreut.

Eidesstattliche Versicherung

Diese Dissertation wurde selbstständig und ohne unerlaubte Hilfe erarbeitet.

München, 09.09.2020

_____

Martin Domnowski

Dissertation eingereicht am:	09.09.2020
1.Gutachter:	Prof. Dr. Wolfgang Frieß
2.Gutachter:	Prof. Dr. Gerhard Winter
Mündliche Prüfung am:	15.10.2020

„Alles, worauf Aufmerksamkeit fällt, verändert sich.“

Michael „Curse“ Kurth

Acknowledgements

I would like to express my deepest gratitude to my supervisors Professor Dr. Wolfgang Frieß and Dr. Jan Jaehrling. I appreciated all the inspiring scientific discussion, their advice and guidance and I am grateful for all the motivating Self-I-E meetings at MorphoSys and at the LMU.

Thanks to Prof. Dr. Wolfgang Frieß, Prof. Dr. Gerhard Winter and Prof. Dr. Olivia Merkel, representative for the Department of Pharmaceutical Technology and Biopharmaceutics for giving me the opportunities to gain insights into the pharmaceutical point of view coming from the biochemistry and biotechnology perspective.

I am thankful to my colleagues from AK Frieß, AK Winter and AK Merkel for the great time we had and for the various social activities. Beside this, the scientific discussion within the groups were always valuable and contributed to my professional development. I want to thank Oliver Blümel for our thrilling scientific and personal conversations, which were enabled by the great coffee each afternoon.

Thanks to all the MorphoSys colleagues for the help and contribution to the project. Above all, I would like to thank Dr. Jan Jaehrling as the scientific supervisor of the project for all the genuine and honest feedback on experiments, analyses, abstracts, posters and manuscripts. Thank you for having your door always open for questions, ideas and comments. I really enjoyed working with you together throughout my time at MorphoSys.

I would like to thank Dr. Stefan Mitterreiter who contributed to this project as a grant manager and controlled the project from the background with great dedication.

Thanks to the Analytics Teams, the Production Teams as well as to the Core Technology at MorphoSys for providing a great working and research atmosphere. Thank you for your experimental contribution to the project which helped a lot to reach the project goals in time. Above all, I would like to thank the participants of the manuscripts coming from this project: Felix Kummer, Benjamin Hackner, Marco Dehling, Josef Reindl, Lucille Lehmann, Meike Wolber, Marion Satzger and Tobias Neuber.

I am also grateful for the research stay abroad at Osaka University in 2018. Beside the technical skills I learned regarding HDX-MS and AUC, I gained insights into the Japanese way of life, which still influence my thoughts today. Thanks to Prof. Susumu Uchiyama and his team for the great time and experience.

My greatest thanks go to my wife Tina for her never-ending patience and support. Thank you for motivating me during tough times and for carefully curtail my enthusiasm whenever it was necessary. Your love and organization helped me to get things done in time without losing myself in details.

Finally, I want to thank my family and friends for their endless support and patience throughout my professional education.

Funding acknowledgements

The project “Self-Interaction and targeted Engineering of monoclonal antibodies (Self-I-E) and this work was funded by the Bayerische Forschungsstiftung (AZ: 1251-16).

Table of Contents

Chapter 1 General introduction

1.1 Self-interaction of monoclonal antibodies

Attractive self-interaction of proteins, also referred to as self-association, reflects a process, in which native, monomeric proteins of the same species form dimers and oligomers. If oligomers are the functional entity of these proteins, attractive self-interaction will lead to activation of components as shown for enzymes and enzymatic cascades.[1, 2] For monoclonal antibodies, self-interaction can be linked to unwanted phenomena such as protein aggregation and particle formation as well as exceptional increase in viscosity.[3–10] This introduction will give an overview of the mechanism underlying the self-interaction process as well as a description of the commonly used analytical techniques to characterize mAb self-interaction. Additionally, influencing factors are presented and discussed.

1.1.1 The driving forces of mAb self-interaction

Protein interaction processes are driven either by repulsive or attractive forces. If antibodies are regarded as colloids, the interaction can be described by the DLVO theory.[11] Accordingly, the net interaction forces depend on the distance between the surface layers of the molecules. At low protein concentration, large distances between molecules can lead to repulsive interactions dominated by the electric double layers that surround each colloid. Upon increase in concentration, distances between molecules become smaller leading to prevalence of attractive Van der Waals forces. The theory of proximity energies provides an energetic framework to these high concentration environments, where not only proteins but also the whole solution composition as a mixture of differently charged components is considered.[12, 13] Non-specific charge-charge, charge-dipole and dipole-dipole interactions contribute to the overall long distance electrostatic forces whereas attractive hydrophobic forces are present at short distances.[13, 14] Crowding at high protein concentration leads to very short distances, which favor the presence of hydrophobic, attractive forces. Therefore, close proximity of the molecules will raise the probability to attractive interaction and thus, to the formation of protein oligomers.[3]

Monoclonal antibodies are multi-domain proteins consisting of two Fab and one Fc domains. All domains can be involved in the self-interaction mechanism. Under low ionic strength conditions, Fc-Fc interaction were observed which led to liquid-liquid phase separation.[15] Fab-Fc interactions were also identified in a formulation dependent manner,

with enhanced oligomerization at higher pH and elevated sodium chloride concentration.[16] Fab-Fab interactions were also described for mAbs and they also depend on ionic strength and pH, which underlines the heterogeneity of this type of non-specific protein-protein interaction.[17] So far, it is not possible to clearly predict distinct self-interaction sites based on primary sequence and structural modeling. Work and cost extensive studies are necessary to investigate this kind of weak protein-protein interaction in order to enhance the molecule specificity, manufacturability and overall developability.

1.1.2 A brief overview of suitable analytical techniques

The analysis of protein-protein interactions is well established in various fields of scientific research. High affine interactions such as antibody-antigen binding can be easily assessed by ELISA or SPR measurements. For the detection of weak interaction processes such as mAb self-interaction, other techniques with different sensitivity and assay principle are used. Analytical Ultracentrifugation (AUC) is regarded as the gold-standard to analyze weak protein-protein interaction processes enabling to calculate the second virial coefficient B_{22} as interaction parameter.[18] It was used in several studies to investigate the extent of self-interaction[9, 19–21] Whereas AUC provides high quality data and characteristic physical numbers, its throughput is very limited. Light scattering techniques such as Dynamic Light Scattering (DLS) can be applied in high throughput to determine the diffusion interaction parameter k_D.[21–23] Emerging techniques such as Affinity Capture Self-Interaction Nanoparticle Spectroscopy (AC-SINS), Bio-Layer-Interferometry (BLI) and Hydrogen-Deuterium Exchange Mass Spectrometry (HDX-MS) have been used recently to characterize mAb self-interaction processes and to rank mAbs by their self-interaction propensity.[24–27] In particular, HDX-MS was used to identify key residues contributing to the self-interaction of mAbs.[16, 24, 28–30] The published work is limited to either a comparison of different mAbs in one formulation or of various formulations of one mAb. Because self-interaction is formulation dependent, the combination of both would be highly useful to characterize mAb candidates in early stages of discovery. Further advantages and disadvantages of the abovementioned methods are discussed in detail in chapter 2 of this thesis. The methods described here differ in their assay and detection principle, which makes it challenging to compare data sets and studies. To this end, the multi method characterization of one particular model system may disclose new correlations and understandings of the results from the various analytical methods providing more comprehensive insights into the self-interaction process.

1.1.3 Factors affecting self-interaction of mAbs

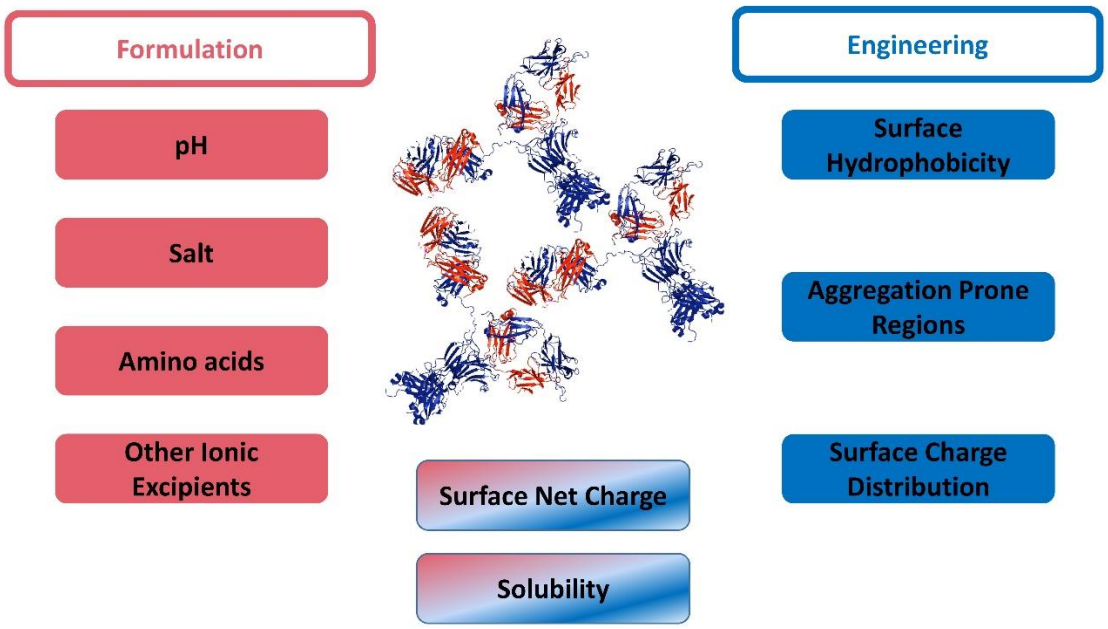

Figure 1 *Formulation and rational engineering as two approaches to influence factors that impact mAb self-interaction.*

MAb self-interaction processes are driven by electrostatic and hydrophobic forces depending on the molecules proximity.[31] Various factors influence the self-interaction propensity, which are related to i) the formulation composition or b) intrinsic properties of the mAb, which can be affected by engineering (Figure 1). During discovery phase and lead candidate optimization, intrinsic properties of a protein can be adjusted by engineering, whereas in later stages of development, when a lead candidate has already been defined, formulation development can affect the self-interaction and its consequences.

1.1.4 Formulation of mAbs

A biopharmaceutical formulation typically consists of a buffer at a specific pH and ionic and non-ionic excipients that should protect the biotherapeutic from chemical, conformational and colloidal degradation. The latter is strongly affected by mAb self-interaction. Thus, the selection of formulation components to prevent strong attractive self-interaction of mAbs is important to reduce aggregation and viscosity. Various examples can be found in literature and a few are highlighted in the following. Sodium chloride as ionic excipient effectively lowers the viscosity of a mAb at high protein concentration and both, different cations and anions affect the solution properties reducing the self-interaction

propensity.[9, 32] In addition to sodium chloride, arginine hydrochloride was described as viscosity reducing agent by lowering the attractive self-interaction propensity. [32, 33] Recently, dipicolinic acid was shown to reduce viscosity by lowering intermolecular attractions.[34] Specifically the pH significantly influences the self-interaction behavior of mAbs.[35–38] The pH dictates the surface charge distribution of the protein molecules which are key for the interactions. Thus, a formulations pH far away from the pI might reduce self-interaction by increasing overall electrostatic repulsion, but may not necessarily reduce the viscosity at high protein concentration if charge heterogeneity on the surface acts as the main driver.[18]

1.1.5 Engineering of mAbs

As depicted in figure 1, engineering approaches can be used to change the surface charge distribution, the overall surface hydrophobicity and aggregation prone regions. These properties were shown to be associated with mAb self-interaction. Yadav et al. demonstrated the effect of the proteins charge on the rheological characteristics of two mAbs, which differed mainly in their CDR regions, and one of which showed high self-interaction propensity and high viscosity at elevated concentration whereas the other did not.[4, 14, 18, 39] They generated "charge-swap" mutants and the resulting variants showed decreased viscosity and pronounced repulsive intermolecular interaction.[39] Apgar et al. generated 40 variants of a mAb, which exhibited high viscosity at 80 mg/ml and a strong self-interaction propensity in AC-SINS.[40] They identified a high net negative charge within the variable region as most promising engineering area. Only some variants showed decreased viscosity although the mutations were of the similar nature indicating that the interplay between structure, viscosity and self-interaction is not clearly understood.

For another mAb, three hydrophobic residues were identified by HDX-MS to be responsible for its aberrant self-interaction behavior which could be resolved by mutation.[29] Wu et al. identified a hydrophobic triad consisting of phenylalanine, histidine and tryptophan within the HCDR3 of the mAb CNTO607 as a key driver for its low solubility and high self-interaction propensity.[41] The exchange of these residues against more hydrophilic residues such as alanine improved the solubility but diminished target binding.[41, 42] The precursor molecule of CNTO607 was included in this thesis and is referred to as mAb1 in Chapter VI.

Calculations for predicting aggregation prone regions (APR) were developed to understand the effect of hydrophobicity, β-sheet propensity and on the probability for polypeptides and small proteins mainly consisting of secondary structure elements to build amyloidic fibrils.[43] The approach to predict the APRs was transferred to large antibodies by Chennamsetty et al. using the "spatial-aggregation propensity (SAP)" based on a three dimensional simulation of a full IgG1 molecule.[44] The SAP depends on the surface accessible area of a residue and its hydrophobicity. The authors selected sites for rational engineering and generated variants with reduced SAP score in the C_H2 domain which showed less turbidity upon shaking and a higher apparent unfolding temperature.[44] Nichols et al. designed variants by disrupting the APR of a model mAb.[45] Introducing a single mutation in this region led to destabilization and a loss of antigen binding. In contrast, variants with a mutation in spatial proximity retained their target binding properties and showed slightly improved physicochemical properties although k_D, as a measure for attractive self-interaction, was not significantly influenced.[45]

Thus, rational engineering can improve the physicochemical properties of mAbs but antigen binding was impaired in most cases, indicating that the link between structure, self-interaction behavior and target binding is not clearly understood. Thus, application of different predictive tools for APRs or surface hydrophobicity for rational mutagenesis and detailed analytical characterization of resulting variants would by highly valuable.

1.2 Developability of mAbs

Developability assessments of monoclonal antibodies are the investigation of properties of a therapeutic compound that are linked to an overall low risk of failure during chemistry, manufacturing, control (CMC), preclinical and clinical development.

The term developability of a mAb includes different aspects which are important for success along the road to a market product. To this end, an "ideal" drug candidate can be produced with high yields and high quality, if possible using a platform bioprocess.[46] High quality includes low heterogeneity and high storage stability. Moreover, a candidate should enable the use of high concentration solutions, which simplifies processing and administration.

The very early evaluation during discovery and candidate selection based on *in silico* approaches and experimental data from extended characterization and forced degradation

studies can be used to decide for a candidate with the most favorable properties for subsequent development. [46, 47]

In general, an early developability assessment of a mAb consists of at least three major parts, depending of the project progress and availability of material. First, computational tools are applied to predict various properties of a protein including pI, presence of free cysteine residues and N-glycosylation sites in CDRs.[46] If homology modeling is appropriate, common chemical degradation sites such as surface exposed deamidation and oxidation sites can be predicted.[46–48]

Computational predictions of the colloidal stability and the aggregation propensity can be based on physics or statistics.[49] Physics based predictions do not require prior experimental data. In contrast, the statistical methods, implemented as machine learning approaches and the generation of artificial intelligence, rely on previously obtained experimental data and the accuracy depends on the data quality used to train the prediction method.[49, 50] Aggregation prone regions of mAbs can be predicted by a variety of algorithms such as *AggreScan3D 2.0* and *AggScore*, which are based on homology modeling of the variable region of a mAb on available 3D models of Fab fragments.[51, 52] A "developability index" based on spatial aggregation propensity and net charge was correlated with long-term stability and successfully applied to unknown mAb candidates.[53] The limitation to a certain segment was overcome by Jain et al. who published a database of 12 biophysical properties of 137 clinical stage or approved mAbs.[54] This dataset includes various properties commonly connected to "good" developability characteristics such as drug-like specificity[55], high conformational as well as high colloidal stability. Based on machine learning approaches and subsequent analysis of homology models of 56 antibodies, developability guidelines for mAbs considering five metrics were proposed: 1) total length of CDRs, 2) surface hydrophobicity, 3) abundance of positive and 4) negative charges in CDR and 5) asymmetric distribution of surface charges.[56] *Protein-sol* is another tool based on the publication of Jain et al. to model clusters according to charge and hydrophobicity and to predict biophysical properties of mAbs based on the primary sequence of the variable fragment.[57]

The second step is the small-scale production of promising candidates. Expression and purification titer can be used to tell whether a mAb should be well producible or bears a higher risk for extended optimization effort. After production of typically less than 100 candidates, biophysical characterization is performed with high-throughput assays which

require only little sample, which includes e.g. analysis of thermal stability and monomer content. At this stage, assessment of the self-interaction propensity could be included. Clone Self-Interaction Bio-Layer-Interferometry (CSI-BLI) as well as Affinity-Capture Self-Interaction Nanoparticle Spectroscopy (AC-SINS) are assays which only require small amounts of material and can be run in high-throughput.[25, 26, 58] However, neither of these assays is suitable to assess the impact of formulation on self-interaction. Thus, the risk of excluding promising candidates due to challenges, which could be easily covered by formulation development, is high. Because the developability assessments typically do not include formulation screenings or considerations, implementation of preformulation studies in the second step of the assessment might be useful.

In the third step of a developability assessment, forced degradation studies are performed to explore degradation pathways and to rank the remaining candidates based on their stability profiles.[47] Due to the low number of candidates, production processes can be scaled up to provide material for further in-depth characterization of the candidates. For the analysis of self-interaction, assays can be used that require medium to high sample amounts like SLS and DLS and even viscosity measurements.[59–61] These physico-chemical results can be combined with data from pharmacokinetics and pharmacodynamics as well as manufacturability experiments to get the full picture of the potential candidates for decision making.[46, 47]

References

1. Hüttl S, Fiebig J, Kutter S, et al. Catalytically active filaments - pyruvate decarboxylase from Neurospora crassa. pH-controlled oligomer structure and catalytic function. 2012. FEBS J 279: 275–284.

2. Kutter S, Spinka M, Koch MHJ, König S. The influence of protein concentration on oligomer structure and catalytic function of two pyruvate decarboxylases. 2007. Protein J 26: 585–591.

3. Wang W, Roberts CJ. Protein aggregation - Mechanisms, detection, and control. 2018. Int J Pharm 550: 251–268.

4. Yadav S, Shire SJ, Kalonia DS. Factors affecting the viscosity in high concentration solutions of different monoclonal antibodies. 2010. J Pharm Sci 99: 4812–4829.

5. Shire SJ, Shahrokh Z, Liu J. Challenges in the development of high protein concentration formulations. 2004. J Pharm Sci 93: 1390–1402.

6. Roberts CJ. Therapeutic protein aggregation: mechanisms, design, and control. 2014. Trends Biotechnol 32: 372–380.

7. Pindrus MA, Shire SJ, Yadav S, Kalonia DS. The Effect of Low Ionic Strength on Diffusion and Viscosity of Monoclonal Antibodies. 2018. Mol Pharm 15: 3133–3142.

8. Neergaard MS, Kalonia DS, Parshad H, et al. Viscosity of high concentration protein formulations of monoclonal antibodies of the IgG1 and IgG4 subclass - prediction of viscosity through protein-protein interaction measurements. 2013. Eur J Pharm Sci 49: 400–410.

9. Liu J, Nguyen MDH, Andya JD, Shire SJ. Reversible self-association increases the viscosity of a concentrated monoclonal antibody in aqueous solution. 2005. J Pharm Sci 94: 1928–1940.

10. Li L, Kumar S, Buck PM, et al. Concentration dependent viscosity of monoclonal antibody solutions: explaining experimental behavior in terms of molecular properties. 2014. Pharm Res 31: 3161–3178.

11. Arzenšek D, Kuzman D, Podgornik R. Colloidal interactions between monoclonal antibodies in aqueous solutions. 2012. J Colloid Interface Sci 384: 207–216.

12. Laue TM, Shire SJ. The Molecular Interaction Process. 2020. J Pharm Sci 109: 154–160.

13. Laue T. Proximity energies: a framework for understanding concentrated solutions. 2012. J Mol Recognit 25: 165–173.

14. Yadav S, Liu J, Shire SJ, Kalonia DS. Specific interactions in high concentration antibody solutions resulting in high viscosity. 2010. J Pharm Sci 99: 1152–1168.

15. Nishi H, Miyajima M, Wakiyama N, et al. Fc domain mediated self-association of an IgG1 monoclonal antibody under a low ionic strength condition. 2011. J Biosci Bioeng 112: 326–332.

16. Arora J, Hu Y, Esfandiary R, et al. Charge-mediated Fab-Fc interactions in an IgG1 antibody induce reversible self-association, cluster formation, and elevated viscosity. 2016. MAbs 8: 1561–1574.

17. Gentiluomo L, Roessner D, Streicher W, et al. Characterization of Native Reversible Self-Association of a Monoclonal Antibody Mediated by Fab-Fab Interaction. 2020. J Pharm Sci 109: 443–451.

18. Yadav S, Laue TM, Kalonia DS, et al. The influence of charge distribution on self-association and viscosity behavior of monoclonal antibody solutions. 2012. Mol Pharm 9: 791–802.

19. Lerch TF, Sharpe P, Mayclin SJ, et al. Infliximab crystal structures reveal insights into self-association. 2017. MAbs 9: 874–883.

20. Sarangapani PS, Weaver J, Parupudi A, et al. Both Reversible Self-Association and Structural Changes Underpin Molecular Viscoelasticity of mAb Solutions. 2016. J Pharm Sci 105: 3496–3506.

21. Connolly BD, Petry C, Yadav S, et al. Weak interactions govern the viscosity of concentrated antibody solutions: high-throughput analysis using the diffusion interaction parameter. 2012. Biophys J 103: 69–78.

22. Menzen T, Friess W. Temperature-ramped studies on the aggregation, unfolding, and interaction of a therapeutic monoclonal antibody. 2014. J Pharm Sci 103: 445–455.

23. Esfandiary R, Parupudi A, Casas-Finet J, et al. Mechanism of reversible self-association of a monoclonal antibody: role of electrostatic and hydrophobic interactions. 2015. J Pharm Sci 104: 577–586.

24. Arora J, Hickey JM, Majumdar R, et al. Hydrogen exchange mass spectrometry reveals protein interfaces and distant dynamic coupling effects during the reversible self-association of an IgG1 monoclonal antibody. 2015. MAbs 7: 525–539.

25. Sun T, Reid F, Liu Y, et al. High throughput detection of antibody self-interaction by bio-layer interferometry. 2013. MAbs 5: 838–841.

26. Geng SB, Wittekind M, Vigil A, Tessier PM. Measurements of Monoclonal Antibody Self-Association Are Correlated with Complex Biophysical Properties. 2016. Mol Pharm 13: 1636–1645.

27. Geng SB, Cheung JK, Narasimhan C, et al. Improving monoclonal antibody selection and engineering using measurements of colloidal protein interactions. 2014. J Pharm Sci 103: 3356–3363.

28. Majumdar R, Middaugh CR, Weis DD, Volkin DB. Hydrogen-deuterium exchange mass spectrometry as an emerging analytical tool for stabilization and formulation development of therapeutic monoclonal antibodies. 2015. J Pharm Sci 104: 327–345.

29. Dobson CL, Devine PWA, Phillips JJ, et al. Engineering the surface properties of a human monoclonal antibody prevents self-association and rapid clearance in vivo. 2016. Sci Rep 6: 38644.

30. Geoghegan JC, Fleming R, Damschroder M, et al. Mitigation of reversible self-association and viscosity in a human IgG1 monoclonal antibody by rational, structure-guided Fv engineering. 2016. MAbs 8: 941–950.

31. Kumar V, Dixit N, Zhou LL, Fraunhofer W. Impact of short range hydrophobic interactions and long range electrostatic forces on the aggregation kinetics of a monoclonal antibody and a dual-variable domain immunoglobulin at low and high concentrations. 2011. Int J Pharm 421: 82–93.

32. Inoue N, Takai E, Arakawa T, Shiraki K. Specific decrease in solution viscosity of antibodies by arginine for therapeutic formulations. 2014. Mol Pharm 11: 1889–1896.

33. Dear BJ, Hung JJ, Truskett TM, Johnston KP. Contrasting the Influence of Cationic Amino Acids on the Viscosity and Stability of a Highly Concentrated Monoclonal Antibody. 2017. Pharm Res 34: 193–207.

34. Ke P, Batalha IL, Dobson A, et al. Novel salts of dipicolinic acid as viscosity modifiers for high concentration antibody solutions. 2018. Int J Pharm 548: 682–688.

35. Yadav S, Scherer TM, Shire SJ, Kalonia DS. Use of dynamic light scattering to determine second virial coefficient in a semidilute concentration regime. 2011. Anal Biochem 411: 292–296.

36. Sule SV, Cheung JK, Antochshuk V, et al. Solution pH that minimizes self-association of three monoclonal antibodies is strongly dependent on ionic strength. 2012. Mol Pharm 9: 744–751.

37. Sahin E, Grillo AO, Perkins MD, Roberts CJ. Comparative effects of pH and ionic strength on protein-protein interactions, unfolding, and aggregation for IgG1 antibodies. 2010. J Pharm Sci 99: 4830–4848.

38. Tomar DS, Kumar S, Singh SK, et al. Molecular basis of high viscosity in concentrated antibody solutions: Strategies for high concentration drug product development. 2016. MAbs 8: 216–228.

39. Yadav S, Sreedhara A, Kanai S, et al. Establishing a link between amino acid sequences and self-associating and viscoelastic behavior of two closely related monoclonal antibodies. 2011. Pharm Res 28: 1750–1764.

40. Apgar JR, Tam ASP, Sorm R, et al. Modeling and mitigation of high-concentration antibody viscosity through structure-based computer-aided protein design. 2020. PLoS ONE 15: e0232713.

41. Wu S-J, Luo J, O'Neil KT, et al. Structure-based engineering of a monoclonal antibody for improved solubility. 2010. Protein Eng Des Sel 23: 643–651.

42. Bethea D, Wu S-J, Luo J, et al. Mechanisms of self-association of a human monoclonal antibody CNTO607. 2012. Protein Eng Des Sel 25: 531–537.

43. Caflisch A. Computational models for the prediction of polypeptide aggregation propensity. 2006. Curr Opin Chem Biol 10: 437–444.

44. Chennamsetty N, Voynov V, Kayser V, et al. Design of therapeutic proteins with enhanced stability. 2009. Proc Natl Acad Sci U S A 106: 11937–11942.

45. Nichols P, Li L, Kumar S, et al. Rational design of viscosity reducing mutants of a monoclonal antibody: hydrophobic versus electrostatic inter-molecular interactions. 2015. MAbs 7: 212–230.

46. Jarasch A, Koll H, Regula JT, et al. Developability assessment during the selection of novel therapeutic antibodies. 2015. J Pharm Sci 104: 1885–1898.

47. Xu Y, Wang D, Mason B, et al. Structure, heterogeneity and developability assessment of therapeutic antibodies. 2019. MAbs 11: 239–264.

48. Sharma VK, Patapoff TW, Kabakoff B, et al. *In silico* selection of therapeutic antibodies for development: viscosity, clearance, and chemical stability. 2014. Proc Natl Acad Sci U S A 111: 18601–18606.

49. Kuroda D, Tsumoto K. Engineering Stability, Viscosity, and Immunogenicity of Antibodies by Computational Design. 2020. J Pharm Sci 109: 1631–1651.

50. Gentiluomo L, Roessner D, Augustijn D, et al. Application of interpretable artificial neural networks to early monoclonal antibodies development. 2019. Eur J Pharm Biopharm 141: 81–89.

51. Kuriata A, Iglesias V, Pujols J, et al. Aggrescan3D (A3D) 2.0: prediction and engineering of protein solubility. 2019. Nucleic Acids Res 47: W300-W307.

52. Sankar K, Krystek SR, Carl SM, et al. AggScore: Prediction of aggregation-prone regions in proteins based on the distribution of surface patches. 2018. Proteins 86: 1147–1156.

53. Lauer TM, Agrawal NJ, Chennamsetty N, et al. Developability index: a rapid *in silico* tool for the screening of antibody aggregation propensity. 2012. J Pharm Sci 101: 102–115.

54. Jain T, Sun T, Durand S, et al. Biophysical properties of the clinical-stage antibody landscape. 2017. Proc Natl Acad Sci U S A 114: 944–949.

55. Starr CG, Tessier PM. Selecting and engineering monoclonal antibodies with drug-like specificity. 2019. Curr Opin Biotechnol 60: 119–127.

56. Raybould MIJ, Marks C, Krawczyk K, et al. Five computational developability guidelines for therapeutic antibody profiling. 2019. Proc Natl Acad Sci U S A 116: 4025–4030.

57. Hebditch M, Warwicker J. Charge and hydrophobicity are key features in sequence-trained machine learning models for predicting the biophysical properties of clinical-stage antibodies. 2019. PeerJ 7: e8199.

58. Liu Y, Caffry I, Wu J, et al. High-throughput screening for developability during early-stage antibody discovery using self-interaction nanoparticle spectroscopy. 2014. MAbs 6: 483–492.

59. Gentiluomo L, Svilenov HL, Augustijn D, et al. Advancing Therapeutic Protein Discovery and Development through Comprehensive Computational and Biophysical Characterization. 2020. Mol Pharm 17: 426–440.

60. Lavoisier A, Schlaeppi J-M. Early developability screen of therapeutic antibody candidates using Taylor dispersion analysis and UV area imaging detection. 2014. MAbs 7: 77–83.

61. Calero-Rubio C, Saluja A, Sahin E, Roberts CJ. Predicting High-Concentration Interactions of Monoclonal Antibody Solutions: Comparison of Theoretical Approaches for Strongly Attractive Versus Repulsive Conditions. 2019. J Phys Chem B 123: 5709–5720.

Aim and outline of this thesis

MAbs play a major role in the treatment of various severe diseases. To increase patient comfort and compliance, high concentration liquid formulations are developed which enable subcutaneous applications. Several challenges are associated with the high concentration approach including increased protein aggregation and a viscosity which is not suited for injection through fine needles and some steps in manufacturing. These challenges can be partially explained by the intrinsic propensity of a protein to self-interact, depending on the protein structure itself and on the formulation conditions.

This thesis should give insights into the self-interaction behavior of mAbs. The investigated set of model proteins comprised three mAbs derived from the phage display HuCAL library of the MorphoSys AG, four derived from the phage display Ylanthia library of the MorphoSys AG and two commercially available mAbs. The goal was to investigate and understand the connection between molecule structure, formulation composition, target binding and self-interaction propensity. The topic was approached in three steps. First, orthogonal techniques were established to characterize the self-interaction propensity of the mAbs. Subsequently, the self-interaction behavior of the mAbs was studied in detail. Lastly, self-interaction hot spots identified for three model mAbs were modified by rational mutagenesis and the mAb variants were characterized regarding their self-interaction propensity and target binding properties.

Chapter 2 describes the establishment of an analytical technique to determine the self-interaction propensity of mAbs in a formulation dependent manner (SI-BLI), which can be applied in high throughput. In this context, the newly established method is compared to other, well-known techniques such as dynamic light scattering.

In **Chapter 3**, the SI-BLI assay is applied in a developability assessment combined with preformulation screening for mAbs derived from the Ylanthia library. The assay can predict rankings of formulations regarding the increase in viscosity at higher protein concentration.

In **Chapter 4**, self-interaction of the model mAb Infliximab is characterized under pharmaceutically relevant formulation conditions using a multi-method approach comprising AUC, DLS, viscosimetry, HDX-MS, SI-BLI and small angle X-ray scattering.

Chapter 5 describes the detailed analysis of the formulation dependent self-interaction and the identification of hot spots by both, *in silico* and *in vitro* approaches for one mAb from the HuCAL library. Based on these results, variants were generated and characterized.

In **Chapter 6**, an engineering approach for two mAbs from the HuCAL library is presented, which is based on computational methods. Results from the experimental characterization of these variants is compared to predictions of *protein-sol*.

Chapter 7 is a summary and conclusion of this thesis, which contains suggestion for future analysis of mAb self-interaction and guidance for next-generation mAb design.

Chapter 2 Assessment of antibody self-interaction by bio-layer-interferometry as a tool for early stage formulation development

This chapter is published as:

M. Domnowski[1,2], J. Jaehrling[2], W. Frieß[1]

Assessment of Antibody Self-Interaction by Bio-Layer-Interferometry as a Tool for Early Stage Formulation Development.

In Pharmaceutical Research, 2020, 37:29

[1]Department of Pharmacy: Pharmaceutical Technology and Biopharmaceutics; Ludwig-Maximilians-Universitaet Muenchen, Butenandtstrasse 5, 81377 Munich, Germany
[2]MorphoSys AG, Semmelweisstraße 7, 82152 Planegg

Note from the authors:

The version included in this thesis is identical with the published article apart from minor changes.

The published article can be assessed online via:

https://doi.org/10.1007/s11095-019-2722-4

Author contributions:

M.D., J.J. and W.F. conceived and designed the study. M.D. conducted and analyzed mAb production, SI-BLI, DLS experiments and performed statistical analysis. M.D. wrote the manuscript. J.J. and W.F. reviewed and revised the manuscript.

Keywords: Self-interaction, bio-layer-interferometry, diffusion interaction parameter, antibody, high concentration formulation,

Abbreviations: AUC – Analytical ultracentrifugation; BLI – Bio-layer-interferometry; DLS – Dynamic light scattering; HCLF – high (protein) concentration liquid formulation; HDX-MS – Hydrogen-Deuterium exchange mass spectrometry; mAb – Monoclonal antibody; PBS – Phosphate buffered saline; SI-BLI – Self-interaction assay based on Bio-layer-interferometry; SIC – Self-interaction chromatography; SLS – Static Light Scattering

2.1 Abstract

Purpose:

To speed up the drug development process in the biopharmaceutical industry, high throughput methods are indispensable for assessing drug candidates and potential lead formulations, in particular during late stages of discovery and early phases of development. This study aimed to establish a bio-layer-interferometry based high throughput assay for assessing formulation dependent mAb self-interaction (SI-BLI) and to compare the results with k_D values obtained by dynamic light scattering (DLS).

Methods:

Self-interaction of proprietary and commercially available mAbs was analyzed by SI-BLI and dynamic light scattering (DLS).

Results:

We found significant correlations of the SI-BLI results and k_D-values obtained by DLS for both, different mAbs in one platform formulation and for mAbs formulated in several buffer compositions. In total, we assessed self-interaction propensity of different mAbs in 58 formulations and found significant Pearson correlation ($p<0.05$) between k_D and results of SI-BLI.

Conclusions:

The SI-BLI results correlate with k_D and enable fast ranking of both different drug candidates and potential lead formulations. Thus, SI-BLI might decrease the risk to lose potent mAb candidates during transition from discovery to development, and help to accelerate the development of high concentration liquid formulations.

2.2 Introduction

By 2020, 70 monoclonal antibodies products will be available on the market and the world-wide sales will be nearly $125 billion.[1] These delicate biomolecules are prone to various forms of instabilities which have to be kept minimal in the course of manufacturing, storage and delivery to the patient. In particular, mAb molecules as colloids exhibit attractive and repulsive forces amongst each other. Pronounced attractive self-interaction is linked to protein oligomerization or aggregation as well as drastically increased solution viscosity at elevated protein concentration.[2, 3] High mAb concentrations may be essential to enable

subcutaneous administration. High viscosities can lead to problems during purification, formulation, filtration or injection of mAb solutions.

Self-interaction at high mAb concentrations can be triggered by charge-charge interactions, charge-dipole and dipole-dipole interactions. Additionally, short range forces such as hydrophobic or van der Waals interactions are present at high protein concentrations where the distance between the mAb molecules is low.[3, 4] Attractive forces between mAb molecules might lead to cluster formation of up to nine mAb molecules, and the size of the cluster correlates with solution viscosity at high protein concentrations.[5]

Development of high concentration formulations is mostly initiated in advanced stages of antibody development when more protein material is available and one or two lead candidates have been selected. Several studies show the influence of buffer composition, pH and presence of excipients on the self-interaction propensity of a mAb.[3, 6–10]

To find suitable antibody candidates for development, various assessments are performed during early stages of the development phase. This includes developability assessment to reduce the risk of costly failure during later stages due to physico-chemical deficiencies of the mAb molecule. Such evaluation often includes evaluation of production performance like yield and protein titer as well as colloidal, conformational and chemical stability. As these assessments are performed during early stages, the number of mAbs to be screened is high and material availability is limited. Computational tools are available to link primary structure to the proteins behavior at high concentration but cannot advise how to change the formulation composition in order to solve self-interaction related problems.[11] Thus, decisions based on these computational tools may erroneously exclude highly potent mAbs in early phase. Therefore, predictive methods with minimal protein consumption suitable for high throughput are sought after.

The colloidal stability of mAbs is an important parameter to be assessed in early development, which is typically evaluated via the diffusion interaction parameter k_D and the second virial coefficient.[8, 12] Using a well-plate based light scattering device, the required volume of sample is reduced. A mAb dilution series is required to assess protein self-interaction. Consequently, the material requirements increase and insufficient mAb quantities may be available during early stages of development, especially to evaluate the mAb behavior in different formulations. Another method to assess mAb self-interaction is self-interaction chromatography based on the retention of a mAb on a column with a

stationary phase to which the mAb of interest is covalently coupled.[13] Column preparation as well as the chromatography itself requires several milligrams of protein material making the self-interaction chromatography hardly available for a single assessment during early development stages. Affinity-capture self-interaction nanoparticle spectroscopy is a very recent method for assessing mAb self-interaction in a high throughput manner.[14, 15] This technique requires low sample amounts and is dedicated for developability screenings but includes labor intensive steps such as conjugation of capture antibodies to gold nanoparticles.

Additionally, analytical ultracentrifugation (AUC) is used to describe the self-interactions of mAbs via the second virial osmotic coefficient.[16, 17] Major disadvantages of this technique are its low throughput and enormous material consumption. On the other hand, this method provides the possibility to investigate the formulation dependency of the oligomerization in detail. A bio-layer interferometry (BLI) -based technique was introduced by Sun et al. to describe self-interaction processes of mAbs.[18] The method can be run in high throughput with low sample consumption. Commercial anti-human-Fc biosensors, a capture level of 0.8 nm and a mAb concentration of 1 µM during the assessed self-interaction event were found to result in the best assay condition for the screening. By analyzing nine different mAbs in PBS, they found a good correlation of the assay results obtained from self-interaction chromatography and cross-interaction chromatography.[18]

To our knowledge, there is no analytical methodology published that combines ranking of mAbs and formulations by self-interaction propensity in high throughput fashion. We therefore tried to establish BLI on a 96 biosensor system, improving loading, quenching and baseline steps in order to enhance reproducibility. Our goal was to show a correlation between k_D and responses from the SI-BLI assay. We therefore analyzed a larger set of mAbs formulated in PBS and a selection of mAbs formulated in different commonly used buffers. We chose proprietary mAbs, which showed problematic behavior during downstream processing and functional assays. Additionally we included adalimumab into our sample set as it is marketed in a high concentration liquid formulation. To verify the applicability of formulation dependent SI-BLI we used Omalizumab, because of its known self-interaction propensity, influenced by formulation composition.[18, 19]

2.3 Materials and methods

2.3.1 Materials

Phosphate buffered saline (Thermo Fisher Scientific, MA), L-histidine (Merck KGaA, Germany), sodium chloride (Carl Roth GmbH + Co. KG, Germany), hydrochloric acid (Merck KGaA, Germany), citric acid monohydrate (Merck KGaA, Germany), sodium phosphate monobasic (Merck KGaA, Germany), L-Arginine (Merck KGaA, Germany), L-tryptophan (Merck KGaA, Germany), L-phenylalanine (Merck KGaA, Germany) were all of analytical grade.

Adalimumab (Humira®) and Omalizumab (Xolair®) were purchased and buffer exchanged into PBS including polysorbate 20 removal by protein A chromatography using Äkta Avant (GE Healthcare, Chicago, IL). mAb stock solutions were concentrated using 30 kDa Amicon Ultra-15 centrifugal devices (Merck KGaA, Germany) to 10 mg/ml.

MorphoSys mAb1 to mAb8 were expressed in HKB11 cells and purified via Protein A chromatography. Antibodies were formulated by dialysis overnight. mAb stock solutions were concentrated using 30 kDa Amicon Ultra-15 centrifugal devices (Merck KGaA, Germany) to 5 mg/ml.

The mAb concentration was determined by UV absorbance at 280 nm using a Nanodrop device (Thermo Fisher Scientific, MA) by applying the theoretical extinction coefficient of the individual mAb. Molar extinction coefficients were calculated based on primary structure only and without further consideration of higher order structure or glycan content. Extinction coefficients vary between 206000 and 237000 M-1/cm. After downstream processing, mAbs were analyzed by UHPLC-SEC. All mAbs showed a monomer content of >90%.

Disulfide-linked human Fc protein was expressed in HKB11 cells and purified via Protein A chromatography and buffer exchanged into PBS using PD10 columns and gravity flow (GE Healthcare, Chicago, IL). The protein was concentrated using 30 kDa Amicon Ultra-15 centrifugal devices (Merck KGaA, Germany) to 5 mg/ml.

2.3.2 Determination of the diffusion interaction parameter k_D by DLS

DLS experiments were performed using a DynaPro plate reader (Wyatt Technologies, Santa Barbara, CA). Samples were 0.22 µm filtrated and measured at 25°C as triplicates in 384 well plates with 12 acquisitions for 5 s. The mutual diffusion coefficient D of the

antibodies was calculated for at least 5 different protein concentrations by applying cumulant fit analysis. k_D was calculated as described by Connolly *et al.*.[8] The concentrations used for determining the k_D were in the range of 0.5 mg/ml to 10 mg/ml depending on the available sample amount. Exemplary raw data of k_D determination are presented in the supplemental material (Figure S1)

2.3.3 Detection of mAb self-interaction by SI-BLI

The method described by Sun *et al.* was adapted for high throughput on an Octet HTX system (FortéBio, CA), which is able to address up to 96 samples in parallel.[18] Anti-hIgG Fc capture (AHC) biosensors (FortèBio, CA) were used. In the first assay step, a baseline was established in PBS for at least 60 s, followed by capture of the mAb of interest at 25 nM in PBS until the BLI signal increased by approximately 1 nm (Fig. 1). Remaining binding capacity of the capture sensors was saturated for 600 s with 1 µM of human Fc in PBS. Subsequently, a second baseline was acquired in the formulation composition of interest for 60 s, followed by incubation with 2 µM mAb in the respective formulation for at least 1200 s. Preliminary experiments demonstrated that this time span was sufficient to reach equilibrium binding. As shown by Sun et al., the mAb concentration during association can affect the signal to noise ratio (BLI response difference between capture level and association equilibrium) in BLI measurements. They chose an IgG concentration of 1 µM for the screening condition.[18] We performed experiments indicating that with 2 µM IgG concentration the largest assay window could be achieved (data are shown in the supplemental material, Figure S2). The response at equilibrium was used for further calculations. To compensate for differences in the amount of captured mAb, the self-interaction signal normalized to the amount of captured mAb (R_{rel}), was calculated according to Equation 1.

$$R_{rel} = \frac{Response_{Association\ equilibrium}\ [nm]}{Response_{capture\ step}[nm]} \quad (1)$$

As negative controls, sensors were used without captured IgG, i.e. which were only saturated with human Fc protein. Even if the protein of interest showed an association behavior to the human Fc-protein, this was also regarded as potential self-association, which could have been caused by Fab-Fc or Fc-Fc interactions. Further, unspecific binding to the biosensor surface itself cannot be excluded by using only this negative control.

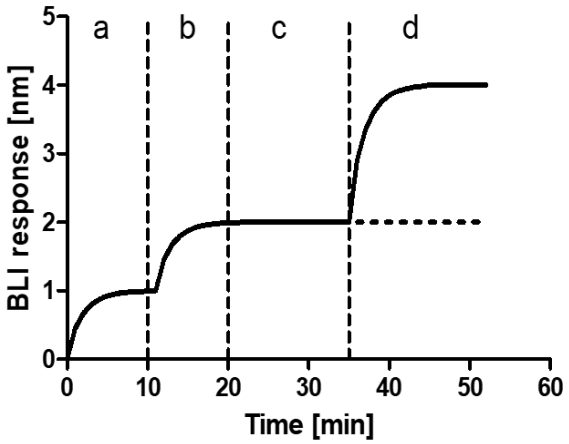

Figure 1 *Schematic overview of the BLI-based self-interaction assay (a – Capture of mAb, b – Saturation of remaining binding sites of the biosensor, c – Baseline acquisition in the formulation of interest, d – Association reaction in formulation of interest until equilibrium)*

2.3.4 Preparation of mAb3 formulations

The mAb was formulated by dialysis and concentrated to 10 mg/ml using Amicon Ultra-15 centrifugal devices (Merck KGaA, Germany).

Table 1 *Formulations of mAb3*

Formulation	Buffer system	pH	Excipient
F1	25 mM Na-phosphate	7.0	---
F2	25 mM Na-phosphate	7.0	25 mM NaCl
F3	25 mM Na-phosphate	7.0	25 mM Trp
F4	25 mM Na-phosphate	7.0	25 mM Phe
F5	25 mM Na-phosphate	7.0	25 mM Arg-HCl
F6	25 mM His-HCl	6.0	---
F7	25 mM His-HCl	6.0	25 mM NaCl
F8	25 mM His-HCl	6.0	25 mM Trp
F9	25 mM His-HCl	6.0	25 mM Phe
F10	25 mM His-HCl	6.0	25 mM Arg-HCl
F11	25 mM Na-citrate	5.0	---
F12	25 mM Na-citrate	5.0	25 mM NaCl
F13	25 mM Na-citrate	5.0	25 mM Trp
F14	25 mM Na-citrate	5.0	25 mM Phe
F15	25 mM Na-citrate	5.0	25 mM Arg-HCl

2.3.5 Calculation of statistical significance

In order to evaluate the suitability of the BLI-based self-interaction assay, Pearson correlation as well as Spearman correlation analysis of results obtained by DLS and BLI was performed using the software PRISM 5.04. A significance level of p = 0.05 was applied.

2.4 Results and discussion

2.4.1 k_D and SI-BLI of different mAbs in PBS

The diffusion interaction parameter k_D is widely used to describe intermolecular interactions of proteins.[8, 16] It can be calculated based on a first-order approximation of the concentration dependence of the apparent diffusion coefficient. We analyzed nine different antibodies formulated in PBS.

Table 2 *R_{rel} ± SD and k_D ± SD of different mAbs in PBS.*

mAb	R_{rel}	k_D [ml/g]
Adalimumab	0.19 ± 0.02	-6.8 ± 1.83
mAb1	0.16 ± 0.17	-1.4 ± 0.66
mAb2	0.38 ± 0.02	-56.4 ± 10.31
mAb3	0.04 ± 0.02	-26.8 ± 3.49
mAb4	0.99 ± 0.06	-114.4 ± 8.82
mAb5	0.68 ± 0.06	-44.8 ± 5.80
mAb6	0.32 ± 0.00	-6.5 ± 0.82
mAb7	0.32 ± 0.02	-9.6 ± 1.28
mAb8	2.21 ± 0.20	-80.9 ± 3.00

For mAb1, mAb6 and mAb7 as well as adalimumab, k_D values were slightly negative, whereas we observed strongly negative k_D values for mAb8 and mAb4 (Table 2). mAbs2, 3 and 5 also exhibit net attractive protein-protein interaction in PBS but to a different extent. mAb1 showed no significant attractive interactions in PBS. These results indicate a wide spectrum of attractive self-association behavior of our chosen model proteins in PBS.

The same sample set was characterized by SI-BLI (Table 2). The results indicate strong self-interaction propensity of mAb8 and mAb4, followed by mAb5. Adalimumab, as well as mAb1 and mAb3 showed low signals in the SI-BLI assay. As the standard deviation of

the triplicates was low, a ranking of the mAbs regarding the self-interaction propensity was possible. mAbs with prominent behavior like mAb4 and mAb8 which showed strongly negative k_D values also gave high signals in the SI-BLI assay. In contrast, adalimumab showed rather low interaction propensity as determined by DLS as well as by SI-BLI. However, we observed differences between the results e.g. for mAb4 and mAb8. Whereas mAb4 showed the most negative k_D, mAb8 showed the highest in SI-BLI signal. In the SI-BLI assay, one binding partner is attached to the sensor surface and the other one is free in solution. If oligomerization takes place as a consequence of mAb self-interaction, the oligomers can be large in size. If such large oligomers either bind to the attached mAb at the BLI sensor surface, the signal is increased compared to binding signals based on dimerization. In DLS, the formation of only few large oligomers will not affect the measurements especially, if these oligomers are present over the whole concentration range analyzed. This effect might explain this deviation between DLS and SI-BLI observed but we do not have any information on the nature of interactions for these mAbs. A Pearson correlation analysis of the results obtained by both methods showed a non-significant correlation ($p > 0.05$). We then analyzed the data based on self-interaction ranking of the different mAbs in PBS and found significant Spearman correlation ($p < 0.05$). We therefore conclude that ranking of different mAbs in a platform formulation like phosphate buffered saline is possible by using SI-BLI.

2.4.2 Assay variability of SI-BLI

According to the assay setup, each experiment is performed on one AHC biosensor. To study the assay variability of the proposed setup, we analyzed the self-interaction propensity of mAb3, mAb4 and adalimumab in PBS with 6 different biosensors for each antibody (Fig. 2). Overall, the standard deviations are low and the results are reproducible. Adalimumab showed the highest relative standard deviation (7.5 %) compared to mAb3 (4.0 %) and mAb4 (2.2 %). For mAbs with a high tendency for self-interaction, the absolute standard deviation is higher, indicating that these interactions include unspecific interactions as well as oligomerization processes. In case of low self-interaction propensity, the absolute standard deviations are smaller but relative standard deviations are higher due to very low R_{rel} values. Comparing different mAbs in different formulations, ranking of formulations seems to be more difficult for formulations showing low mAb self-interaction propensity.

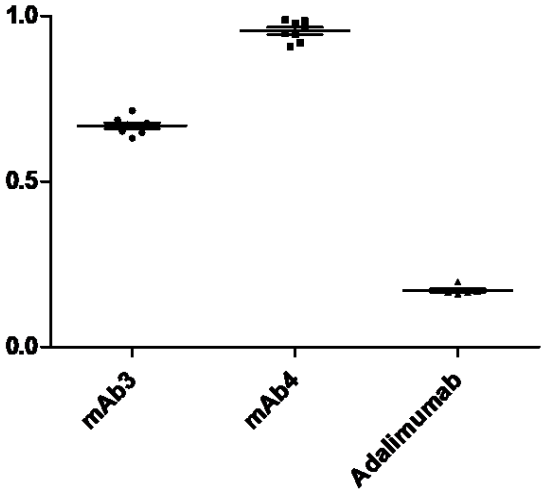

Figure 2 *Assay variability of SI-BLI for mAb3, mAb4 and adalimumab in PBS. Error bars represent the relative standard deviation.*

2.4.3 Characterization of formulation dependent self-interaction behavior of mAbs using k_D and SI-BLI

In addition to screening different mAbs in the same formulation, in our case PBS, we evaluated SI-BLI for screening the formulation dependency of self-interaction exemplarily for mAb3 and compared the obtained R_{rel} with the k_D values from DLS. We varied pH values, buffer type and added sodium chloride, arginine hydrochloride, tryptophan or phenylalanine, excipients known for affecting self-interaction of mAbs.[6] We ranked the formulations based on the measured self-interaction propensity of mAb3. A strong negative k_D value was ranked with a high number, whereby a slightly negative k_D was ranked with a low number (Raw data are listed in the supplemental material in table S1). The most negative k_D-value of mAb3 and therefore the highest ranking was observed in 25 mM histidine hydrochloride pH 6.0 without further excipients (F6) (Fig. 3). An increase in ionic strength, (F7 – 25 mM sodium chloride; F10 – 25 mM arginine hydrochloride) led to charge shielding and reduced electrostatic repulsion. Correspondingly, k_D was reduced. In general, mAb3 showed stronger attractive interactions in histidine hydrochloride based formulations compared to sodium citrate formulations (F11-F15). k_D in sodium phosphate pH 7.0 (F1) without excipients was higher than in histidine hydrochloride at pH 6.0, indicating that attractive self-interaction was more pronounced at pH 6.0. Contrary to the results for F7 and F10, adding 25 mM sodium chloride (F2) or 25 mM arginine hydrochloride (F5) did not influence the k_D of mAb3 in sodium phosphate buffer. But k_D

was decreased by addition of hydrophobic amino acids like L-tryptophan (25 mM, F3) and L-phenylalanine (25 mM, F4).

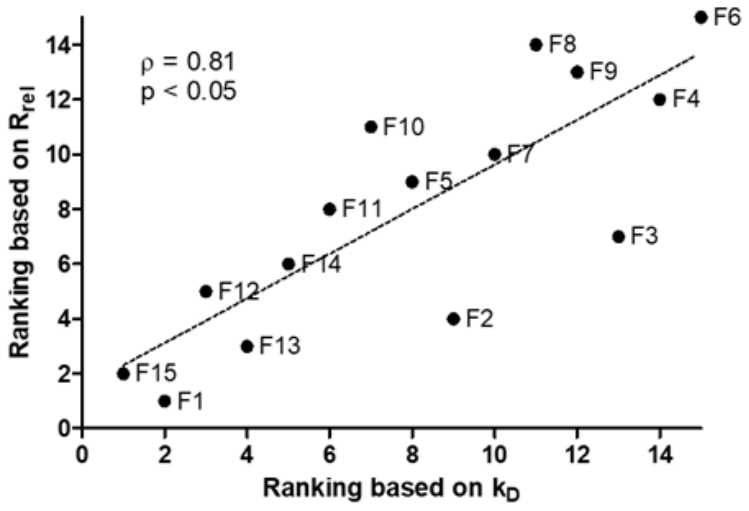

Figure 3 *Spearman correlation plot of R_{rel} and k_D for mAb3 in 15 different formulations.*

We ranked the formulations based on the R_{rel} obtained by SI-BLI. A high response correspond to a high ranking. Similar to the k_D results, the sodium citrate based formulations showed low R_{rel} compared to the histidine hydrochloride based formulations. Furthermore, the self-interaction propensity as observed by SI-BLI was reduced by addition of sodium chloride and arginine hydrochloride to histidine formulations (F7, F10). R_{rel} was not significantly affected by adding charged excipients to sodium phosphate based formulation (F2, F5) but was increased by adding L-tryptophan to the formulation (F4).

Overall, the k_D and SI-BLI results correlated well. Formulations that triggered self-interaction of mAb3 as indicated by strongly negative k_D –values also showed increased R_{rel} in SI-BLI. mAb3 showed attractive interactions in all formulations. A correlation analysis of the results obtained by DLS and SI-BLI showed significant Spearman correlations ($p < 0.05$), whereas a Pearson correlation remained non-significant ($p > 0.05$).

Additionally, mAb2 and mAb3 were formulated at different pH values and buffer concentrations. Figure 4A depicts a high in self-interaction propensity of mAb2 at pH of 5.5 to 6.0. At a buffer concentration of 7 mM, this strong attractive interaction is also found at higher pH, whereas the SI-BLI signal decreases at higher buffer concentrations. We hypothesize that self-interaction of this mAb is reduced at higher buffer concentration due to charge shielding of protonated amino acids at pH 7.0. mAb2 and mAb3 have a similar framework region and only differ in their complementary determining regions. At pH 4.5,

self-interaction of the two mAbs is similar, but at higher pH mAb2 showed significantly higher response (Fig. 4B). mAb3 contains an N-glycosylation site within its CDR which could decrease the self-interaction propensity. Thus, the BLI-based self-interaction assay was able to differentiate self-interaction propensity between different mAbs in dependence of formulation conditions.

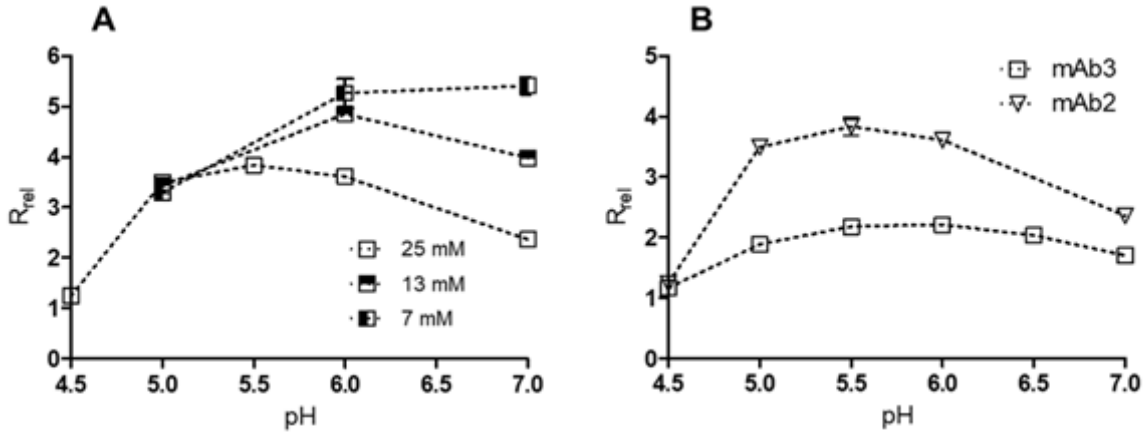

Figure 4 *R_{rel} of mAb2 in sodium phosphate/sodium citrate buffer at different pH and buffer concentration (A) and mAb2 and mAb3 as a function of pH in 25 mM sodium phosphate/sodium citrate buffer (B).*

2.4.4 Characterization of self-interaction propensity of Omalizumab by SI-BLI

Omalizumab has been shown to exhibit a marked increase in viscosity with increasing concentration triggered by self-interaction.[20] The kinematic viscosity of a formulation containing 16 mM Histidine pH 6.0, 266 mM sucrose, 0.03 % PS20 and 125 mg/ml mAb was 80 cSt. The addition of 100 mM sodium chloride to a 125 mg/ml Omalizumab solution reduced the viscosity by a factor of 4 from 80 cSt to 20 cSt.[20] Therefore, we challenged the SI-BLI assay with this extreme, studying the effect of salt, pH and buffer strength on the self-interaction of Omalizumab.

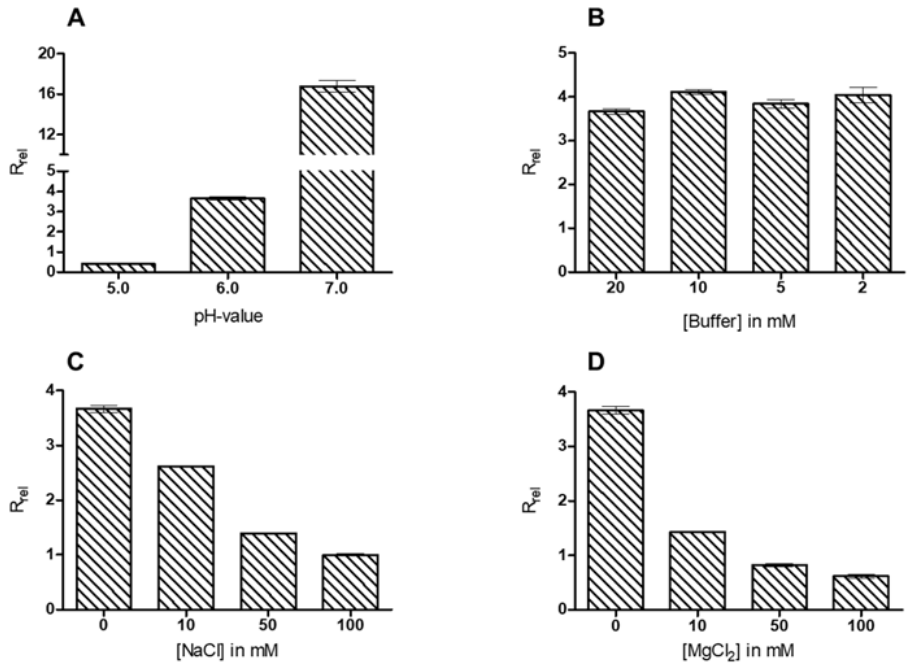

Figure 5 *Formulation dependent self-interaction behavior of Omalizumab determined by SI-BLI in dependence of formulation pH-value in 20 mM histidine buffer (A), of histidine buffer concentration at pH 6.0 (B), of sodium chloride concentration in 20mM histidine buffer pH 6.0 (C) and of magnesium chloride concentration in 20 mM histidine buffer pH 6.0 (D).*

The formulation pH had tremendous impact on the self-interaction propensity of Omalizumab (Fig. 5A). At pH 7.0, the theoretical isoelectric point of Omalizumab[20], the BLI signal was 40-fold higher compared to pH 5.0. Increasing the net surface charge of the antibody by lowering the pH below the pI resulted in stronger electrostatic repulsion and in a lower R_{rel}. Although addition of salt caused a strong decrease in R_{rel}, the self-interaction propensity of Omalizumab was not significantly affected by the concentration of the histidine buffer at pH 6.0 in a range from 2 to 20 mM (Fig. 5B). The R_{rel} of 3.7 in 20 mM histidine hydrochloride pH 6.0 substantially decreased with addition of sodium chloride (Fig. 5C). The decrease was more pronounced with magnesium chloride (Fig. 5D). This reduction of attractive self-interaction with higher ionic strength is in line with findings reported in literature.[20] The addition of salt results in a disruption of attractive electrostatic interactions.

2.4.5 Correlation of k_D obtained by DLS and R_{rel} obtained by SI-BLI

During this study, in total 58 mAb formulations were analyzed by DLS and SI-BLI regarding the self-interaction propensity. Overall, a more negative k_D-value is associated with a higher response of the SI-BLI assay. We found significant Spearman correlation

coefficients for smaller sample sets of both different antibodies formulated in PBS and for one mAb formulated in different buffer compositions. In order to assess, if the SI-BLI assay can be used as a high throughput alternative to k_D determination by DLS, we used all corresponding DLS and SI-BLI results and looked for Spearman and Pearson correlation. First we analyzed our complete data set for Gaussian distribution and found non-significant differences for our data set ($p > 0.05$). For the 58 samples we found significant Spearman correlation between R_{rel} and k_D ($\rho = -0.77$, $p < 0.0001$) as well as statistically significantly correlation ($p < 0.0001$) with a Pearson correlation coefficient of -0.72 (Fig. 6). Thus, ranking of the self-interaction propensity of different mAb formulations by SI-BLI is possible. In addition, R_{rel} can be used as a predictor for k_D.

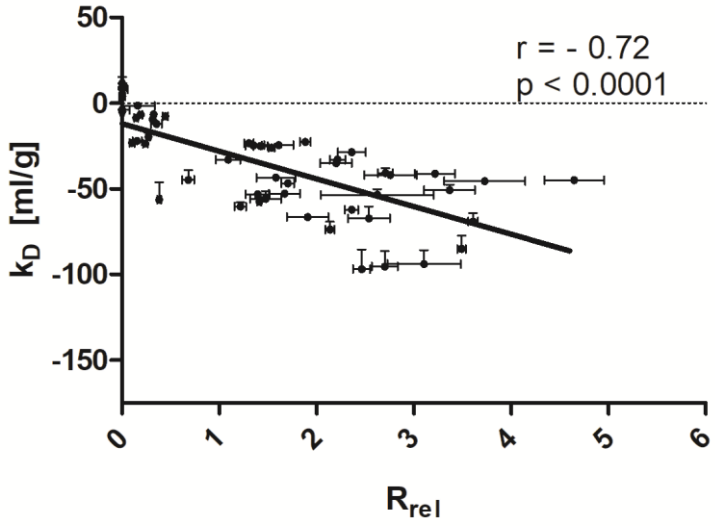

Figure 6 *Correlation of R_{rel} obtained by SI-BLI- and k_D obtained by DLS for different mAbs in different formulations.*

2.4.6 Using the SI-BLI assay for developability assessments and preformulation

Various studies show the correspondence of net attractive mAb self-interaction as indicated by negative k_D with the viscosity increase of antibody formulations at high protein concentration.[8,21,22] In order to predict the self-interaction propensity at early stages of development, promising *in silico* tools are available.[23] But these tools do not consider excipient and formulation effects. The formulation dependent self-interaction behavior can be studied by DLS techniques in a high throughput manner. However, sample preparation including dialysis and preparation of a dilution series are labor intensive. Furthermore,

excipients such as sucrose and trehalose can affect the results obtained by DLS.[24] The SI-BLI assay setup was described by Sun et al.[18] They used this method to screen for suitable antibody clones in discovery. It was proposed that mAbs which showed higher self-interaction response as adalimumab should be considered as potentially problematic for later development steps. They used PBS as platform formulation only. We transferred the assay to a 96 well setup which enables interaction assessment with only 21 µg of mAb material per formulation at a single concentration of 0.3 mg/ml (2 µM). This setup was applied to screen the self-interaction of various mAbs in different formulations. The 58 samples rendered a significant correlation of the R_{rel} from SI-BLI and the k_D from DLS.

At early development stage either mAbs which show low viscosity at high concentration have to be selected or mAb candidates require optimization by mutagenesis or the formulation composition needs to be adapted. This can be supported by analysis of protein-protein interaction in high throughput with minimal sample consumption and preparation effort. All these attributes are combined in the SI-BLI assay which makes it suitable for use already during transition from discovery to development stage. This early assessment of protein-protein interactions is of high value for candidate selection and for formulation selection in the discovery phase. It cannot replace detailed analysis of the protein behavior, specifically at high concentration at later stages of development.

2.4.7 Limitations of the SI-BLI assay

The SI-BLI assay setup included the essential mAb capture step. The utilized anti-hIgG Fc capture sensors have a high affinity to human Fc and this binding was shown to be stable for the whole assay duration.[18] Nevertheless, we observed loss of binding capacity of the biosensor in acetate buffers below pH 4.0. Furthermore, by losing the captured IgG and Fc protein, the association reaction will be overestimated. Further, a possible association reaction cannot be safely attributed to self-interaction, as this association curve can also be caused by binding of IgG to the biosensor itself, which at least lost part of the captured IgG and blocking Fc.

Self-interaction processes of mAbs can be triggered by Fab-Fc domain interactions or by Fab-Fab domain interactions.[25–27] Also Fc-Fc domain interactions are possible as well. Especially in the latter case, association of the free mAb molecules with the Fc-protein used for saturation after the capture step might interfere. To avoid this, other biosensors like anti-

hFab-CH1 capture sensors or sensors based on covalent binding of analyte (amino reactive biosensors) can be used.

The optical thickness of the layer on the sensor surface is a result of association of protein molecules. Net repulsive interactions can therefore not be analyzed. Thus, the SI-BLI assay cannot discriminate between molecules and conditions which show weak attractive interaction and repulsive interaction. But it can cover the range of critical substantial attractive interactions.

During k_D analysis, diffusion coefficients of the mAb molecules are determined with the analyte in solution. Similar to self-interaction chromatography, the SI-BLI method studies the interaction of mAb molecules bound to the sensor surface with molecules in solution, which potentially restricts their movement, flexibility and accessibility sterically. We therefore suggest using SI-BLI as a rapid screening method for suitable formulations, and k_D analysis for in-depth characterization of self-interaction for selected final formulations.

2.4.8 Comparison to other SI analyzing techniques

As discussed, SI-BLI seems to be a powerful tool for early stage formulation development or developability assessments, when only small amounts of protein material are available and the number of candidates and possible formulations is high. SI-BLI is a relatively new technique for analyzing mAb self-interaction behavior compared to other techniques such as AUC, DLS and SIC. AUC provides the second virial coefficient, but consumes substantial amounts of material and offers low throughput. Methods of medium throughput are DLS and SLS. Both are also based on molecular interactions present in solution. As it was mentioned for AUC, DLS and SLS can provide information on the second virial coefficient and k_D. But to assess self-interaction propensity by these techniques, a dilution series of the mAb formulation is necessary starting at concentrations of several g/L. Upconcentration and dilution make these methods more labor intensive and can lead to material loss, which increases material consumption. Both SIC and AC-SINS require several preparation steps including conjugation to either suitable chromatographic beads or via a capture antibody conjugated to gold nanoparticles. Both methods study interactions of immobilized mAb with mAb molecules in solution. A very recent technique for analyzing mAb self-association is HDX-MS. It enables to detect the mAb structures involved on peptide level or potentially even higher resolution. If mutagenesis is an option to reduce the self-interaction propensity of a lead candidate, HDX-MS can give important

advice. It is specifically of use at later stages of development when more protein material is available. We summarize a comparison of the techniques for analyzing mAb self-interaction in Figure 7 and Table 2.

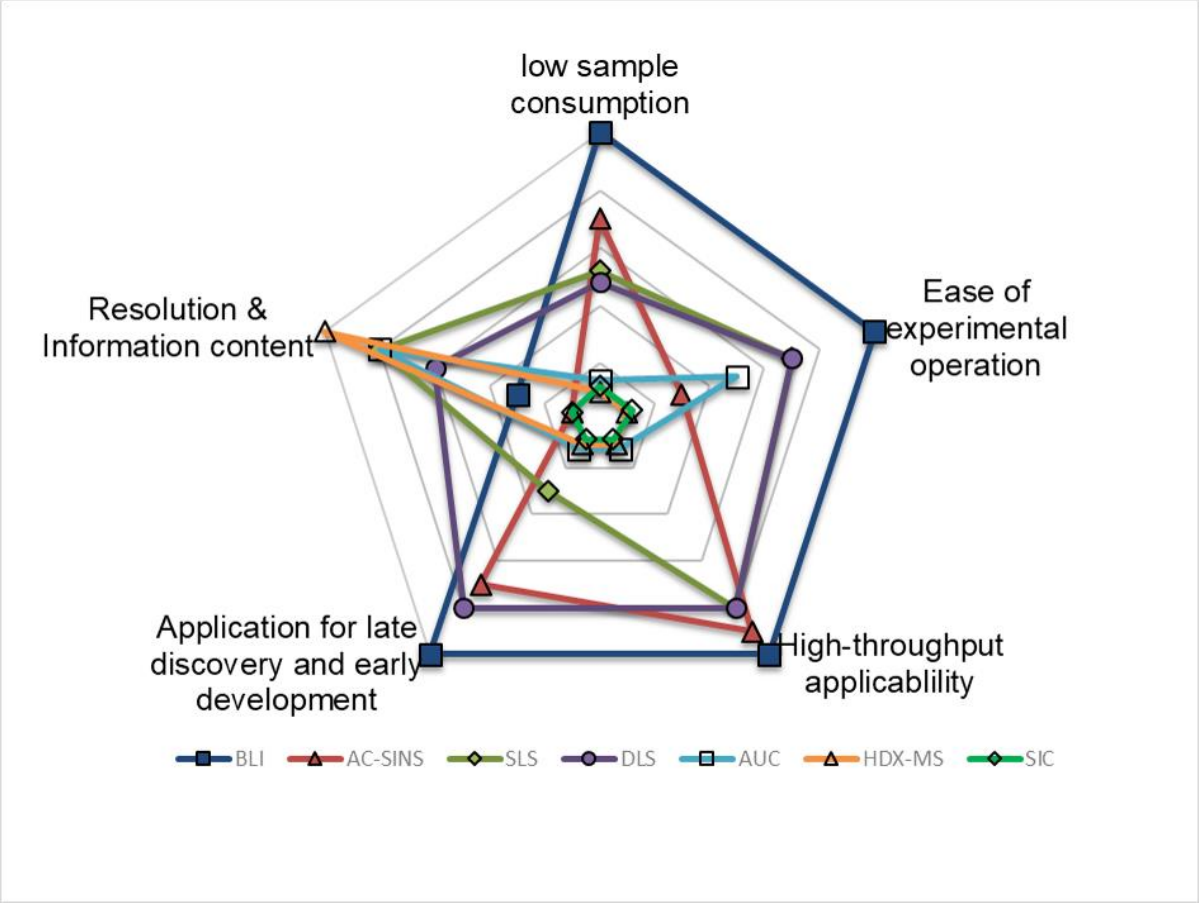

Figure 7 *Comparison of different techniques to assess mAb self-interactions.*

Table 3 *Overview of methods to analyzed mAb self-interaction.*

Method	SI-BLI	AC-SINS	SIC	DLS/SLS	AUC	HDX-MS
Interaction partners	Immobilized / in solution	Immobilized / immobilized	Immobilized / in solution	in solution	in solution	in solution
Assay read out	Binding normalized to amount of captured sample, R_{rel}	Wavelength shift caused by binding $\Delta\lambda$ [28]	Retention factor [29]	Diffusion interaction parameter k_D	Sedimentation coefficient, second virial coefficient, hydrodynamic non-ideality coefficient[19, 30]	Differences in deuterium uptake [26]
Required protein amount	Very low, approx. 24 µg per antibody and formulation	Very low, approx. 0.5 µg per antibody solution [28]	High (column preparation); low for analysis (5-10 µg sample) [29]	Moderate, approx. 500 µg per antibody and formulation[8]	High, 15 mg per antibody and formulation[16]	High, 30 mg per antibody and formulation [26]
Sample preparation	Dilution or buffer exchange. Working concentration: 0.3 mg/ml	Preparation of gold nanoparticles with capture antibody. Working concentration: 0.05 mg/ml	Immobilization of mAbs to stationary phase at a concentration of 15 mg/ml; Injection of protein solutions of 2.5 mg/ml to 10 mg/ml	Buffer exchange, upconcentration, preparation of dilution series from 0.5 mg/ml to 10 mg/ml	Buffer exchange, upconcentration and preparation of dilution series to high protein concentrations (up to 150 mg/ml)	Lyophilization or dialysis and reconstitution in D2O containing reconstitution buffer [25]. No technical limitations in protein concentration.
Application for early development	Yes	Yes	No	Yes	No	No
Advantages	Very low sample consumption; high throughput;	Low sample consumption; High–throughput, no interference with compounds from supernatants	Moderate throughput , automated sampling, standard LC equipment required	Moderate sample consumption & throughput; Assessment in solution	Interaction parameter are directly accessible. Direct measurement of oligomerisation possible.	High resolution of self-interaction sites
Disadvantages	Unspecific binding needs to be excluded, buffers must be compatible with capture (pH above 4.0), only rank order of mAbs and formulations possible, weak attractive or repulsive interactions cannot be measured	only ranking of mAbs relative to each other, no formulation dependent SI measurements published [14]	High sample consumption (SIC), Moderate throughput (sequential sampling)	Low - moderate sample consumption & throughput, limitations at low-ionic strength and sugar containing formulations[24]	Low throughput, high sample consumption, expensive AUC devices required	Very low throughput, expensive HDX-MS devices required complex evaluation, time-consuming method development

2.5 Conclusion

We were able to differentiate the self-interaction behavior of different mAbs in PBS as a platform formulation both by k_D analysis via DLS as well as by SI-BLI. The self-interaction rankings of the mAbs obtained from the two methods correlated significantly. Additionally, we analyzed the self-interaction behavior of one mAb in different formulations using both methods. Again, we found a significant correlation between the results from both methodologies, k_D and R_{rel}, based on a sample set of 58 different conditions. Thus, SI-BLI is suitable to rank the self-interaction propensity of mAbs in a formulation dependent manner. Over and above our proprietary mAbs, we analyzed the self-interaction behavior of Omalizumab, which is commercially available and well described in the literature. Our SI-BLI and DLS data corroborated the reduction of attractive self-interaction with increasing ionic strength and decreasing pH value from pH 7.0 to 5.0, as described in literature. Whereas the SI-BLI assay allows to characterize the self-interaction behavior of mAbs for ranking purpose, this assay cannot provide a physico-chemical interaction parameter like k_D. Furthermore, the SI-BLI assay provides information based on the interaction of mAb molecules in solution with non-covalently surface attached mAb molecules and cannot replace interaction assays where both interaction partners are free in solution. These aspects have to be weighed against the clear benefits of the SI-BLI assay, low material requirements and working at one diluted concentration only, which enables analysis of the formulation effect already at very early stages.

In summary, SI-BLI appears to be a powerful tool for early stage formulation development when only limited amount of protein is available and the number of antibody candidates is high. By implementing this approach in developability assessments of mAbs, the risk to lose potential lead candidates based on highly attractive self-interaction propensity can be decreased.

2.6 Acknowledgements

This study was part of the project “Self-Interaction and targeted Engineering of monoclonal antibodies (Self-I-E)”. This project is funded by the Bayerische Forschungsstiftung and MorphoSys AG. The authors would like to thank Dr. Daniel Weinfurtner and Dr. Roy Eylenstein for their support during the initial phase of this project.

References

1. Ecker DM, Jones SD, Levine HL. The therapeutic monoclonal antibody market. 2014. MAbs 7: 9–14.

2. Shire SJ, Shahrokh Z, Liu J. Challenges in the development of high protein concentration formulations. 2004. J Pharm Sci 93: 1390–1402.

3. Yadav S, Liu J, Shire SJ, Kalonia DS. Specific interactions in high concentration antibody solutions resulting in high viscosity. 2010. J Pharm Sci 99: 1152–1168.

4. Laue T. Proximity energies: a framework for understanding concentrated solutions. 2012. J Mol Recognit 25: 165–173.

5. Lilyestrom WG, Yadav S, Shire SJ, Scherer TM. Monoclonal antibody self-association, cluster formation, and rheology at high concentrations. 2013. J Phys Chem B 117: 6373–6384.

6. Esfandiary R, Parupudi A, Casas-Finet J, et al. Mechanism of reversible self-association of a monoclonal antibody: role of electrostatic and hydrophobic interactions. 2015. J Pharm Sci 104: 577–586.

7. Binabaji E, Ma J, Zydney AL. Intermolecular Interactions and the Viscosity of Highly Concentrated Monoclonal Antibody Solutions. 2015. Pharm Res 32: 3102–3109.

8. Connolly BD, Petry C, Yadav S, et al. Weak interactions govern the viscosity of concentrated antibody solutions: high-throughput analysis using the diffusion interaction parameter. 2012. Biophys J 103: 69–78.

9. Le Brun V, Friess W, Bassarab S, et al. A critical evaluation of self-interaction chromatography as a predictive tool for the assessment of protein-protein interactions in protein formulation development: a case study of a therapeutic monoclonal antibody. 2010. Eur J Pharm Biopharm 75: 16–25.

10. Dear BJ, Hung JJ, Truskett TM, Johnston KP. Contrasting the Influence of Cationic Amino Acids on the Viscosity and Stability of a Highly Concentrated Monoclonal Antibody. 2017. Pharm Res 34: 193–207.

11. Agrawal NJ, Helk B, Kumar S, et al. Computational tool for the early screening of monoclonal antibodies for their viscosities. 2016. MAbs 8: 43–48.

12. Hofmann M, Winzer M, Weber C, Gieseler H. Prediction of Protein Aggregation in High Concentration Protein Solutions Utilizing Protein-Protein Interactions Determined by Low Volume Static Light Scattering. 2016. J Pharm Sci 105: 1819–1828.

13. Hedberg SHM, Heng JYY, Williams DR, Liddell JM. Self-Interaction Chromatography of mAbs: Accurate Measurement of Dead Volumes. 2015. Pharm Res 32: 3975–3985.

14. Liu Y, Caffry I, Wu J, et al. High-throughput screening for developability during early-stage antibody discovery using self-interaction nanoparticle spectroscopy. 2014. MAbs 6: 483–492.

15. Estep P, Caffry I, Yu Y, et al. An alternative assay to hydrophobic interaction chromatography for high-throughput characterization of monoclonal antibodies. 2015. MAbs 7: 553–561.

16. Saito S, Hasegawa J, Kobayashi N, et al. Behavior of monoclonal antibodies: relation between the second virial coefficient (B (2)) at low concentrations and aggregation propensity and viscosity at high concentrations. 2012. Pharm Res 29: 397–410.

17. Hopkins MM, Lambert CL, Bee JS, et al. Determination of Interaction Parameters for Reversibly Self-Associating Antibodies: A Comparative Analysis. 2018. J Pharm Sci 107: 1820–1830.

18. Sun T, Reid F, Liu Y, et al. High throughput detection of antibody self-interaction by bio-layer interferometry. 2013. MAbs 5: 838–841.

19. Zhang Z, Liu Y. Recent progresses of understanding the viscosity of concentrated protein solutions. 2017. Current Opinion in Chemical Engineering 16: 48–55.

20. Liu J, Nguyen MDH, Andya JD, Shire SJ. Reversible self-association increases the viscosity of a concentrated monoclonal antibody in aqueous solution. 2005. J Pharm Sci 94: 1928–1940.

21. Li L, Kumar S, Buck PM, et al. Concentration dependent viscosity of monoclonal antibody solutions: explaining experimental behavior in terms of molecular properties. 2014. Pharm Res 31: 3161–3178.

22. Yadav S, Scherer TM, Shire SJ, Kalonia DS. Use of dynamic light scattering to determine second virial coefficient in a semidilute concentration regime. 2011. Anal Biochem 411: 292–296.

23. Tomar DS, Kumar S, Singh SK, et al. Molecular basis of high viscosity in concentrated antibody solutions: Strategies for high concentration drug product development. 2016. MAbs 8: 216–228.

24. Sorret LL, DeWinter MA, Schwartz DK, Randolph TW. Challenges in Predicting Protein-Protein Interactions from Measurements of Molecular Diffusivity. 2016. Biophys J 111: 1831–1842.

25. Arora J, Hu Y, Esfandiary R, et al. Charge-mediated Fab-Fc interactions in an IgG1 antibody induce reversible self-association, cluster formation, and elevated viscosity. 2016. MAbs 8: 1561–1574.

26. Arora J, Hickey JM, Majumdar R, et al. Hydrogen exchange mass spectrometry reveals protein interfaces and distant dynamic coupling effects during the reversible self-association of an IgG1 monoclonal antibody. 2015. MAbs 7: 525–539.

27. Kanai S, Liu J, Patapoff TW, Shire SJ. Reversible self-association of a concentrated monoclonal antibody solution mediated by Fab-Fab interaction that impacts solution viscosity. 2008. J Pharm Sci 97: 4219–4227.

28. Geng SB, Wittekind M, Vigil A, Tessier PM. Measurements of Monoclonal Antibody Self-Association Are Correlated with Complex Biophysical Properties. 2016. Mol Pharm 13: 1636–1645.

29. Hedberg SHM, Heng JYY, Williams DR, Liddell JM. Micro scale self-interaction chromatography of proteins: A mAb case-study. 2016. J Chromatogr A 1434: 57–63.

30. Yang D, Correia JJ, Stafford Iii WF, et al. Weak IgG self- and hetero-association characterized by fluorescence analytical ultracentrifugation. 2018. Protein Sci 27: 1334–1348.

Supplementary data

Table S1 *k_D and R_{rel} of different formulations of mAb3. Mean and standard deviation (SD) were calculated based on n=3.*

	k_D [ml/g]		R_{rel}	
	mean±SD	Rank	mean±SD	Rank
Formulation 1	-24.3±2.4	2	1.2±0.1	1
Formulation 2	-33.2±1.3	9	1.4±0.1	4
Formulation 3	-55.9±4.5	13	1.5±0.2	7
Formulation 4	-57.5±2.6	14	2.4±0.0	12
Formulation 5	-33.0±0.7	8	1.9±0.1	9
Formulation 6	-93.9±8.1	15	3.1±0.4	15
Formulation 7	-34.9±1.6	10	2.2±0.2	10
Formulation 8	-40.8±2.8	11	2.7±0.1	14
Formulation 9	-53.6±3.4	12	2.6±0.6	13
Formulation 10	-28.7±0.9	7	2.4±0.1	11
Formulation 11	-26.1±0.6	6	1.5±0.0	8
Formulation 12	-24.6±0.6	3	1.4±0.1	5
Formulation 13	-24.6±1.5	4	1.4±0.1	3
Formulation 14	-25.1±0.7	5	1.4±0.1	6
Formulation 15	-23.5±0.5	1	1.3±0.0	2

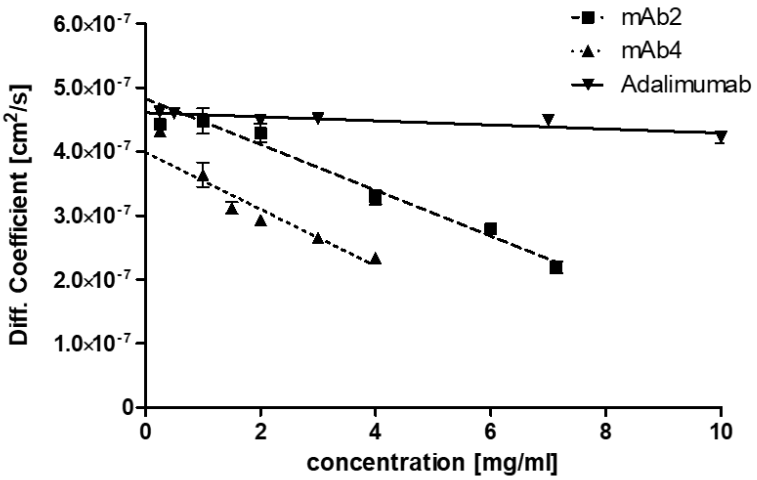

Figure S1 *Exemplary data of k_D determination for adalimumab, mAb2 and mAb4.*

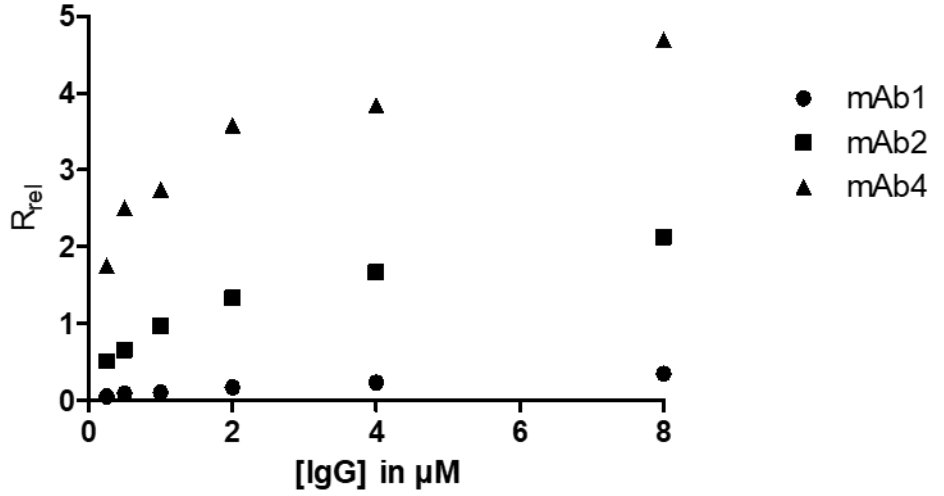

Figure S2 *Linearity check of R_{rel} in dependence on used mAb concentration for association.*

Chapter 3 Analysis of antibody self-interaction by bio-layer interferometry as tool to support lead candidate selection during preformulation and developability assessments

This chapter is published as:

M. Domnowski[1,2], B. Hackner[2], T. Neuber[2], J. Jaehrling[2], W. Frieß[1]

Analysis of antibody self-interaction by bio-layer interferometry as tool to support lead candidate selection during preformulation and developability assessments.

In International Journal of Pharmaceutics, 2020, Vol. 589

[1]Department of Pharmacy: Pharmaceutical Technology and Biopharmaceutics; Ludwig-Maximilians-Universitaet Muenchen, Butenandtstrasse 5, 81377 Munich, Germany
[2]MorphoSys AG, Semmelweisstraße 7, 82152 Planegg

Note from the authors:

The version included in this thesis is identical with the published article apart from minor changes.

The published article can be assessed online via:

https://doi.org/10.1016/j.ijpharm.2020.119854

Author contributions:

M.D., B.H. and J.J. conceived and designed the study. M.D. conducted and analyzed SI-BLI, DLS, nanoDSF measurements. B.H. performed and analyzed viscosimetry experiments. T.N. conducted and analyzed SI-BLI measurements. J.J. performed SI-BLI experiments. M.D., B.H., T.N., J.J. and W.F contributed to the writing of the manuscript.

Keywords: Protein formulation; Self-interaction; Self-association; Monoclonal antibody; Bio-layer interferometry; Developability; Preformulation

3.1 Abstract

Developability assessment of therapeutic mAb candidates before entering CMC development mitigates the risk of later failure because of manufacturing and stability issues. For mAbs derived from library based screenings, such evaluation starts with the first panning and ends with the selection of a lead candidate. This candidate should show, amongst others, high affine target binding and beneficial conformational as well as chemical stability. In addition, colloidal stability, reflected by the self-interaction propensity, should be superior in order to reduce aggregate formation and unacceptably high viscosity at elevated protein concentrations. Here, we present a study demonstrating the application of self-interaction bio-layer interferometry (SI-BLI) in a developability assessment, including the evaluation of preformulations. We reveal that the formulation rankings based on SI-BLI, DLS and viscosity measurements correlate. SI-BLI provides a deeper understanding of influencing factors on mAb self-interaction such as ionic strength or cation species. The attractive mAb self-interaction propensity was significantly more suppressed by Mg^{2+} compared to Na^{+}. SI-BLI can be performed in high throughput with minimal material and sample preparation needs. Therefore, it can be applied in early stages of developability assessment going beyond the use of a platform formulation and a small number of analysis, to screen more parameters before proceeding with candidate selection and further extensive development.

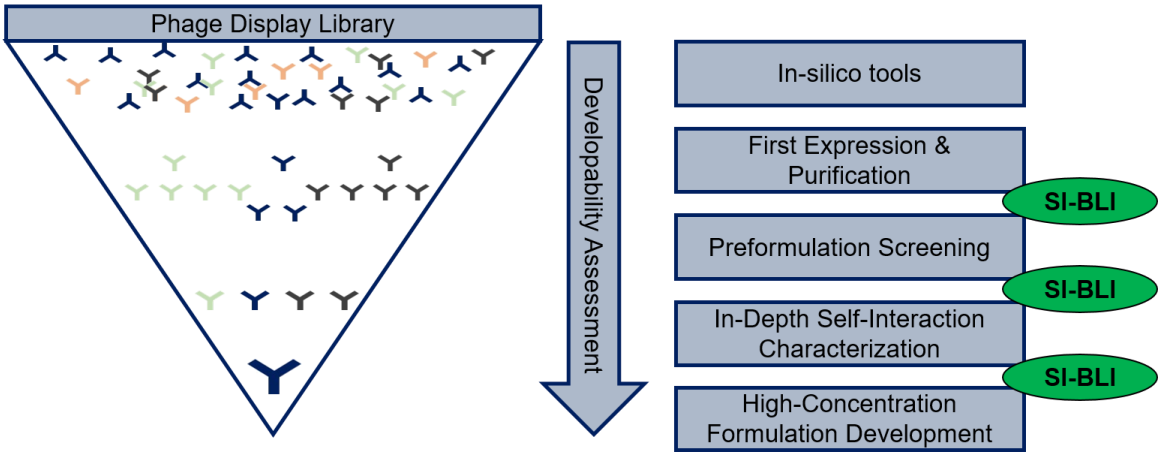

Graphical abstract *Analysis of antibody self-interaction by bio-layer interferometry as tool to support lead candidate selection during preformulation and developability assessments*

3.2 Introduction

A major challenge in early stages of development of therapeutic monoclonal antibodies (mAbs) is the efficient and rational selection of the best candidate for moving forward into CMC and clinical development. The lead candidate should provide functionality and sufficient stability during manufacturing, filling and storage. Thus, analytical tools have to be applied to evaluate the chemical, conformational and colloidal stability of the potential candidates. This developability assessment starts in an early phase when hundreds to thousands of molecules have to be screened. To this end, methodologies capable of high throughput and low sample consumption, as well as *in silico* tools have to be employed.[1] In an intermediate phase, tens to hundreds of molecules can be tested to obtain a better mechanistic understanding of processes. Finally, few candidates are characterized in-depth to decide for a lead and a backup candidate.[2, 3] This decision path should mitigate the risk of failure in subsequent CMC development.

The colloidal stability in terms of protein-protein self-interaction can be described by the second virial coefficient B_{22} or the related diffusion interaction parameter k_D.[4–6] Both parameters are typically assessed by light scattering techniques [7, 8] since other analytical methods come with throughput limitations or require extensive amounts of sample like AUC and self-interaction chromatography.[9–11] Although SIC analyses can be performed in high throughput on HPLC systems requiring only small injection amounts, the preparation of the stationary phase requires several milligrams. The light scattering based methodologies can be used in a high throughput manner if corresponding instruments are available. But sample preparation steps including concentration and preparation of a dilution series still requires 500 µg of sample.[12] The self-interaction can be assessed with even less material in high throughput manner by using bio-layer interferometry (SI-BLI). Sun et al. applied this technique to distinguish between different antibodies based on their self-interaction propensity in a platform formulation.[13] Because self-interaction processes are dependent on the formulations composition [14–20], we developed the assay further and showed its correlation with k_D.[12]

Here we present the applicability of this assay for the final stage of mAb assessment when the decision for a lead and backup candidate has to be taken. We used SI-BLI for a preformulation study to determine the effect of buffer, ionic strength, pH and excipients on

the self-interaction propensity of four different mAbs. These mAbs, derived from phage display library [21], target the same epitope of the antigen and were matured based on one common parental mAb. They were produced by comparable upstream and downstream processes and have theoretical isoelectric points between 9.3 and 9.4. We screened 19 different formulations for each mAb by SI-BLI and found remarkable effects on self-interaction propensity. The findings could be confirmed by dynamic light scattering and viscosimetry for selected formulations. Additionally, we differentiated between a general effect of ionic strength and a more specific metal ion modality for one dedicated mAb. Thus, we successfully applied the SI-BLI assay as a high-throughput approach for preformulation and for follow-up studies, which demonstrated its usefulness for fast and reliable screening of the formulation dependent self-interaction propensity of mAbs.

3.3 Materials and methods

3.3.1 MAb production and formulation

Four mAbs were expressed in HKB11 stable cell pools and purified via affinity Protein A chromatography. To reach at least 95 % monomeric content, preparative size exclusion chromatography was performed followed by buffer exchange to 150 mM histidine hydrochloride pH 6.0. The protein concentration was adjusted to 10 mg/ml. For preformulation assessment, samples were diluted to 1 mg/ml with the respective formulation buffer. For the follow up studies, the 10 mg/ml protein solution was dialyzed over night against the formulations F1-F4 (Table 1) by using Slide-A-Lyzer dialysis cassettes with a MWCO of 30 kDa (Thermo Fisher Scientific, MA). Formulations F5 to F11 were prepared by dilution to the SI-BLI assay concentration (0.3 mg/ml) after dialysis to water over night (Table 1).

A D-Optimal Design approach was applied for preformulation screening (MODDE, Sartorius Stedim, Sweden). As formulation factors, histidine hydrochloride at pH 5.0, 6.0 and 7.0, sodium chloride, magnesium chloride, arginine hydrochloride and surfactant were used. These factors were combined to reach a theoretical osmolarity of 300 mOsm in each formulation. A detailed overview of the compositions of the preformulations can be found in the supplemental material (Table S1). Results were statistically analyzed by applying multivariate data analysis, which is implemented in the DoE software. After model

refinement by excluding combination factors, statistically estimated effects were calculated for the linear terms pH, sodium chloride, arginine hydrochloride, magnesium chloride and surfactant.

Table 1 *Overview of the formulations used.*

	Buffer	pH	NaCl [mM]	$MgCl_2$ [mM]	Ionic strength
F1	15 mM Histidine-HCl	6.0	-	-	
F2	15 mM Histidine-HCl	6.0	130		
F3	15 mM Histidine-HCl	6.0	130	0.5	
F4	15 mM Histidine-HCl	6.0	-	90	
F5	50 mM Na-Acetate	5.5		100	0.342
F6	50 mM Na-Acetate	5.5	100		0.142
F7	50 mM Na-Acetate	5.5		50	0.192
F8	50 mM Na-Acetate	5.5	200		0.242
F9	50 mM Na-Acetate	5.5	-	-	0.042
F10	25 mM Na-Acetate	5.5	-	-	0.021
F11	10 mM Na-Acetate	5.5	-	-	0.008

3.3.2 Self-Interaction Bio-Layer Interferometry

The SI-BLI method was performed as previously described.[12] Briefly, anti-hIgG Fc capture (AHC) biosensors were used on an Octet HTX system (Sartorius AG, FortéBio, CA) in a 384 well plate format. A baseline was established in PBS, followed by capture of the mAb of interest at 25 nM in PBS until the BLI signal increased by approximately 1 nm followed by saturation of the sensor with 1 µM of human Fc in PBS. Subsequently, a second baseline was acquired in the formulation composition, followed by an association step with 2 µM mAb in the same formulation. The response at equilibrium normalized to the amount of captured mAb (R_{rel}) was used for further calculations:

$$R_{rel} = \frac{Response_{Association\ equilibrium}\ [nm]}{Response_{capture\ step}[nm]} \quad (1)$$

As control, sensors saturated with human Fc without IgG capture were used.

3.3.3 Dynamic Light Scattering

Dynamic light scattering was conducted on a DynaPro® Plate Reader (Wyatt Technology, CA). 80 µl of sample were filtrated using 96 well filter plates (0.22 µm, Merck Millipore, Germany). Afterwards, 20 µl of sample were transferred to a 384 well plate (Corning INC, NY) in triplicates. Wells were sealed with silicone oil and then centrifuged at 400xg for 2 min. Diffusivity was measured with 5 acquisitions à 10 s at 25 °C. Data were processed using Dynamics 7.8 (Wyatt Technology, CA). Five different protein concentrations between 0.5 and 10 mg/ml were analyzed to determine the diffusion interaction parameter k_D via linear regression using PRISM 5 (GraphPad Software Inc., CA) [22].

3.3.4 Viscosimetry

Viscosity of mAb solutions was analyzed using a Viscosizer TD capillary system (Malvern, UK) at mAb concentrations between 1.5 and 80 mg/ml. A constant pressure of 1000 mbar was applied at a capillary temperature of 20 °C with UV detection at 280 nm. The relative values were referenced to 1 mg/ml caffeine solution in H_2O. The concentration dependent increase in viscosity was characterized by the slope B_1 of logarithmized viscosity values based on $\ln \eta = \ln \eta_0 + B_1 \cdot c$.

3.3.5 nano Dynamic Scanning Fluorimetry

1 mg/ml mAb samples were filled in standard nanoDSF glass capillaries and measurements were performed using a Prometheus NT.48 (NanoTemper Technologies, Germany). Intrinsic fluorescence at 330 nm and 350 nm was evaluated during a temperature ramp from 20 °C to 90 °C at 1 K/min. Transition onset and inflection points were determined from the first derivative using the PR.Control software (NanoTemper, Germany).

3.4 Results

3.4.1 SI-BLI preformulation screening as part of a developability assessment

We evaluated the effect of pH and excipients on the self-interaction of the four candidate mAbs by SI-BLI as a preformulation screening before initiation of subsequent extensive stability studies. This enables the evaluation of the colloidal stability under formulation conditions with low self-interaction propensity. We varied pH, buffer concentration as well as the concentration of different excipients based on a DoE approach according to Table S1 (Supplemental material). MAb self-interaction was remarkably decreased if ionic excipients were included in the formulation. The addition of magnesium chloride minimized the BLI response (exemplarily shown for mAbA in Figure 1).

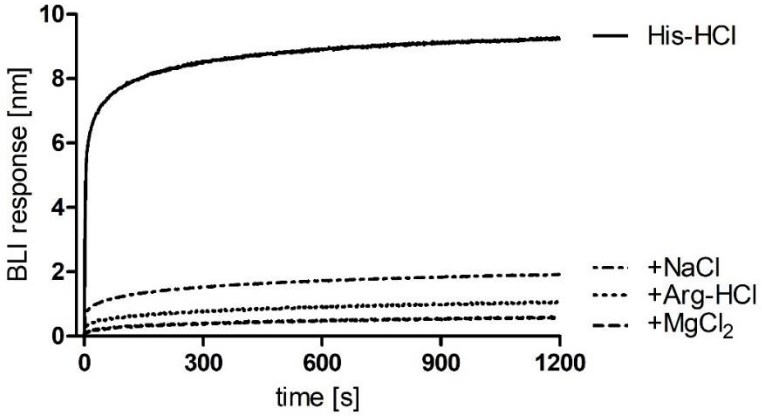

Figure 1 *SI-BLI association reaction of mAbA in 15 mM His pH 7.0, 0.05% PS20 (His-HCl; PF13), 15 mM His pH 7.0, 0.05% PS20, 135 mM NaCl (+NaCl; PF16), 15 mM His pH 7.0, 0.05% PS20, 135 mM Arg-HCl (Arg-HCl; PF15), 15 mM His pH 7.0, 0.05% PS20, 90 mM $MgCl_2$ (+$MgCl_2$; PF14).*

The results of the preformulation study were statistically analyzed and effects were calculated. The effect plot showed comparable results for all mAbs (Figure 2 shows the effects exemplarily for mAbA). We determined a significant, negative effect on attractive self-interaction for magnesium chloride ($p<0.001$). In addition, a higher pH increased attraction of the mAb molecules significantly ($p<0.001$), whereas surfactant concentration as well as addition of NaCl and Arg-HCl did not show a significant effects. These results suggest, that a formulation comprising magnesium chloride at slightly acidic pH would

reduce the self-interaction propensity of the mAb und thus, the response of the SI-BLI assay.

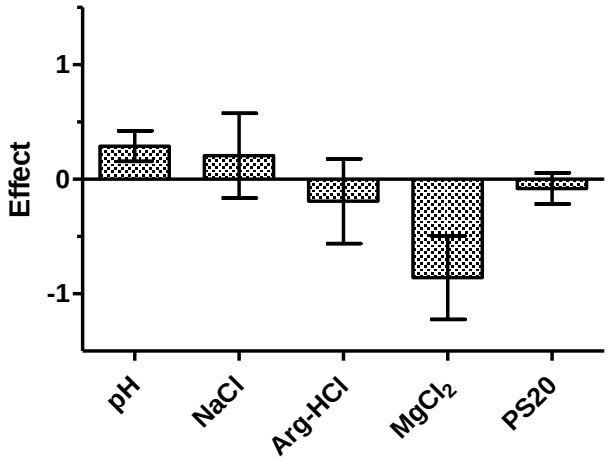

Figure 2 *Effect plot of the DoE-based SI-BLI preformulation screening of mAbA. Error bars represent the 95 % confidence interval.*

3.4.2 Assessment of self-interaction propensity by DLS for selected formulations

The effects of pH and $MgCl_2$, although not all salts, point to electrostatics as an important trigger for self-interaction of the mAbs. Therefore, we conducted a more detailed investigation of all four mAbs in four formulations, 15 mM His pH 6.0 containing either no salt, 130 mM NaCl, 130 mM NaCl + 0.5 mM $MgCl_2$ or 90 mM $MgCl_2$ (F1 – F4, Table 1). We analyzed k_D by DLS, R_{rel} as indicator of attractive self-interaction by SI-BLI and the viscosity as a function of protein concentration.

The concentration dependent diffusivity of mAbB is exemplarily shown in Figure 3A. We observed negative slopes for all mAbs in all formulations with the most negative for the His buffer without additional salt (F1) and the least negative with addition of 90 mM $MgCl_2$ (F4). Thus, the most negative k_D values indicating strong attractive self-interaction was observed in absence of salts (Figure 3B). With addition of salt, k_D increased and at the high $MgCl_2$ concentration the only slightly negative k_D values reflect diminished self-interaction. Comparing NaCl (F2) and NaCl + $MgCl_2$ (F3), the addition of only 0.5 mM $MgCl_2$ did not have a significant impact on a formulation already containing 130 mM NaCl.

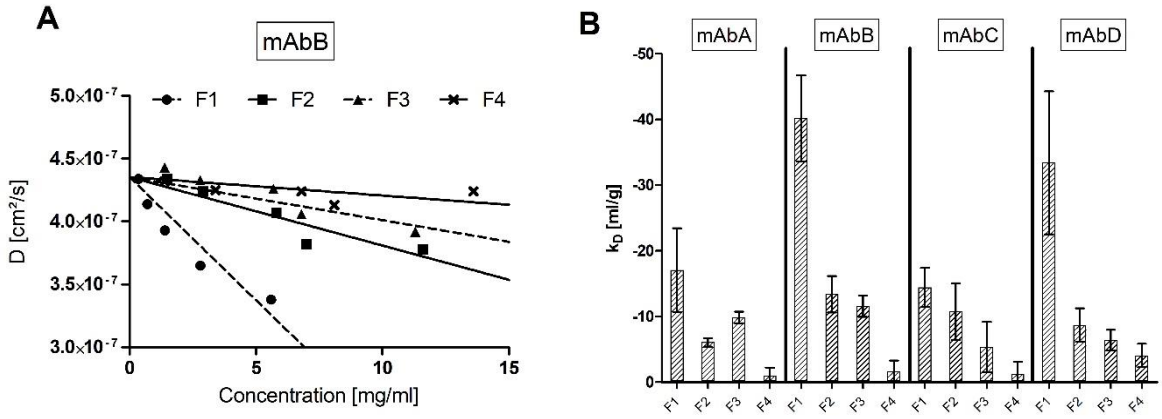

Figure 3 *k_D analysis of the four mAbs in 15 mM His pH 6.0 without salt (F1), 15 mM His pH 6.0 + 130 mM NaCl (F2),15 mM His pH 6.0 + 130 mM NaCl + 0.5 mM $MgCl_2$ (F3) and 15 mM His pH 6.0 + 90 mM $MgCl_2$ (F4) by DLS. A) concentration dependent diffusivity of mAbB (for mAbA, mAbC and mAbD see Figure S1); B) k_D values (± SD).*

3.4.3 Assessment of self-interaction propensity by SI-BLI for selected formulations

The self-Interaction propensity of the mAbs was additionally assessed by SI-BLI. Association curves of mAbC are exemplarily shown in Figure 4A. The highest R_{rel} values for all mAbs and formulations indicating strong attractive self-interaction resulted from His buffer without additional salt (F1) (Figure 4B). R_{rel} decreased in salt containing formulations. Formulation F4, containing a high $MgCl_2$ concentration, resulted in low R_{rel} values, indicating that self-interaction was diminished in these formulations. The addition of a low amount of $MgCl_2$ to a 130 mM NaCl formulation only slightly influenced the attractive self-interaction (F2 vs. F3).

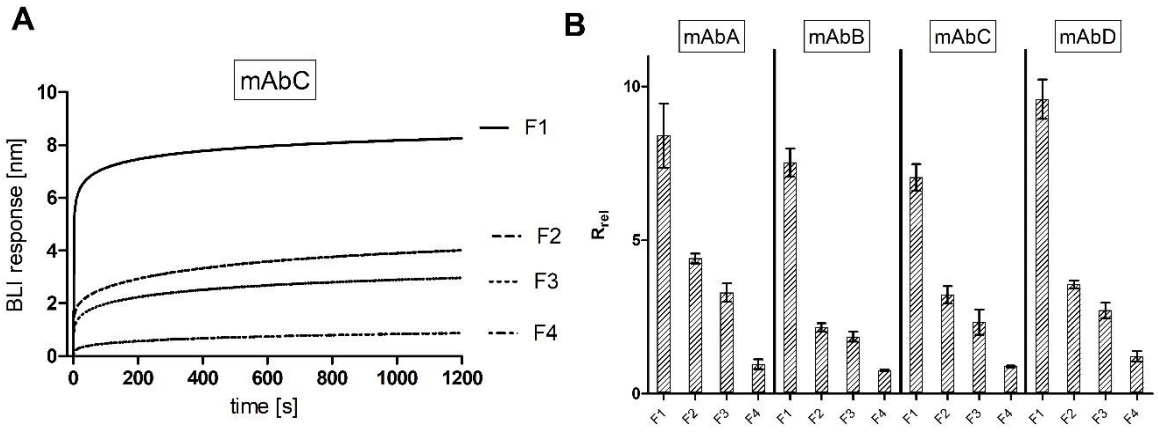

Figure 4 *SI-BLI results of the four mAbs in in 15 mM His pH 6.0 without salt (F1), 15 mM His pH 6.0 + 130 mM NaCl (F2),15 mM His pH 6.0 + 130 mM NaCl + 0.5 mM $MgCl_2$ (F3) and 15 mM His pH 6.0 + 90 mM $MgCl_2$ (F4). A) Association curve of the self-interaction of mAbC (for mAbA, mAbB and mAbD see Figure S2); B) Overview of calculated R_{rel} values (± SD).*

3.4.4 Analysis of mAb concentration dependent viscosity for selected formulations

All mAbs showed a formulation dependent increase of viscosity with increased concentration (Figure 5). The dynamic viscosity of mAbD formulations increased exponentially from 1.0 mPa*s at 2.7 mg/ml to 1.5 mPa*s at 43 mg/ml in F1 without salt. The addition of $MgCl_2$ (F4) led to a reduced increase from 1.0 mPa*s (4.9 mg/ml) to 1.1mPa*s (39 mg/ml). For formulations 2 and 3, the viscosity increased from 1.0 mPa*s to 1.2 mPa*s at 27 mg/ml and 35 mg/ml, respectively. We linearized the data for determination of the slope of the increased dynamic viscosity (Figure 5A). The slope was used to compare the formulations and mAbs. As shown in figure 5B, the strongest increase in viscosity was observed for F1 containing only histidine. The addition of NaCl in F2, as well as NaCl + 0.5 mM MgCl2 in F3 significantly reduced the slope for all mAbs except for mAbC, which showed the same trend, which was not significant though. The slope of the increased viscosity was the lowest for all mAbs in formulation F4 containing a high amount of $MgCl_2$.

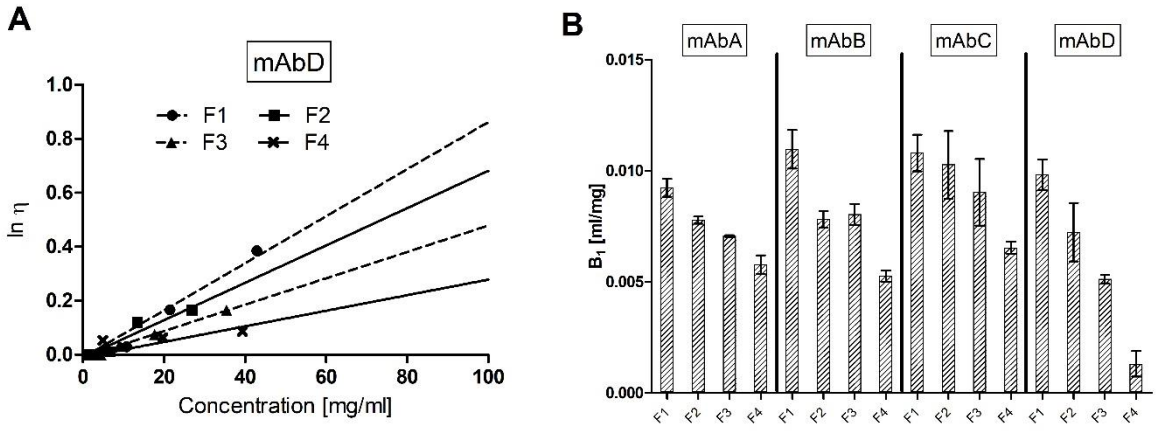

Figure 5 *Viscosity of the four mAbs in in 15 mM His pH 6.0 without salt (F1), 15 mM His pH 6.0 + 130 mM NaCl (F2),15 mM His pH 6.0 + 130 mM NaCl + 0.5 mM $MgCl_2$ (F3) and 15 mM His pH 6.0 + 90 mM $MgCl_2$ (F4). A) Concentration dependent viscosity of mAbD (natural log of the dynamic viscosity in mPa*s) (for mAbA, mAbB and mAbC see Figure S3); B) Overview of calculated slopes of the concentration dependent dynamic viscosity (B_1).*

3.4.5 Correlation of results obtained by SI-BLI, DLS and Viscosimetry

SI-BLI, DLS and Viscosimetry were performed to analyze the self-interaction propensity of the four model mAbs in four different formulations differing in ionic strength and the cation type. Comparable rankings of the formulations for all mAbs were observed by all methods. We calculated significant Pearson correlation coefficients for results of R_{rel} and k_D ($r = 0.82$, $p < 0.001$) (Fig S4) as also reported previously [12]. Additionally, the correlation of R_{rel} and B_1, reflecting the concentration dependent viscosity increase, was also significant ($r = 0.68$, $p < 0.01$).

3.4.6 The Mg^{2+} effect on mAb self-interaction propensity

Since the self-interaction propensity was decreased in high ionic strength formulation and was further reduced by $MgCl_2$ at higher concentration, we performed additional SI-BLI and nanoDSF experiments. To differentiate between the effect of ionic strength and a specific or non-specific effect of the divalent ion Mg^{2+}, we formulated mAbC exemplarily in formulations based on sodium acetate buffer pH 5.5 with NaCl and $MgCl_2$ concentrations (F5-F8) and with different buffer strength (F9-F11).

The self-interaction propensity of mAbC decreased with an increase in ionic strength of the buffer only formulations (Figure 6). The supplement of salt reduced attractive self-interaction generally. In addition, the R_{rel} was lower in solutions containing the same concentration of chloride, but Mg^{2+} instead of Na^{+}. Further, R_{rel} was lower in the formulation containing 50 mM $MgCl_2$ compared to 200 mM NaCl although the ionic strength of the latter was higher.

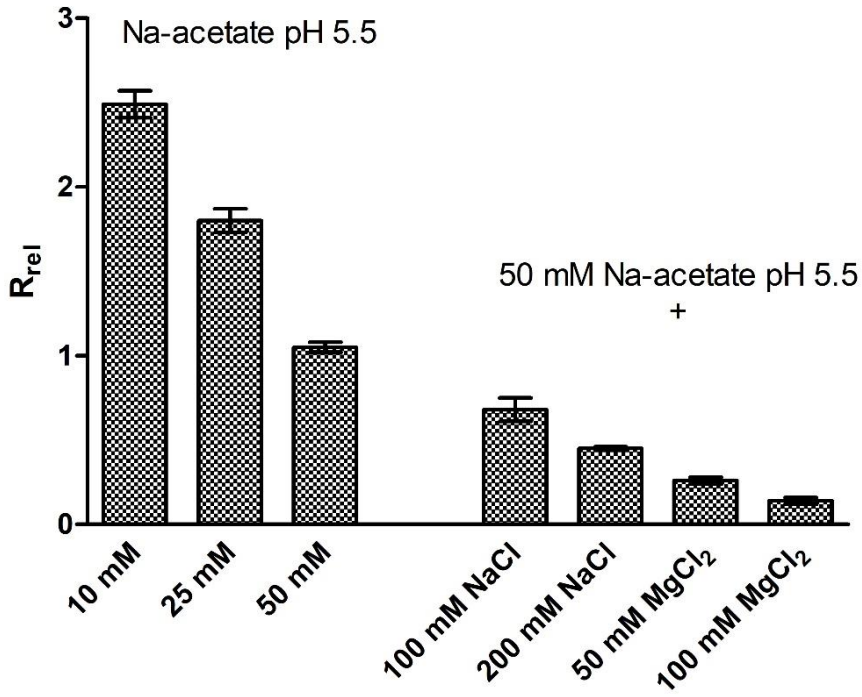

Figure 6 *SI-BLI results for mAbC in formulations containing different buffer concentrations and low and high concentration of ionic excipients.*

To determine if the effect of $MgCl_2$ on self-interaction arises from specific Mg^{2+} binding to the mAb, we performed nanoDSF for mAbC in 10 mM sodium acetate, 50 mM sodium acetate without salt, 50 mM sodium acetate + 100 mM NaCl and 50 mM sodium acetate + 50 mM $MgCl_2$. A specific interaction should alter the conformational stability of the protein.[23] The apparent unfolding temperature varied between 64.9°C as the lowest temperature in the formulation containing NaCl and 66.0°C in 10 mM sodium acetate as the highest temperature (See Table S2). We did not observe significant differences in T_m comparing formulations with NaCl or $MgCl_2$ and therefore consider the interaction of Mg^{2+} and the mAbs as unspecific and not targeted to specific interaction sites of the protein molecules.

3.5 Discussion

To minimize cost and time, platform approaches are widely used in the development of biopharmaceutical products.[24, 25] This includes the use of platform formulations considering a narrow pH range and standard excipients derived from commercially available products especially in early phases of development.[26–28] In addition to surfactants like polysorbate 20 or 80, ionic modifiers and sugars are used to stabilize the product. For the development of high concentration mAb formulations, the assessment of protein self-interaction is of utmost importance as this propensity drives viscosity and colloidal instability. [9,18,29,30] Limiting this analysis to platform formulations bears the risk of dismissing high potential candidate molecules in early stages due to inadequately high viscosity or colloidal instability. We established a workflow, which makes use of SI-BLI during candidate screening to analyze candidates in a high number of formulations with minimal effort and material requirements. This enables the combination of both candidate assessment and preformulation in the development of high concentration mAb formulations. Recent studies applied k_D to train artificial neural networks to predict the formulation behavior of therapeutic protein candidates.[31] The SI-BLI datasets obtained in high throughput could be included to improve model accuracy and precision by including the formulation dependent attractive self-interaction propensity.

In addition to the assessment of colloidal stability and viscosity, the evaluation of conformational properties can be included both in developability assessments and preformulation work.[31] As the apparent unfolding temperature of a mAb can be easily analyzed in high throughput by DSF, mAbs with lower stability can be excluded prior to subsequent lab extensive parts of developability assessments.

With regard to developability, computational tools such as Therapeutic Antibody Profiler (TAP) and Developability Index (DI) have been generated to predict developability challenges based on the structural properties of the variable domains of a mAb.[32, 33] In case of TAP, these structural properties include CDR length, surface hydrophobicity, surface exposed positive and negative charged properties as well as charge symmetry at pH 7.4.[32].The DI is based on spatial aggregation propensity and net charge.[33] Thus, DI can reflect pH dependence of surface charge and the probability of electrostatic interactions. Because SI-BLI can be performed in high-throughput at different pH values, the

combination of data from *in silico* tools such as DI and experimental data from SI-BLI may support the assessment at early stages of discovery. Thus, the development of mAb candidates, which are suitable for high concentration formulations can be initiated earlier which can save time and effort at later stages of development.

We analyzed four mAbs in four different formulations containing different NaCl or $MgCl_2$ levels. R_{rel} from SI-BLI was increased for formulations without salt and was remarkably reduced by the addition of ionic excipients. Ions potentially influence the self-interaction process by shielding electrostatically driven interactions. Thus, attractive self-interaction was decreased in formulations containing NaCl and was further minimized by $MgCl_2$. Based on k_D we identified strong attractive interactions in formulations without salt and less attractive interaction in formulations containing salt. With both methods, we observed comparable rankings of the formulations which confirmed the correlation of SI-BLI and DLS results[12]. We further evaluated the effect of protein concentration on the dynamic viscosity of the formulations. Viscosity increased exponentially with protein concentration which was consistently described for other mAbs. [9,14,17,18,30,34,35] However, the increase was overall small but we were able to rank the formulation based on the slope of this increase. We observed a stronger increase in formulations without salt for all mAbs. The addition of 90 mM $MgCl_2$ minimized the viscosity. To this end, the ion effect on the attractive self-interaction of the mAbs was confirmed by all methodologies used. The results of SI-BLI, DLS and viscosimetry correlate significantly and confirm previous findings.[4,22,36] In this context, rankings based on R_{rel} values may reflect a new approach to predict the solution behavior at high protein concentration and to generate developability rankings. A limitation which has to be kept in mind is the fact that net repulsive interactions cannot be assessed by SI-BLI.[4]

Since the attractive self-interaction of the investigated mAb samples could be significantly reduced by salts, we tested different facets of this factor with SI-BLI: the effect of different Cl^-concentration, of mono- or divalent cations and of overall ionic strength. As depicted in figure 6, attractive self-interaction was less pronounced in formulations containing 50 mM $MgCl_2$ compared to 200 mM NaCl, although the ionic strength as well as the Cl^- concentration of the 200 mM NaCl containing formulation was higher. Thus the divalent cation Mg^{2+} reduces attractive self-interaction distinctively more than Na^+ or a general increase in ionic strength. This may indicate the salting-in effect of Mg^{2+}, which has been

described before [37], although different proteins were studied and higher $MgCl_2$ concentrations were required to observe significant effects. In addition, we could not confirm specific binding of cations to the protein by nanoDSF and therefore hypothesize that the observed behavior is caused by the combination of two effects: a preferential, although rather unspecific, interaction of Mg^{2+} with the mAbs, and the effect of increasing ionic strength of the solution. A special attractive interaction and viscosity decreasing effect of cations on mAbs has been demonstrated for cationic amino acids [34] and we observed a decrease in R_{rel} for mAbA upon addition of Arg-HCl. Screening of different ionic species, e.g. by SI-BLI can improve the chances of successfully developing high concentration formulations by minimizing electrostatically driven self-interaction processes.

3.6 Conclusion

We described the application of SI-BLI in a preformulation screening as part of the developability assessment of mAbs. We analyzed four mAbs in 19 different formulations and identified significant effects on mAb self-interaction. After formulation selection, self-interaction propensity was analyzed by DLS and SI-BLI. Additionally, the viscosity at elevated protein concentration was determined. We observed a significant correlation of rankings based on k_D obtained by DLS, R_{rel} obtained by SI-BLI and the increase in viscosity. Additionally, SI-BLI enabled us to understand the influence of different ions on the self-interaction behavior. Based on our findings, SI-BLI could be helpful to predict the solutions behavior at high protein concentration and thus to mitigate risks in CMC development of high concentration protein formulations. As this assay only requires a single, low concentration of protein for determination of attractive self-interaction, it can be applied in very early stages of development where the number of potential candidates is high and the available amount of protein material is limited. This could accelerate the design of high concentration liquid formulations for subcutaneous administration and thus decrease effort and shorten timelines for late stage CMC development.

3.7 Acknowledgements

This study was part of the project “Self-Interaction and targeted Engineering of monoclonal antibodies (Self-I-E)”, which was funded by the Bayerische Forschungsstiftung.

References

1. Agrawal NJ, Helk B, Kumar S, et al. Computational tool for the early screening of monoclonal antibodies for their viscosities. 2016. MAbs 8: 43–48.

2. Jameel F, Skoug JW, Nesbitt RR. 2020. Development of Biopharmaceutical Drug-Device Products, Cham: Springer International Publishing. 888 p.

3. Jarasch A, Koll H, Regula JT, et al. Developability assessment during the selection of novel therapeutic antibodies. 2015. J Pharm Sci 104: 1885–1898.

4. Woldeyes MA, Qi W, Razinkov VI, et al. How Well Do Low- and High-Concentration Protein Interactions Predict Solution Viscosities of Monoclonal Antibodies? 2019. J Pharm Sci 108: 142–154.

5. Roberts D, Keeling R, Tracka M, et al. The role of electrostatics in protein-protein interactions of a monoclonal antibody. 2014. Mol Pharm 11: 2475–2489.

6. Le Brun V, Friess W, Bassarab S, et al. A critical evaluation of self-interaction chromatography as a predictive tool for the assessment of protein-protein interactions in protein formulation development: a case study of a therapeutic monoclonal antibody. 2010. Eur J Pharm Biopharm 75: 16–25.

7. Gentiluomo L, Roessner D, Streicher W, et al. Characterization of Native Reversible Self-Association of a Monoclonal Antibody Mediated by Fab-Fab Interaction. 2020. J Pharm Sci 109: 443–451.

8. Calero-Rubio C, Ghosh R, Saluja A, Roberts CJ. Predicting Protein-Protein Interactions of Concentrated Antibody Solutions Using Dilute Solution Data and Coarse-Grained Molecular Models. 2018. J Pharm Sci 107: 1269–1281.

9. Kanai S, Liu J, Patapoff TW, Shire SJ. Reversible self-association of a concentrated monoclonal antibody solution mediated by Fab-Fab interaction that impacts solution viscosity. 2008. J Pharm Sci 97: 4219–4227.

10. Hedberg SHM, Heng JYY, Williams DR, Liddell JM. Micro scale self-interaction chromatography of proteins: A mAb case-study. 2016. J Chromatogr A 1434: 57–63.

11. Hedberg SHM, Lee D, Mishra Y, et al. Mapping the mAb Aggregation Propensity Using Self-Interaction Chromatography as a Screening Tool. 2018. Anal Chem 90: 3878–3885.

12. Domnowski M, Jaehrling J, Frieß W. Assessment of Antibody Self-Interaction by Bio-Layer-Interferometry as a Tool for Early Stage Formulation Development. 2020. Pharm Res 37: 29.

13. Sun T, Reid F, Liu Y, et al. High throughput detection of antibody self-interaction by bio-layer interferometry. 2013. MAbs 5: 838–841.

14. Tomar DS, Kumar S, Singh SK, et al. Molecular basis of high viscosity in concentrated antibody solutions: Strategies for high concentration drug product development. 2016. MAbs 8: 216–228.

15. Garidel P, Blume A, Wagner M. Prediction of colloidal stability of high concentration protein formulations. 2015. Pharm Dev Technol 20: 367–374.

16. Esfandiary R, Parupudi A, Casas-Finet J, et al. Mechanism of reversible self-association of a monoclonal antibody: role of electrostatic and hydrophobic interactions. 2015. J Pharm Sci 104: 577–586.

17. Yadav S, Shire SJ, Kalonia DS. Factors affecting the viscosity in high concentration solutions of different monoclonal antibodies. 2010. J Pharm Sci 99: 4812–4829.

18. Liu J, Nguyen MDH, Andya JD, Shire SJ. Reversible self-association increases the viscosity of a concentrated monoclonal antibody in aqueous solution. 2005. J Pharm Sci 94: 1928–1940.

19. Pindrus MA, Shire SJ, Yadav S, Kalonia DS. The Effect of Low Ionic Strength on Diffusion and Viscosity of Monoclonal Antibodies. 2018. Mol Pharm 15: 3133–3142.

20. Sahin E, Grillo AO, Perkins MD, Roberts CJ. Comparative effects of pH and ionic strength on protein-protein interactions, unfolding, and aggregation for IgG1 antibodies. 2010. J Pharm Sci 99: 4830–4848.

21. Tiller T, Schuster I, Deppe D, et al. A fully synthetic human Fab antibody library based on fixed VH/VL framework pairings with favorable biophysical properties. 2013. MAbs 5: 445–470.

22. Connolly BD, Petry C, Yadav S, et al. Weak interactions govern the viscosity of concentrated antibody solutions: high-throughput analysis using the diffusion interaction parameter. 2012. Biophys J 103: 69–78.

23. Arakawa T. Protein-solvent interaction. 2018. Biophys Rev 10: 203–208.

24. Yang X, Xu W, Dukleska S, et al. Developability studies before initiation of process development: improving manufacturability of monoclonal antibodies. 2013. MAbs 5: 787–794.

25. Man A, Luo H, Levitskaya SV, et al. Optimization of a platform process operating space for a monoclonal antibody susceptible to reversible and irreversible aggregation using a solution stability screening approach. 2019. J Chromatogr A 1597: 100–108.

26. Warne NW. Development of high concentration protein biopharmaceuticals: the use of platform approaches in formulation development. 2011. Eur J Pharm Biopharm 78: 208–212.

27. Goldberg DS, Lewus RA, Esfandiary R, et al. Utility of High Throughput Screening Techniques to Predict Stability of Monoclonal Antibody Formulations During Early Stage Development. 2017. J Pharm Sci 106: 1971–1977.

28. Uchiyama S. Liquid formulation for antibody drugs. 2014. Biochim Biophys Acta 1844: 2041–2052.

29. Binabaji E, Ma J, Zydney AL. Intermolecular Interactions and the Viscosity of Highly Concentrated Monoclonal Antibody Solutions. 2015. Pharm Res 32: 3102–3109.

30. Li L, Kumar S, Buck PM, et al. Concentration dependent viscosity of monoclonal antibody solutions: explaining experimental behavior in terms of molecular properties. 2014. Pharm Res 31: 3161–3178.

31. Gentiluomo L, Roessner D, Augustijn D, et al. Application of interpretable artificial neural networks to early monoclonal antibodies development. 2019. Eur J Pharm Biopharm 141: 81–89.

32. Raybould MIJ, Marks C, Krawczyk K, et al. Five computational developability guidelines for therapeutic antibody profiling. 2019. Proc Natl Acad Sci U S A 116: 4025–4030.

33. Lauer TM, Agrawal NJ, Chennamsetty N, et al. Developability index: a rapid *in silico* tool for the screening of antibody aggregation propensity. 2012. J Pharm Sci 101: 102–115.

34. Dear BJ, Hung JJ, Truskett TM, Johnston KP. Contrasting the Influence of Cationic Amino Acids on the Viscosity and Stability of a Highly Concentrated Monoclonal Antibody. 2017. Pharm Res 34: 193–207.

35. Lilyestrom WG, Yadav S, Shire SJ, Scherer TM. Monoclonal antibody self-association, cluster formation, and rheology at high concentrations. 2013. J Phys Chem B 117: 6373–6384.

36. Xu AY, Castellanos MM, Mattison K, et al. Studying Excipient Modulated Physical Stability and Viscosity of Monoclonal Antibody Formulations Using Small-Angle Scattering. 2019. Mol Pharm 16: 4319–4338.

37. Arakawa T, Bhat R, Timasheff SN. Preferential interactions determine protein solubility in three-component solutions: the magnesium chloride system. 1990. Biochemistry 29: 1914–1923.

Supplementary data

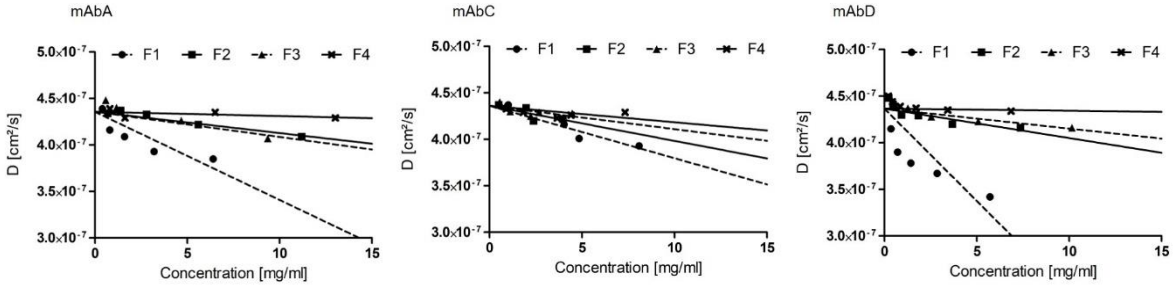

Figure S1 *Diffusivity of mAbA, mAbC and mAbD in Formulations F1 to F4.*

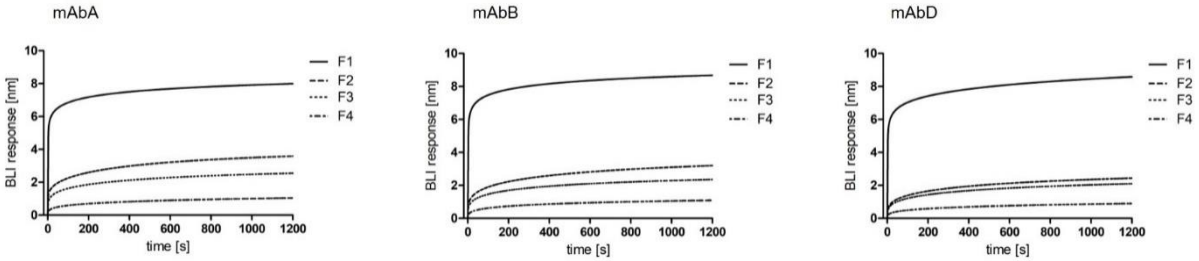

Figure S2 *Association curves of SI-BLI of mAbA, mAbB and mAbD in Formulations F1 to F4.*

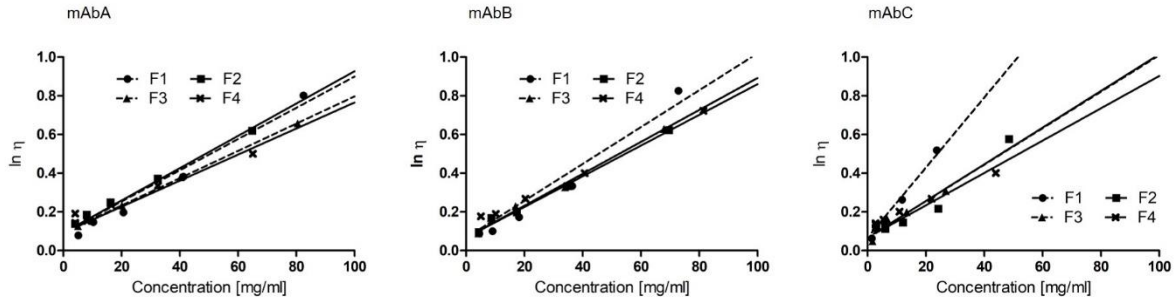

Figure S3 *Viscosity profiles (ln) of mAbA, mAbB and mAbC in Formulations F1 to F4.*

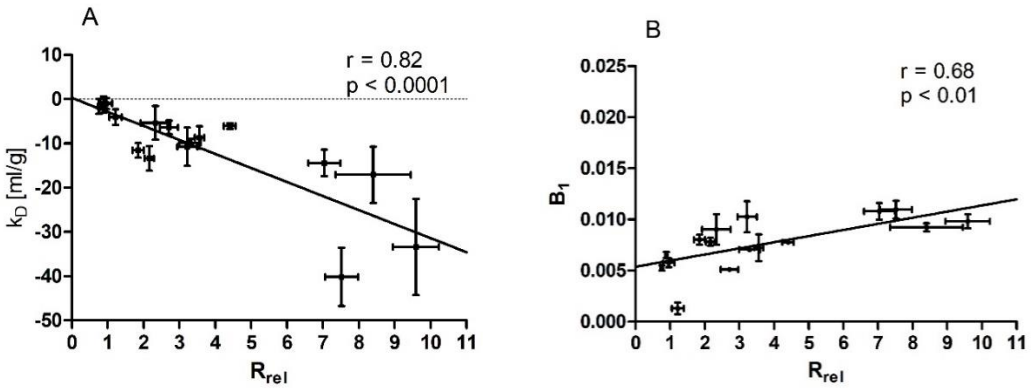

Figure S4 *Correlation plot of R_{rel} and A) k_D and B) B_1.*

Table S1 *Overview of preformulations tested and the results of SI-BLI.*

Preformulation matrix							R_{rel}			
#	Buffer	pH	NaCl	Arg-HCl	$MgCl_2$	PS20	mAbA	mAbB	mAbC	mAbD
PF1	15mM His-HCl	5	---	---	---	---	0.8	0.8	1.5	0.7
PF2		5	---	---	90	---	0.5	1.5	0.6	0.4
PF3		5	---	135	---	---	0.8	3.0	2.0	0.7
PF4		5	135	---	---	---	1.3	0.5	3.6	1.4
PF5		7	---	---	---	---	9.0	12.6	16.1	10.4
PF6		7	---	---	90	---	0.6	2.2	0.5	0.6
PF7		7	---	135	---	---	1.1	1.2	1.7	0.9
PF8		7	135	---	---	---	2.0	1.5	4.0	1.7
PF9		5	---	---	---	0.05	0.9	1.0	1.5	0.7
PF10		5	---	---	90	0.05	0.4	0.5	0.4	0.6
PF11		5	---	135	---	0.05	0.8	0.7	1.1	0.8
PF12		5	135	---	---	0.05	1.1	1.2	1.7	1.7
PF13		7	---	---	---	0.05	8.1	7.0	10.7	7.7
PF14		7	---	---	90	0.05	0.5	0.6	0.5	0.3
PF15		7	---	135	---	0.05	1.0	0.9	1.3	0.8
PF16		7	135	---	---	0.05	1.9	1.8	2.3	1.5
PF17		6	27	54	54	0.025	1.1	0.9	1.3	1.7
PF18		6	27	54	54	0.025	1.0	1.0	1.5	0.8
PF19		6	27	54	54	0.025	1.1	1.2	1.4	0.8

Table S2 *NanoDSF results of mAbC.*

Formulations of mAbC	**T_m [°C] ± SD**	**T_m ^{onset} [°C] ± SD**
10mM Na-Acetate pH 5.5	66.0 ± 0.1	53.0 ± 0.4
50mM Na-Acetate pH 5.5	65.4 ± 0.1	56.4 ± 0.3
50mM Na-Acetate pH 5.5 + 100 mM NaCl	64.9 ± 0.2	55.2 ± 0.2
50mM Na-Acetate pH 5.5 + 50 mM $MgCl_2$	65.4 ± 0.3	55.0 ± 0.2

Chapter 4 A multi-method approach to assess the self-interaction behavior of Infliximab

M. Domnowski[1,2]; T. Maruno[3]; K. Enomoto[3]; F. Kummer[2];

A. Kulakova[4]; P. Harris[4]; S. Uchiyama[3]; J. Jaehrling[2]; W. Frieß[1]

[1] Department of Pharmacy: Pharmaceutical Technology and Biopharmaceutics; Ludwig-Maximilians-Universitaet Muenchen, Butenandtstrasse 5, 81377 Munich, Germany

[2] MorphoSys AG, Semmelweisstraße 7, 82152 Planegg

[3] Osaka University, Department of Biotechnology, Graduate School of Bioengineering, Osaka 565-0871, Japan

[4] Technical University of Denmark, Department of Chemistry, 2800 Kongens Lyngby, Denmark

Author contributions:

M.D., S.U. J.J. and W.F. conceived and designed the study. M.D. conducted and analyzed lyophilization, SEC-MALS, CD, DLS, SI-BLI, HDX-MS and viscosimetry experiments. T.M. conducted and analyzed AUC. K.E. conducted and analyzed HDX-MS. F.K. performed mAb digestion. A.K. conducted and analyzed SAXS experiments. M.D., T.M., F.K., A.K., J.J. and W.F. contributed to the writing of the manuscript. P.H, S.U., J.J. and W.F. reviewed the paper.

Keywords: Infliximab, Self-interaction, Self-association, AUC, SAXS, BLI, HDX-MS

Abbreviations: AUC SV/SE – Analytical Ultracentrifugation Sedimentation Velocity/Sedimentation Equilibrium; CDR – Complementarity determining region; CH – constant heavy chain; CL – constant light chain; DLS – Dynamic Light Scattering; Fab – Antigen binding Fragment; Fc – crystallizable Fragment; HDX-MS – Hydrogen Deuterium Exchange Mass Spectrometry; MALS – Multi Angle Laser Light Scattering; SAXS – Small Angle X-Ray Scattering; VH – variable heavy chain; VL – variable light chain

4.1 Abstract

Attractive self-interaction processes in antibody formulations increase the risk of aggregation and extraordinarily elevated viscosity at high protein concentrations. These challenges affect manufacturing and application. This study aimed to understand the self-interaction process of Infliximab as a model system with pronounced attractive self-interaction. The association mechanism was studied by a multi method approach comprising analytical ultracentrifugation, dynamic light scattering, small angle X-ray scattering, self-interaction bio-layer interferometry and hydrogen-deuterium exchange mass spectrometry. Based on our results, both Fab and Fc regions of Infliximab are involved in self-interaction. We hypothesize a mechanism based on electrostatic interactions of polar and charged residues within the identified areas of the heavy and the light chain of the mAb. The combination of fast and reliable screening methods and low throughput but high resolution methods can contribute to detailed characterization and deeper understanding of specific self-interaction processes.

4.2 Introduction

By 2020, 70 monoclonal antibody (mAb) products will be available on the market and the world-wide sales will be nearly $125 billion.[1] These biomolecules are susceptible to various forms of instability during manufacturing, storage and delivery to the patient. In particular, as colloids mAb molecules exhibit attractive and repulsive interactions with each other.[2] This reversible self-interaction is linked to protein oligomerization or aggregation as well as drastically increased solution viscosity at elevated protein concentration.[3, 4]

mAb self-interaction can either be driven by Fc-Fc interaction, Fab-Fab-interactions or Fab-Fc-interactions[5–9] and the identification of self-interaction sites on an IgG domain level can be highly useful. Analytical ultracentrifugation (AUC)[10], dynamic light scattering (DLS)[11], small-angle X-ray scattering (SAXS)[11] and self-interaction bio-layer interferometry (SI-BLI)[12, 13] have been described for this purpose. The identification requires either digestion of the IgG into Fab and Fc domain or separate expression of the fragments as single proteins. In addition, lab extensive purification is necessary to achieve high sample quality. An even deeper structural understanding of interaction hot spots on a peptide or residue level would be highly beneficial to engineer mAbs and to avoid

unfavorable amino acids and sequences in the primary structure. Results of hydrogen-deuterium-exchange mass spectrometry could provide such high resolution data. In general, this method is used for analyzing highly specific interaction processes during the in-depth characterization process of biopharmaceutical drug development.[14] In addition, this method allows the analysis of weaker protein-protein interactions like in the case of mAb self-interaction processes.[7, 15]

In 2017, Lerch et al. published the self-interaction site of Infliximab based on studies by X-ray crystallography, SEC, SV-AUC and SE-AUC. Based on X-ray crystallography of the Fab fragment, a "head-to-tail orientation" was proposed. The V_L of one Fab builds an interaction interface with the C_L of another Fab. Patches, which indicate hydrophobic interactions have been identified within these chains e.g. Leu_3 of the C_L was shown to stack into a pocket created by Thr_{197}, Lys_{145} and Glu_{143} of V_L. In addition, they identified other interaction sites in other crystal forms indicating that multiple arrangements are possible.[16] But the question arises whether these findings are relevant for pharmaceutical formulations of the protein, in this case Infliximab. High ionic strength buffers and crystallization agents have to be used for crystallization. Furthermore, only the Fab fragment was crystallized, not the full mAb. In addition, the identified interaction sites were present in solid crystals of Infliximab Fab fragments. But do they also play a role in solution, specifically a pharmaceutically relevant formulation?

In our study, we used Infliximab as a model system to generate and challenge a multi-method approach for identifying self-interaction sites based on approaches alternative to X-ray crystallography working in solutions reflecting pharmaceutically relevant formulations and for the whole mAb. DLS, SI-BLI, SAXS and AUC were used to assess the overall propensity for reversible self-interaction on protein level. We further investigated the interaction process after fragmentation of the IgG into Fab and Fc domain by SI-BLI and AUC. Finally, we performed HDX-MS as a high resolution method to identify residues that are involved in the self-interaction process of Infliximab. In our study, we identified that residues in both the Fc and the Fab region trigger the self-interaction of Infliximab. This finding, mostly driven by HDX-MS and AUC results, indicate that interaction hot-spots of mAbs found in solution can differ markedly from the hot-spots identified by crystallography.

4.3 Experimental section

4.3.1 Materials

Phosphate buffered saline (Thermo Fisher Scientific), sodium phosphate monobasic (Merck KGaA), trehalose dihydrate (Merck KGaA) were all of analytical grade. Deuterium oxide (99.96%) was purchased from Eurisotop GmbH.

Infliximab (Flixabi®) was purchased, reconstituted according to the manufacturer's protocol and buffer exchanged into 10 mM sodium phosphate pH 7.2 including polysorbate 20 removal by protein A chromatography using an Äkta Avant (Cytiva). mAb stock solutions were concentrated using Amicon Ultra-15 centrifugal devices (Merck KGaA) to 10 mg/ml.

4.3.2 Digestion

Infliximab (Flixabi®) was reconstituted according to the manufacturer's protocol and buffer exchanged into 150 mM sodium phosphate pH 7.0 using PD10 columns (Cytiva). Digestion was performed using FabALACTICA Fab Kit (Genovis) according to the manual overnight. Purification of Fc fragments was performed using a HiTrap MabSelect SuRe 5 mL pre-packed column (Cytiva) on an Äkta Avant system loading the eluate from the FabALACTICA Fab Kit. Purification of Fab fragments was performed using CaptureSelect IgG-CH1 5 mL pre-packed column (Thermo Fischer Scientific) on an Äkta Avant system loading the flow through of the Fc fragment purification. Fc fragments and Fab fragments were formulated in PBS after purification. Sterile filtration was performed and the fragments were subjected to SEC analysis.

4.3.3 Lyophilization

Lyophilization stoppers (B2 TR coating, West) and DIN 2R Vials (Fiolax®, Schott) were cleaned with ddH_2O and dried at 60 °C for 8 h. The vials were filled with 300 µl and semi-stoppered subsequently. A thermocouple was used for temperature recording throughout the freeze drying process. Both placebo and protein formulations were freeze-dried using a FTS LyostarTM 3 freeze dryer (SP Scientific) by 1) freezing to -50 °C, ramp: 0.5 K/min;

2) primary drying at 0.1 mbar and -25 °C shelf temperature for 20 h followed by a 0.15 K/min ramp to 10 °C; 3) secondary drying at 0.1 mbar and 10 °C for 10 h. The vials were stoppered at 800 mbar after secondary drying and crimped with flip-off seals.

4.3.4 Size-Exclusion-Chromatography combined with Multi Angle Laser Light Scattering

SEC analysis was performed using a Vanquish UHPLC system (Thermo Fisher Scientific,). A Waters BEH200 column (1.7 µm, 4.6 x 150 mm) was used with a flowrate of the mobile phase (50 mM sodium phosphate, 400 mM sodium perchlorate, pH 6.0) of 0.4 ml/min. Routine UV-detection was at 210 nm. All samples were diluted to 5 mg/ml in formulation buffer prior to injection of 0.75 µg. For MALS measurements, samples were directed to a µDAWN MALS detector and a µREX RI detector (both Wyatt Technologies).

4.3.5 Circular Dichroism spectroscopy (CD)

Near-UV spectra of Infliximab were recorded on a Chirascan instrument (Applied Photophysics). Samples were diluted in 6 mM sodium phosphate pH 6.2, 90 mM trehalose to 2 mg/ml and pipetted to quartz cuvettes with a path length of 1 mm. The CD spectra were acquired from 260 nm to 350 nm at 1 nm step size, 0.5 s^{-1} sampling time and 20 °C. Collected spectra (n=6) were blank corrected. The absorbance at 280 nm was used for concentration and MRME calculation.

4.3.6 Dynamic Light Scattering

DLS experiments were performed using a DynaPro plate reader III (Wyatt Technologies). Samples were filtrated through 0.22 µm filters to remove larger particulate impurities and measured at 25 °C as triplicates in 384 well plates with 12 acquisitions for 5 s. Six protein concentrations between 0.5 and 20 mg/ml were measured. Data were processed by the software DYNAMICS V7.8 (Wyatt Technologies). Cumulant fit analysis was applied for determination of the apparent diffusion coefficient and polydispersity, followed by calculation of hydrodynamic radii based on Stokes-Einstein relation.

4.3.7 Self-Interaction Bio-Layer-Interferometry (SI-BLI)

SI-BLI was performed on an Octet HTX device (Sartorius AG, FortéBio) as previously described.[13] Full-length IgG or Fc domain were captured (Anti-hIgG Fc capture (AHC) biosensors) and the association of IgG, Fc and Fab domain analyzed. To capture equal amounts, we captured 1 nm of the full-length IgG or 0.3 nm of the Fc domain which is approximately a third in size.

4.3.8 Hydrogen-Deuterium-Exchange Mass Spectrometry

HDX-MS Experiments using Waters HDX with LEAP system (Waters) were conducted in two independent laboratories 1 and 2. In both laboratories, lyophilized Infliximab was reconstituted to a protein concentration of 60 mg/ml. For the high concentration condition, the reconstituted product was diluted to 20 mg/ml in D_2O containing formulation buffer. For the low concentration condition, the reconstituted product was first diluted to 1.5 mg/ml in formulation buffer and subsequently diluted to the assay concentration of 0.5 mg/ml in D_2O containing formulation buffer. After incubation at 20 °C, the labeling reaction was quenched by 1:1 dilution in quenching buffer followed by online digestion at 15 °C using a Enzymate Pepsin column (300 Å, 5 µm, 2.1x30 mm, Waters) at a flowrate of 80 µl/min (0.1 % Formic acid). Peptides were trapped for 3 minutes at 0 °C using an Acquity UPLC BEH C18 VanGuard column (1.7 µm, 2.1x5 mm, Waters, MA). After trapping, C18 separation was performed on an Acquity UPLC BEH C18 column (1.7 µm, 1.0x100 mm, Waters) at 0 °C and a flowrate of 40 µl/min. A 9 min linear gradient from 8 % to 40 % Acetonitrile was applied and eluting peptides were directed to MS detection. Protein Lynx Global Server (PLGS) version 2.5.3 and DynamX version 3.0 (both Waters) were used to identify peptides and analyze H/D exchange. Statistical analysis was performed using Hybrid Significance Testing.[17] In Lab1, samples were incubated in D_2O containing buffer for 1, 3 and 10 min at 20 °C before quenching 1:1 with 0.1 M potassium phosphate, 4 M guanidine hydrochloride, 0.2 M TCEP at pH 2.6 at 2 °C. The eluate was directed into a Waters Synapt G2Si mass spectrometer for MS/MS-IMS detection.

In Lab2 protein solutions were incubated for 1, 3, 10, 60 and 240 min and quenched with 0.1 M potassium phosphate, 2 M guanidine hydrochloride, 75 mM TCEP pH 2.6 at 4 °C. MS/MS detection was performed on a Waters Synapt G2S mass spectrometer.

4.3.9 Analytical Ultracentrifugation

Experiments were conducted at 20 °C using an Optima XL-I or Optima AUC (Beckman Coulter) equipped with a UV-VIS detection system. Sedimentation velocity experiments were performed with 0.5, 5.0, and 20 mg/mL protein solutions at 42,000 rpm. For 0.5 and 5.0 mg/mL, 390 µL sample was loaded into the sample sector of 12 mm double-sector charcoal-filled epon centerpiece, and 400 µL buffer (6 mM sodium phosphate pH 6.2, 90 mM trehalose) was loaded into the reference sector of centerpiece. For 20 mg/mL sample, 97.5 µL sample was loaded into sample sector of 3 mm double-sector charcoal-filled epon centerpiece, and 100 µL buffer was loaded into the reference sector of centerpiece. The collected data were analyzed using continuous c(s) distribution model of Program SEDFIT ver. 16.2b fitting for the frictional ratio, meniscus, and time-invariant noise and using regularization level of 0.68 for 0.5 and 5.0 mg/mL samples. For the 20 mg/mL sample, the non-ideal distribution model implemented in SEDFIT was used as described previously.[18]

Sedimentation equilibrium experiments were performed at 20 °C with 0.1, 0.5, 1.0, 2.5, 5.0, 10, and 20 mg/mL protein solutions at 5,000, 9,000 and 13,000 rpm. For 0.1, 0.5, 1.0, 2.5, and 5.0 mg/mL, 100 µL sample was loaded into sample sector of the 12 mm 6-channel charcoal-filled epon centerpiece, and 110 µL buffer was loaded into the reference sector of the centerpiece. For 10 and 20 mg/mL sample, 25 µL sample was loaded into sample sector of the 3 mm double-sector charcoal-filled epon centerpiece, and 27.5 µL buffer was loaded into the reference sector of the centerpiece. Data were collected at sedimentation equilibrium at each rotor speed. The average data from eight scans were analyzed using Program SEDPHAT ver. 15.2c. [19, 20]

4.3.10 Small Angle X-ray Scattering

SAXS data collection was performed at the EMBL beamline P12 at the Petra III storage ring (DESY, Hamburg). Data were collected at 0.5, 0.9, 2.5, 5.8, 7.1, 10.3, and 18.7 mg/mL in 6 mM sodium phosphate pH 6.2, 90 mM trehalose. A buffer was measured before and after each sample. The experimental details are shown in Table S2 in supplementary material. Pair-distance distribution function ($p(r)$) and all molecular parameters, including

radius of gyration (R_g), maximum dimension (D_{max}), molecular weight (*MW*), were derived from the experimental data with the graphical data analysis program *PRIMUSQT*.[21, 22]

4.3.11 Viscosimetry

Viscosity measurements were performed on a ViscoSizerTD system (Malvern) at 20 °C. The capillary was flushed with water before applying the sample at a constant pressure of 1500 mbar. Caffeine in water (1 mg/ml) was used as reference.

4.4 Results

4.4.1 Formulation development for self-interaction analysis of Infliximab

At first, we performed a screening of Infliximab for self-interaction to identify formulations which are i) suitable for pharmaceutical application, ii) suitable for freeze-drying in order to expand the pharmaceutical application, use the process for simple water removal to initiate HDX-MS and iii) provide highly attractive interaction for detailed analysis and method evaluation. We observed an increased binding signal at low pH and low buffer concentration (Figure 1). In addition, trehalose up to a concentration of 90 mM did not influence the interaction, whereas the BLI signal was reduced at 120 mM trehalose. As the protein concentration should be higher in the reconstituted product to enable the dilution to the HDX assay concentration with D_2O containing buffers, we performed lyophilization with a diluted formulation containing 20 mg/ml Infliximab in 2 mM sodium phosphate pH 6.2, 30 mM trehalose. The lyophilized product was intended to be reconstituted in a third of the initial volume to a solution ending up in 60 mg/ml Infliximab in 6 mM sodium phosphate pH 6.2, 90 mM trehalose. The integrity of the mAb after lyophilization and reconstitution was confirmed by HPLC-SEC which indicates only 0.3% monomer loss and by CD spectroscopy which indicated structural integrity (Figure S1).

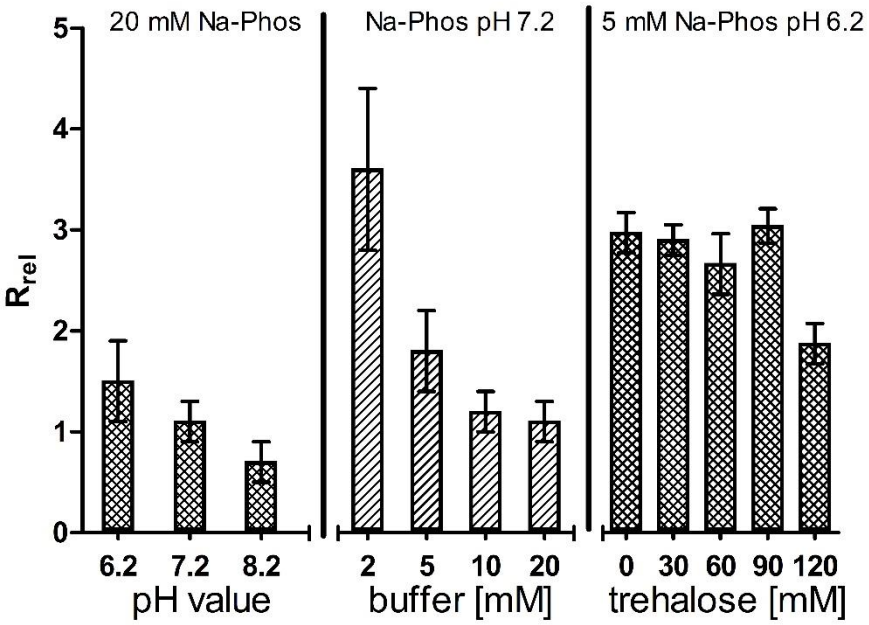

Figure 1 *SI-BLI results of Infliximab to identify formulation conditions suitable for assessing SI behavior and lyophilization in 20 mM sodium phosphate at different pH values, in sodium phosphate buffer pH 7.2 of different concentration, and in 5 mM sodium phosphate pH 6.2 at different trehalose concentrations.*

4.4.2 Characterization of self-interaction of Infliximab by DLS

The apparent diffusion coefficient (D^{app}) of Infliximab in the target formulation of 6 mM sodium phosphate pH 6.2, 90 mM trehalose was analyzed by DLS as a function of protein concentration in order to characterize the self-interaction processes (Figure 2). We observed a non-linear dependence with a strong decrease of the diffusion coefficient at protein concentrations below 2.5 mg/ml.

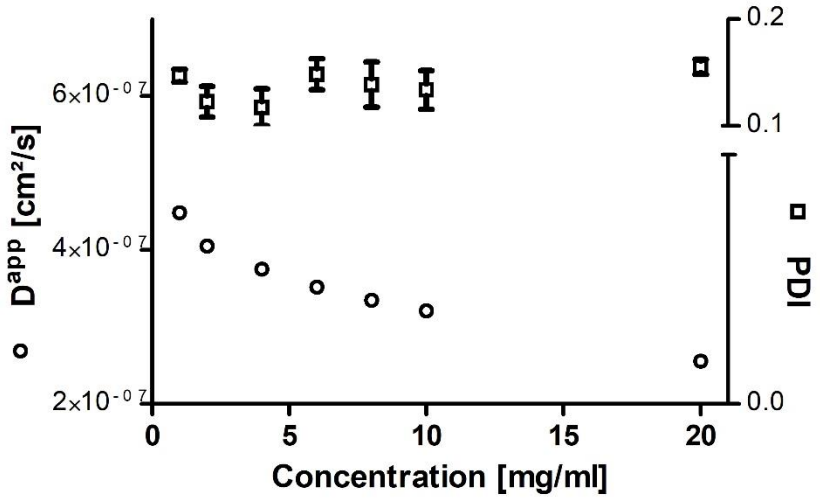

Figure 2 *DLS results (apparent diffusion coefficient D^{app} and polydispersity index PDI) of Infliximab from 1 to 20 mg/ml in 6 mM sodium phosphate pH 6.2, 90 mM trehalose.*

4.4.3 Analysis of self-interaction and oligomerization of Infliximab by SAXS

Subsequently we performed SAXS measurements of Infliximab in the target formulation at different concentrations. The intensity at low *q*-values increased with increasing concentration, pointing towards oligomerization (Figure 3A and B). Additionally, the shape of the *p*(*r*) function changed with concentration and an additional third peak at around 20-25 nm was observed at higher concentrations flagging the formation of larger oligomeric species (Figure 3C). Furthermore the R_g, D_{max}, and MW increased with increasing Infliximab concentration (Figures 3D, E, and F). At 18.3 mg/ml D_{max} reached 60 nm which did not correspond to a monomer with approximately 15 nm[23] or a dimer with 20 to 30 nm[24] D_{max} and indicated the formation of large oligomeric species.

As the first two peaks at approximately 5 and 9 nm of the p(r) profile, which are characteristic for an IgG[23, 24], were preserved at higher Infliximab concentration, we hypothesize that the increasing in R_g, D_{max}, and MW is related to the presence of distinct oligomers and not to unspecific aggregation.

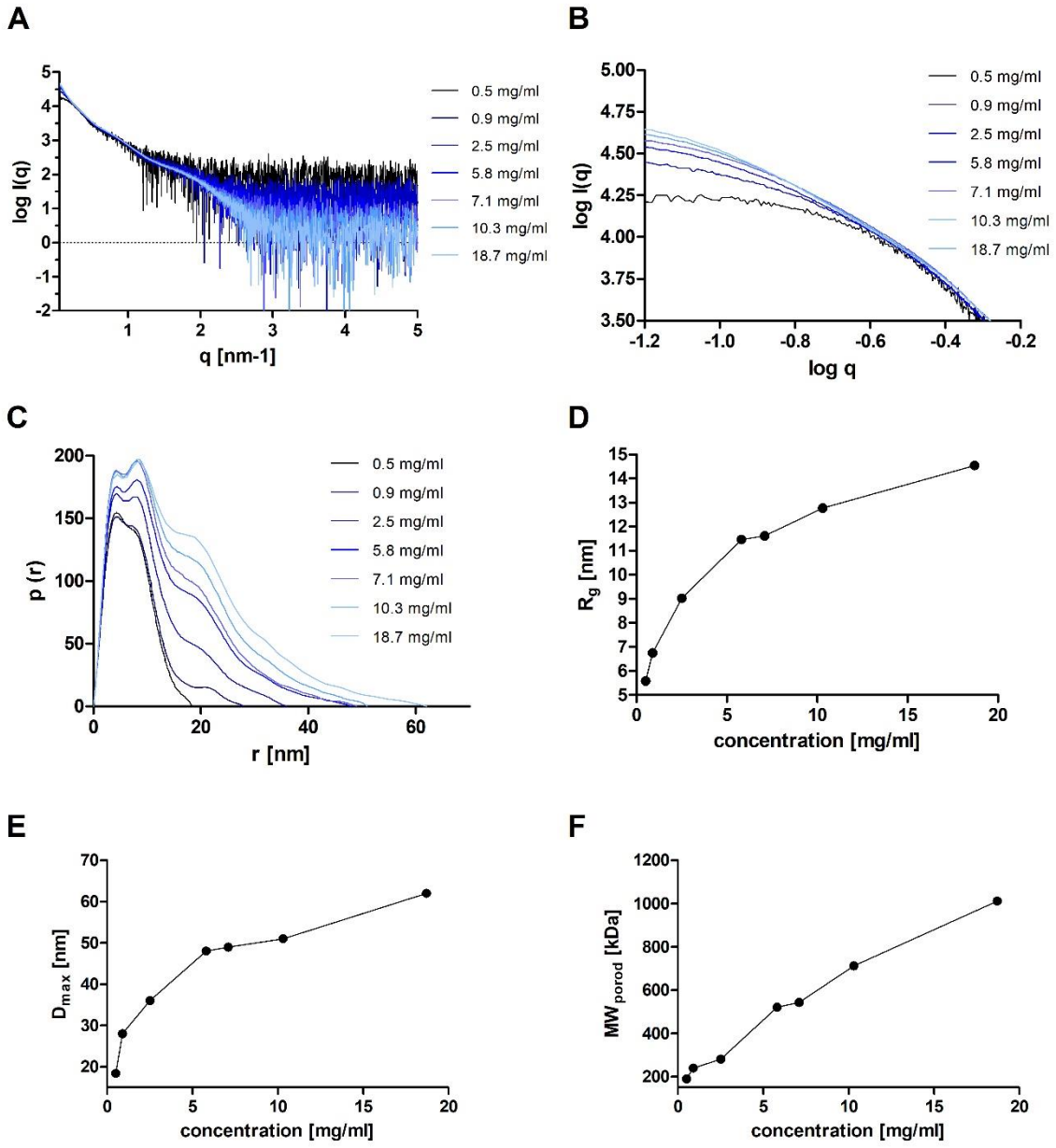

Figure 3 *SAXS data of Infliximab at different concentrations in 6 mM sodium phosphate pH 6.2, 90 mM trehalose. A) SAXS curves, B) zoomed view at low q values C) p(r) functions, D) Rg, E) Dmax, F) MW calculated from porod volume.*

4.4.4 Analysis of self-interaction and dimerization of Infliximab by AUC

In a subsequent step, SV-AUC was performed to determine the size distribution of Infliximab species in solution (Figure 4). At low concentration of 0.5 mg/ml, Infliximab was monodisperse with a sedimentation coefficient ($s_{20,w}$) of 6.6 S which is a typical value of an antibody monomer.[25] At higher concentration of 5 mg/ml we observed two peaks with

6.6 S and 8.3 S which confirmed the observations reported by Lerch et al.[16] The authors described a peak resolution between 6.6 S and 8.2 S at 0.6 mg/ml. However, 8.2 S and, in our case, 8.3 S do not represent a stable and fully dimerized antibody species, which would be expected to sediment at a higher sedimentation coefficient.[25] These results indicate fast kinetics of the weak self-association process of Infliximab. The distribution of the solution at 20 mg/ml obtained by C(s) incorporating non-ideality was monodisperse with 8.3 S, which corresponds to Infliximab dimer. SE-AUC was performed to generate an equilibrium concentration gradient from which the apparent molecular weight reflecting the intermolecular interactions of Infliximab in solution can be deduced. The apparent molecular weight of Infliximab increased with concentration > 1 mg/ml which corresponds to the data acquired by DLS, SAXS and SV-AUC (Table 1). The apparent molecular weight increased to 272 kDa indicating the presence of dimeric species. With increasing the Infliximab concentration from 10 to 20 mg/ml the apparent molecular weight decreased from 272.0 kDa to 224.8 kDa which is consistent with the decrease in S observed in SV-AUC. Additionally, at higher rotor speed of 9,000 and 13,000 rpm, the apparent molecular weight could not be determined at concentrations of 2.5 mg/ml and higher due to a strong increase in turbidity from the entire solution in the cell. This is reflected in decrease in light intensity at 350 nm at the cell bottom (supplemental material figure S2 and S3) suggesting formation of a highly concentrated Infliximab layer at the cell bottom. This layer may arise from a concentration dependent formation of higher order structures which we also observed by DLS and SAXS at protein concentrations of 20 mg/ml. Thus, AUC of full-length Infliximab indicates dimerization of Infliximab in solution, which can be further oligomerize to fast dissociating higher order structures. The inverse of the apparent molecular weight was plotted against the protein concentration (Figure S4). This plot indicated differences in B_{22} below and above 2.5 mg/ml. Below this concentration threshold, a negative B_{22} was observed which indicated attractive interactions between Infliximab molecules. B_{22} was increased at concentrations above 2.5 mg/ml.

Table 1 *Concentration dependent apparent molecular weight of Infliximab in 6 mM sodium phosphate pH 6.2, 90 mM trehalose obtained by SE-AUC at different rotor speeds.*

Rotor Speed [rpm]	**Infliximab Concentration [mg/ml]**						
	0.1	0.5	1	2.5	5	10	20
5,000	166.6	150.0	160.3	237.1	238.6	272.0	224.8
9,000	146.4	154.4	164.2	n.d.	n.d.	n.d.	n.d.
13,000	143.7	154.0	n.d.	n.d.	n.d.	n.d.	n.d.

Unit: kDa; n.d.: Not determined due to the turbidity at cell bottom

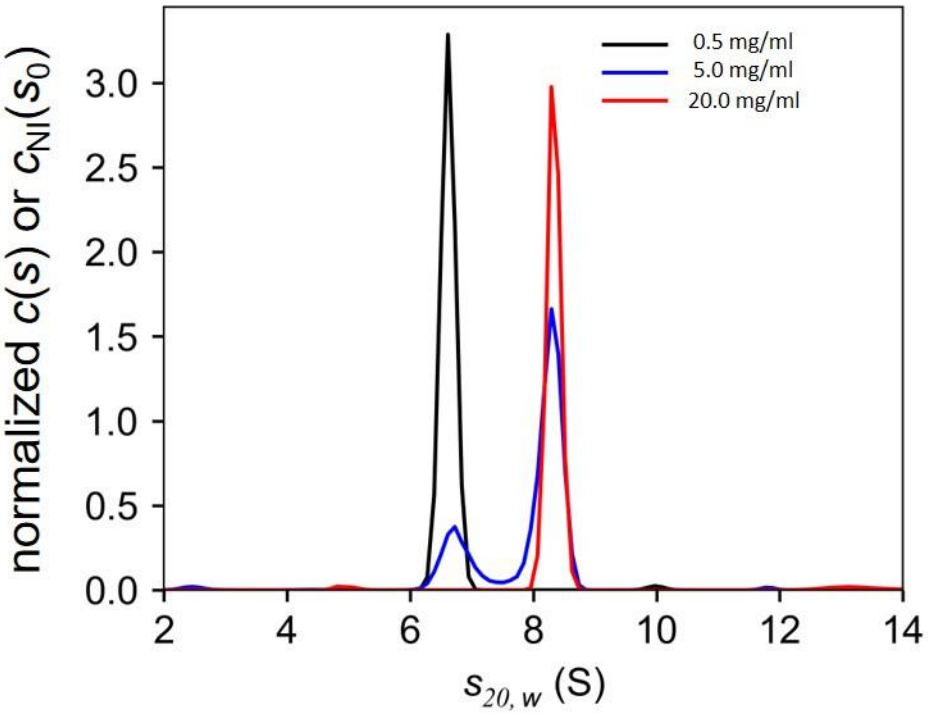

Figure 4 *Distribution of the sedimentation coefficient of Infliximab in 6 mM sodium phosphate pH 6.2, 90 mM trehalose obtained by SV-AUC. Non-ideal c(s) model was used for the analysis of the sedimentation profile obtained at 20 mg/ml Infliximab.*

4.4.5 Viscosity as an indicator for attractive self-interaction of Infliximab

A high self-interaction propensity of mAb molecules frequently correlates with increased viscosity at high protein concentrations.[26–29] We observed an exponential increase in viscosity with increasing Infliximab concentration in 6 mM sodium phosphate pH 6.2, 90 mM trehalose from 1.1 mPa*s at 1.0 mg/ml, which corresponds to the viscosity of the formulation buffer, to 10 mPa*s at 90 mg/ml (supplemental material figure S5). This increase in viscosity indicated the presence of higher order structures due to network formation. These results correspond to our observations from DLS, SAXS and SE-AUC, which also indicated large oligomeric species at elevated protein concentrations.

4.4.6 Analysis of intermolecular interactions of Infliximab fragments by SI-BLI

We wanted to understand, which of the three potential interactions, Fab-Fab, Fc-Fc or Fab-Fc, is or are relevant. We therefore digested the IgG and performed experiments on the two fragments. After purification, SEC-MALS indicated 83.6 % purity of the 53 kDa Fc fragment which contains approx. 8% of a 110 and a 151 kDa species each as impurities and more than 98 % purity of the 51 kDa Fab-fragment.

First, we captured the Fc fragment by using the anti-hFc capture biosensor. Thus, the Fc part was presented on the sensor surface. We did not observe further binding of Fc fragments during the association reaction (Figure 5). In contrast, binding of Fab fragment and the whole IgG was detected. Using the same biosensors, we captured the whole IgG and thus, presented the Fab region. We observed binding of Fc fragment and whole IgG. If we applied the Fab fragment as analyte, no association was seen. In summary, binding processes were identified in BLI assay set ups, where the Fc part was presented on the sensor surface and the Fab fragment was in solution or the Fab fragment was presented on the surface and the Fc part was in solution. In addition, we characterized the self-interaction in the SEC mobile phase used by Lerch et al. for SEC and AUC experiments.[16] Self-interaction was suppressed at pH 7.2 and the high ionic strength conditions and we only detected net attraction between captured IgG and Fc fragment or IgG in solution.

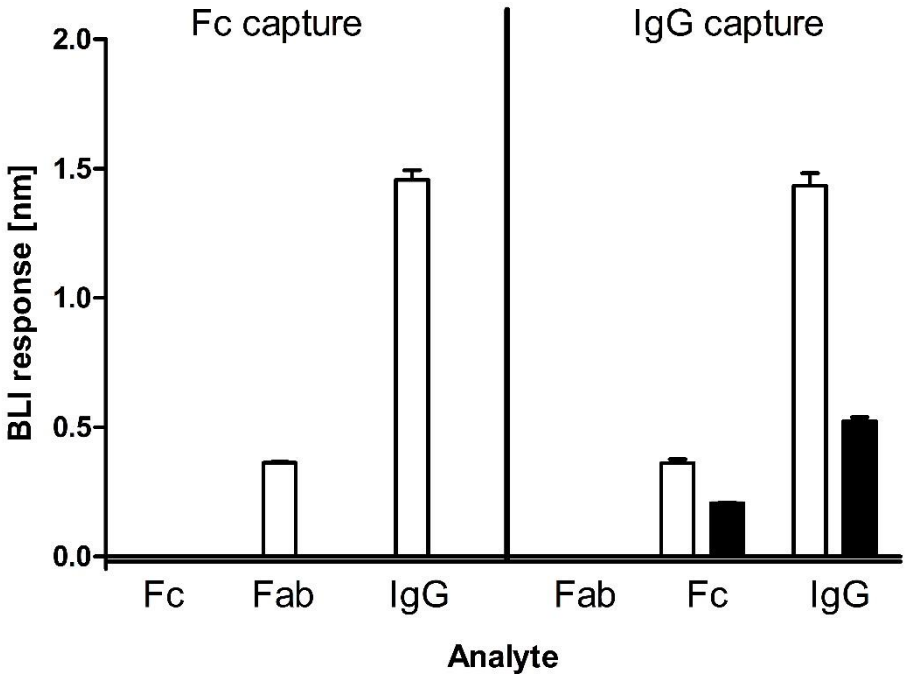

Figure 5 *SI-BLI results for Infliximab fragments with either Fc or whole IgG as capture molecule in 6 mM sodium phosphate pH 6.2, 90 mM trehalose (□) and in 20 mM sodium phosphate, 400 mM sodium chloride (■). The association signals of Fab and Fc only reached a third of the binding signal of an IgG which reflects the difference in molecular size.*

We further performed experiments which involved a capture setup of the Fab fragment. We identified unspecific interactions of Fab, Fc and IgG with the anti-hFab biosensors in these experiments. Thus we could not distinguish clearly between non-specific binding to the underlying sensor, and Fab-Fab interactions in the absence of Fc or whole IgG.

4.4.7 Analysis of intermolecular interactions of Infliximab fragments by AUC

Additional AUC analyses were performed using the Infliximab Fab and Fc fragments to understand the interactions of Infliximab in solution. The maximum concentrations of 34.3 μM Fc (1.7 mg/mL) and 68.7 μM Fab (3.3 mg/mL) tested correspond to 34.3 μM Infliximab (5.0 mg/ml). At lower concentration of 0.33 mg/ml the Fab fragment was monodisperse with a sedimentation coefficient of 3.7 S (Figure 6A). At higher concentration of 3.3 mg/ml two peaks with 3.8 S and 4.7 S corresponding to monomer and

dimer were observed. Also Lerch et al. observed the shift in monomer dimer equilibrium of the Fab fragment at higher concentrations.[16] We did not see an indication for attractive self-interaction of the Fc fragment (Figure 6B), which showed concentration independently 3.9 S. In mixtures of Fab and Fc fragment, a slight shift of the 3.8 S peak to 4.0 S was observed. Additionally, the peak at 4.7 S was shifted to 4.9 S which points towards weak hetero association of Fab and Fc fragment (Figure 6C). We hypothesize that the dissociation of Fab and Fc fragments is fast, and therefore the Fab-Fc complex could not be observed as a distinct and well separated peak by SV-AUC.[19] Additionally we conducted SE-AUC and did not observed the enrichment at the bottom of the cell, unlike for the full-length Infliximab (Figure S2 A-F) Based on these AUC results, we can hypothesize that the self-interaction of infliximab occurs through association of Fab domains, and further oligomerization requires complete IgG molecules containing both, Fab and Fc domains.

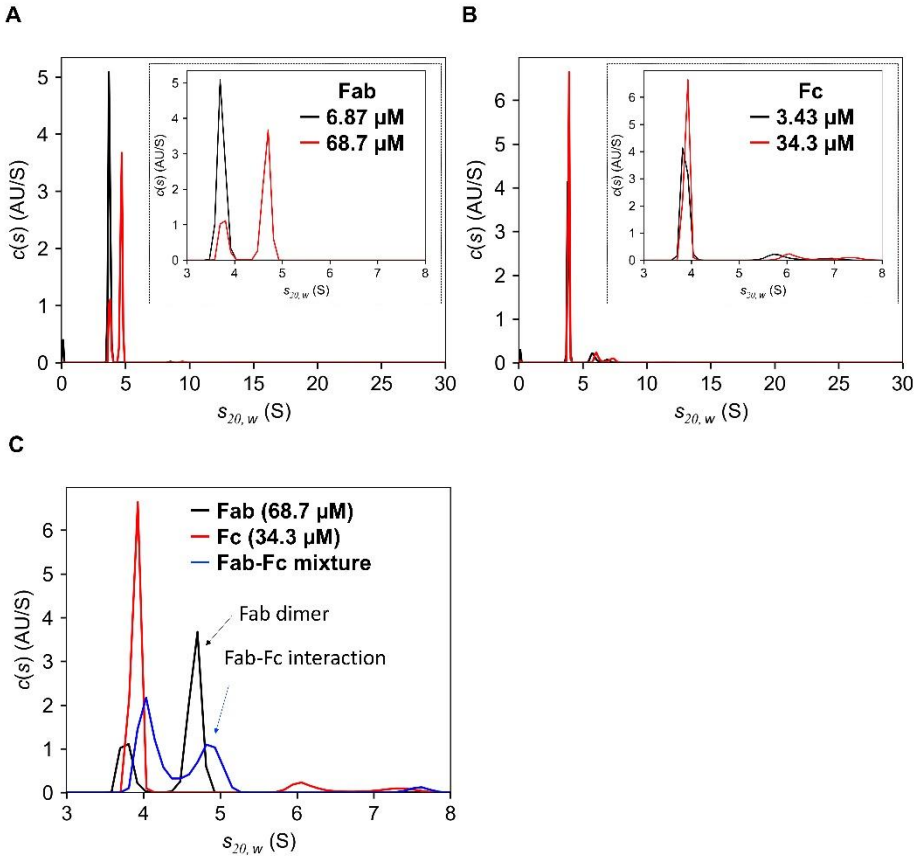

Figure 6 *SV-AUC experiments of Infliximab-Fab and Infliximab-Fc fragment and mixtures thereof. A) Fab fragment at 6.87 µM and 68.7 µM (0.33 mg/ml and 3.3 mg/ml), B) Fc fragment at 3.43 µM and 34.3 µM (0.17 mg/ml and 1.7 mg/ml). C) Fab, Fc and mixture of both at 68.7 and 34.3 µM respectively which corresponds to 5.0 mg/ml whole IgG molecule.*

4.4.8 Identification of peptides involved in self-interaction of Infliximab by HDX-MS

To identify amino acids or peptide sequences involved in the pronounced attractive self-interaction of Infliximab in solution we compared the deuterium uptake incubation in D_2O containing formulation buffer at low (0.5 mg/ml) and high protein concentration (20 mg/ml). As Infliximab tends to form larger structures at 20 mg/ml, we expected that peptides involved in the interaction should show a decreased deuterium uptake at high concentration. To challenge our data for reproducibility, we performed HDX-MS experiments at two different laboratories utilizing two different HDX-MS device settings regarding the MS setup, labeling and quenching conditions as described above. Comparing laboratory 1 and 2, we identified 615 and 1092 data points of peptides / corresponding labeling times respectively, reflecting approx. 90% sequence coverage in both setups. Statistical analysis of the data sets demonstrated comparable findings (Figure 7). We observed a significant decrease in deuterium uptake at 20 mg/ml Infliximab compared to 0.5 mg/ml in the V_H domain region (E_{50}IRSKSINSATHYAESVKGRF$_{70}$) and two regions of the C_H domain of the Fc fragment (K_{329}ALPAPIEKTISKAKGQPREPQV$_{351}$ and V_{430}MHEALHNHYTQKSLSLSPG$_{449}$). In addition, we identified a region in the C_L domain, (K_{149}VDNALQSGNSQESVTEQDSKDSTYSLSSTL$_{179}$). A list of peptides with significant differences in H/D uptake can be found as supplemental material (Table S1).

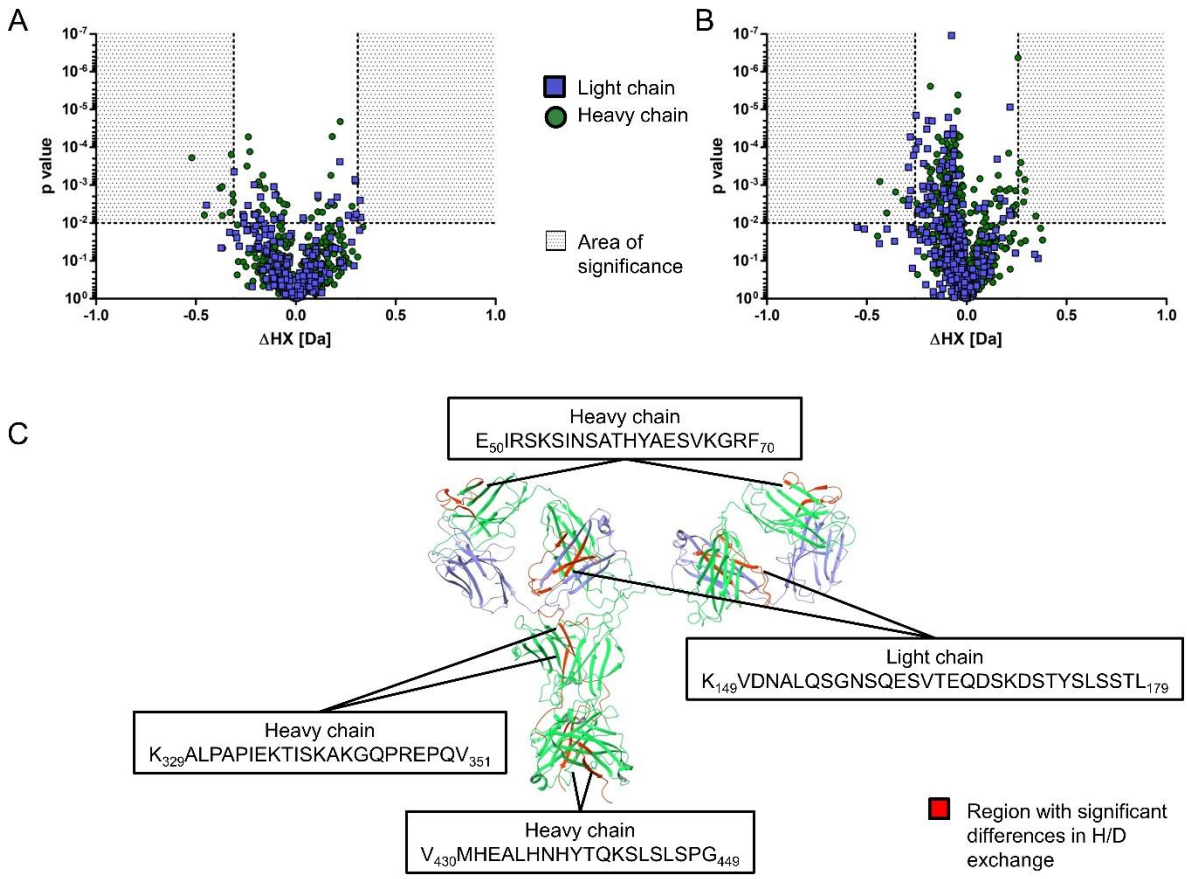

Figure 7 *Overview of HDX-MS results. Infliximab was incubated in 6 mM sodium phosphate pH 6.2, 90 mM trehalose at 0.5 mg/ml and 20 mg/ml for various time frames. A) Volcano plot of results from laboratory 1; B) Volcano plot of results from laboratory 2; C) Annotation of regions with significant differences in H/D exchange on a homology model of Infliximab (pdb: 1HZH)*

4.5 Discussion

4.5.1 Analysis of Infliximab self-interaction on protein resolution level

We chose Infliximab as a model system because the self-interaction process of this protein was described for in-solution conditions and in a solid crystalline state.[16] But the formulations used in literature were not of pharmaceutical relevance as they were either SEC mobile phases or crystallization inducing buffers. Thus we searched for a pharmaceutical formulation which enabled the analysis of the self-interaction behavior and which was capable of lyophilization. SI-BLI revealed insights into the pH dependence of

the self-interaction process of Infliximab and indicated the effect of buffer and trehalose concentration. Based on that, we developed a formulation that displayed the wanted features.

Light scattering techniques such as DLS and SAXS[8, 30, 31] are established methods for analyzing protein-protein interactions and were used in this study to determine self-interaction behavior of Infliximab on a protein level. DLS provides the apparent diffusion coefficient of a scattering agent whereas SAXS can provide the radius of gyration. By analyzing both physical parameters in a concentration dependent manner, attractive protein-protein interactions are indicated by an increase in size with concentration.

Our results indicated attractive interactions between mAb molecules in solution. Usually, reversible self-interaction processes analyzed by DLS include the calculation of the diffusion interaction parameter k_D. This parameter contains both, a thermodynamic as well as a hydrodynamic term.[32] At low protein concentration and in our case at low ionic strength the hydrodynamic effects may cause the non-linearity. Additionally, the SV-AUC (Figure 4) and SAXS results (Figure 3) indicated that Infliximab tends to specifically dimerize at protein concentration above 2.5 mg/ml, which results in a heterogeneous solution at higher protein concentration. Due to this association as a function of concentration, it was not possible to differentiate between unspecific self-interaction, which is represented by k_D and dimerization of Infliximab by the light scattering signal.[33, 8] To this end, we refrained from including quantitative values.. With SAXS, we observed an increase of the radius of gyration and of the molecular weight at a protein concentration of 20 mg/ml indicating oligomerization of Infliximab at higher concentration. Furthermore, the characteristic features from antibodies were still present in the p(r) function suggesting conserved structure and no unspecific aggregation. The increase in R_g and D_{max} pointed into the direction of very large, oligomeric species. The presence of such oligomers may explain the increase in turbidity observed in SE-AUC experiments.

In addition to DLS and SAXS, we performed AUC as a powerful method to assess the intermolecular interaction of macromolecules.[34–36] A weak reversible self-association of Infliximab IgG was confirmed by SV-AUC and SE-AUC at a protein concentration above 2 mg/ml, where the results indicated an apparent molecular weight corresponding to a dimeric species. This dimeric species is predominant at concentrations between 2 and

20 mg/ml. It should be noted that at 20 mg/mL a single species was observed at 6.8S by C(s) for non-interacting systems while this species takes 8.3S by non-ideal C(s) analysis, corresponding to dimer of Infliximab IgG. At higher rotor speeds, we observed a decrease in light transmission towards the cell bottom in SE-AUC which can be explained by further intermolecular interactions.

In fact, the apparent molecular weight in SE-AUC becomes higher than that of a monomer when the initial concentration is above 1 mg/mL, indicating the formation of oligomers. At higher concentrations like 5 mg/ml, the apparent molecular weight reached at a value close to dimer, while light scattering (turbidity) which is a sign of the formation of large oligomers was detected at the bottom of the cell. The volume of the region where light scattering is confirmed increases as the initial concentration and/or the speed of rotation increases. Thus SV-AUC demonstrated Infliximab dimerization while didn't form further large oligomers. B_{22} reflects these observation as was negative below 2.5-5 mg/ml and slightly positive over 5 mg/ml.

Also Nishi et al. reported the property of liquid-liquid phase separation (LLPS) for a mAb .[37]

MAbs with LLPS tendency exist as monomer and small oligomers at low concentration at which LLPS does not occur. Above a certain concentration LLPS can be noted, as in addition to monomer and small oligomers, higher oligomers emerge. These higher oligomers form a phase that has slightly higher density than a phase composed from monomer and small oligomers. Under gravity force, formation of LLPS takes long time. It can be accelerated by centrifugation because higher oligomers sediment faster to the bottom, leading to the formation of a heavy lower phase, and higher oligomers are depleted in the upper phase solution corresponding (Figure 8). These higher order structures were also observed by SAXS reflected by the increase in D_{max} and R_g. Additionally, these oligomeric interactions trigger the formation of networks, which cause the increase in viscosity. Our data show, that the dimerization of Infliximab is not the final state of the self-interaction process. Whereas SV-AUC showed that the dimer is stable at 20 mg/ml, a further increase in concentration confirmed the additional oligomerization and also lead to the increase in the viscosity (Figure S5).

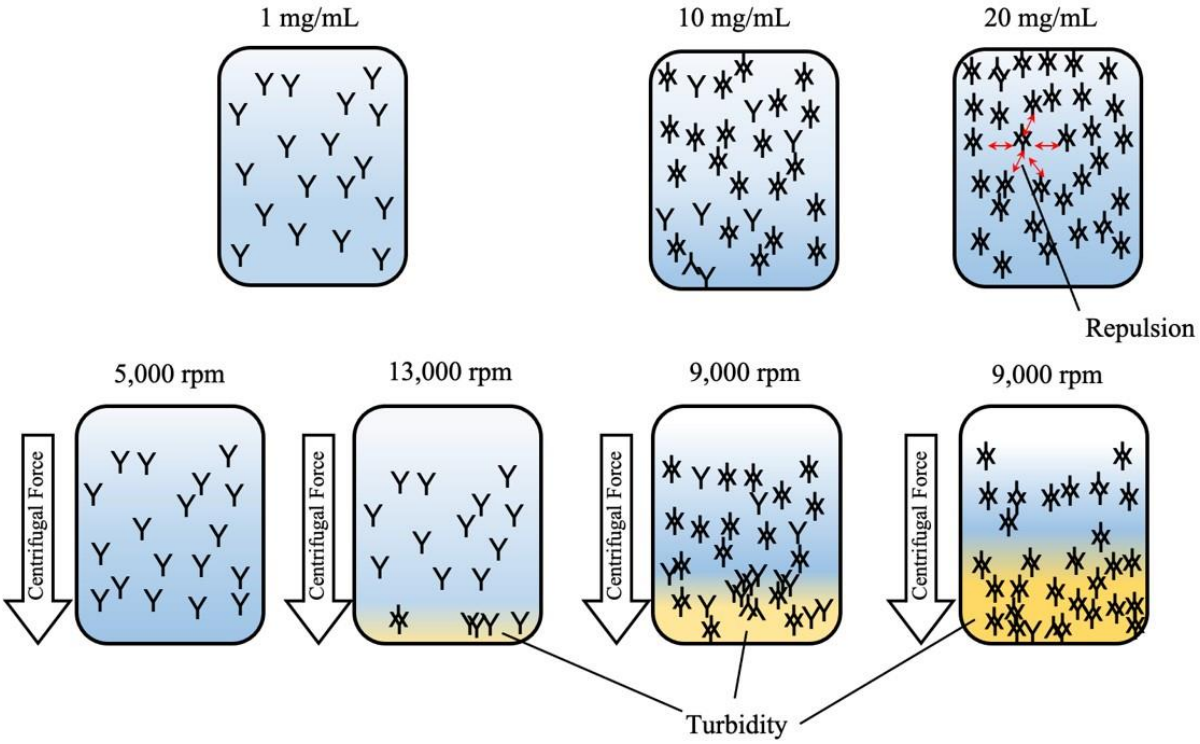

Figure 8 *Schematic overview of phase separation behavior of Infliximab IgG under centrifugal force for the solution below 20 mg/ml.*

4.5.2 Analysis of Infliximab self-interaction on fragment resolution level

For a more detailed understanding of the self-interactions processes, the characterization of the Infliximab Fab and Fc fragments was performed after digestion of the native protein. Several studies showed results based on analysis of self-interaction mechanisms of fragments.[5, 6, 8] Kanai et al demonstrated that the increase in viscosity of a Fab only containing solution was comparable to the solution of the corresponding full length IgG.[5] Nishi et al. showed that a liquid liquid phase separation of a mAb was mainly driven by attractive electrostatic interactions of Fc fragments.[6] Fab-Fc interactions were identified as self-interaction mechanism by Arora et al., demonstrated by HDX-MS experiments.[7] For Infliximab, Lerch et al proposed a Fab-Fab based self-interaction process based on their crystallization, AUC and SEC data.[16] All these references differed in their solution conditions. To this end, we aimed to understand how the formulation affects Infliximab self-interaction and what are the processes occurring in solutions. We used SI-BLI with

captured IgG or Fc fragment on the sensor, and Fab, Fc or native IgG as analyte in solution. A marked attractive interaction of captured Fc with Fab or IgG in solution, as well as of captured IgG with IgG or Fc in solution was observed. Thus, Fab and Fc fragments are involved in the self-interaction process of Infliximab. For further elucidation, we performed SV-AUC experiments. The Fab fragment dimerized at higher protein concentration, whereas the Fc fragment was in its monomeric form at both concentrations. In a Fab Fc mixture, we observed a small shift of the Fc and Fab as well as the Fab-Dimer peak to higher S-values indicating a weak reversible association of Fab-Fc that may coexist with Fab homodimers. Upon concentration during the centrifugation process, only the IgG preparation showed turbidity indicating that the IgG format itself provided interaction sites responsible for larger network formation.

Thus, Fab fragments tended to form concentration dependent dimers in AUC, but IgG-Fab interaction was not observed by SI-BLI. Fab-Fab interaction could not be studied with SI-BLI for technical reasons. Both methods demonstrated Fab-Fc interaction. Additionally, pronounced oligomerization resulting in the marked accumulation of large protein structures at the cell bottom did occur with Infliximab but not in the Fab-Fc mixture. Thus, AUC demonstrated that attractive interactions may not occur in mixtures of Fab and Fc fragments to the same extent and by the very same mechanism as for the full-length mAb. On the same account, we did not find IgG-Fab interactions in SI-BLI. As identified by X-ray crystallography, the Fab tends to form dimers via head-to-tail orientation.[16] Potentially this head-to-tail interaction process cannot proceed after capturing the IgG on a biosensor, or the “tail”-epitope is not accessible in the complete IgG molecule. Overall, we demonstrated that Fab-Fc interactions substantially contribute to the Infliximab self-interaction in solution, on top of the Fab-Fab interactions previously identified.

4.5.3 Analysis of Infliximab self-interaction on peptide resolution level

Lerch et al. identified distinct regions within the Fab fragment by X-ray crystallography that are involved in the self-interaction process of Infliximab. We aimed to identify the sequences, which trigger the self-interaction in solution in particular after the detection of Fc involvement by AUC and BLI measurements. In addition, we targeted for a method, which overcomes the challenge of having results obtained by methods performed under

artificial conditions and the interactions in the pharmaceutically relevant formulation applied to the patient. To this end, we chose HDX-MS as a high resolution technique which can be operated under native circumstances. HDX-MS is an emerging techniques to understand higher order structures of proteins, targeted mutations or chemical modifications.[7, 38, 39] This technique is also used in epitope mapping, where the binding affinity is usually high.[40, 14] In addition, HDX-MS can be used to examine low affine mAb self-interaction.[7, 41, 15] Correspondingly, we compared the H/D exchange of Infliximab in the monomeric state at 0.5 mg/ml and in the oligomerized state at 20 mg/ml.

By analyzing overlapping peptides for the identified heavy chain region, we identified the four residues $H_{61}YAE_{64}$ as present in all peptides that showed significant differences in deuterium uptake. By SI-BLI we showed that the attractive interaction of Infliximab was more pronounced at pH 6.2 compared to pH 7.2 and pH 8.2. Thus, H_{61} may play an important role in the self-interaction process as this residue gets deprotonated at pH 7.2 then becoming a surface exposed neutral residue. E_{64} is deprotonated at pH 6.2. We therefore hypothesize that the protonated state of H_{61}, together with deprotonated E_{64} can interact with other domains via electrostatic interactions or hydrogen bonding. We further identified a region in the CH2 domain of Infliximab Fc fragment (K_{329}ALPAPIEKTISKAKGQPREPQV$_{351}$) which showed less deuterium uptake at higher protein concentration. This area contains several electron-rich residues like–proline and glutamic acid. These residues might interact with H_{61} and E_{64} at pH 6.2 until H_{61} gets deprotonated at pH 7.2 and hydrogen bonds are destabilized. In addition, the C-terminus of the IgG heavy chain (V_{430}MHEALHNHYTQKSLSLSPG$_{449}$) showed significant concentration dependent differences in H/D exchange, confirming that the Fc region is involved in self-interaction as well. As this area contains several histidine residues, the state of protonation might be the trigger for the self-interaction processes of Infliximab. Within the light chain of Infliximab Fab fragment we identified a region consisting of 30 residues (K_{149}VDNALQSGNSQESVTEQDSKDSTYSLSSTL$_{179}$) that showed differences in deuterium uptake at high protein concentration. This region contains several polar amino acids like serine and threonine that are accessible for hydrogen bonding. Because the identified peptides of this region were not well overlapping, a more detailed differentiation might be too speculative.

The regions identified by HDX-MS differ from the sites identified by X-ray crystallography. Thus, the identified self-interactions sites differ between processes present in solution and in a crystal. This indicates the importance of analysis interaction processes by a multi-method approach where various results contribute to the overall picture of a self-interaction mechanism.

In summary, our results indicate that Infliximab self-interaction in solution is driven by a combination of Fab-Fab and Fab-Fc interactions under conditions which are relevant for pharmaceutical formulations. A possible self-interaction process may start with Fab-Fab interactions leading to dimerization. These dimers can further oligomerize by weak Fab-Fc interactions at higher protein concentration. This higher order oligomerization was only observed in the presence of complete IgG molecules which may indicate conformational, sterical and avidity effects contributing to the self-interaction mechanism. Our results complement published data which showed Fab-Fab interaction of Infliximab only. Lerch et al. performed the analysis at high ionic strength for crystallization of Fab fragments followed by X-ray structure determination. The protein crystals are 1) a solid state and 2) did not contain the whole IgG molecule. Here, we present a study in a pharmaceutically relevant formulation considering the whole IgG molecule. We assume that the use of a multi-method approach containing analyses of intact IgG, fragments and peptides led to a clearer picture of the self-interaction process. We found that mAb self-interaction is not only dependent on the protein structure, but that the formulation buffer itself can influence the self-interaction mechanism. Depending on the environment of the molecule, different sites can be involved in self-interaction which may explain the differences between findings of crystallography and in-solution methods. We assume that the ionic strength and the pH impact the nature of the interaction sites. By increasing the ionic strength of the formulation, charge shielding might reduce the ability to form hydrogen or electrostatic bonds between Infliximab molecules. For crystallization, the ionic strength is higher and the protein concentration might further increase during the process of crystal growth. This might increase the probability for hydrophobic interactions because the distance between the molecules becomes smaller. In solution, where the protein concentration is lower, electrostatic interactions are more pronounced than hydrophobic forces.[2] The interplay between the solution parameters and specific residues of the protein also may explain why even for proteins which are prone to self-interact, formulation development or rational

engineering can both be successful strategies for developing stable high concentration liquid formulations.

4.6 Acknowledgements

This study was part of the project “Self-Interaction and targeted Engineering of monoclonal antibodies (Self-I-E)” and funded by the Bayerische Forschungsstiftung. The authors would like to thank Lorenzo Gentiluomo for the helpful discussions of the DLS data.

References

1. Ecker DM, Jones SD, Levine HL. The therapeutic monoclonal antibody market. 2015. MAbs 7: 9–14.

2. Laue TM, Shire SJ. The Molecular Interaction Process. 2020. J Pharm Sci 109: 154–160.

3. Shire SJ, Shahrokh Z, Liu J. Challenges in the development of high protein concentration formulations. 2004. J Pharm Sci 93: 1390–1402.

4. Yadav S, Liu J, Shire SJ, Kalonia DS. Specific interactions in high concentration antibody solutions resulting in high viscosity. 2010. J Pharm Sci 99: 1152–1168.

5. Kanai S, Liu J, Patapoff TW, Shire SJ. Reversible self-association of a concentrated monoclonal antibody solution mediated by Fab-Fab interaction that impacts solution viscosity. 2008. J Pharm Sci 97: 4219–4227.

6. Nishi H, Miyajima M, Wakiyama N, et al. Fc domain mediated self-association of an IgG1 monoclonal antibody under a low ionic strength condition. 2011. J Biosci Bioeng 112: 326–332.

7. Arora J, Hickey JM, Majumdar R, et al. Hydrogen exchange mass spectrometry reveals protein interfaces and distant dynamic coupling effects during the reversible self-association of an IgG1 monoclonal antibody. 2015. MAbs 7: 525–539.

8. Gentiluomo L, Roessner D, Streicher W, et al. Characterization of Native Reversible Self-Association of a Monoclonal Antibody Mediated by Fab-Fab Interaction. 2020. J Pharm Sci 109: 443–451.

9. Esfandiary R, Parupudi A, Casas-Finet J, et al. Mechanism of reversible self-association of a monoclonal antibody: role of electrostatic and hydrophobic interactions. 2015. J Pharm Sci 104: 577–586.

10. Yang D, Correia JJ, Stafford Iii WF, et al. Weak IgG self- and hetero-association characterized by fluorescence analytical ultracentrifugation. 2018. Protein Sci 27: 1334–1348.

11. Connolly BD, Petry C, Yadav S, et al. Weak interactions govern the viscosity of concentrated antibody solutions: high-throughput analysis using the diffusion interaction parameter. 2012. Biophys J 103: 69–78.

12. Sun T, Reid F, Liu Y, et al. High throughput detection of antibody self-interaction by bio-layer interferometry. 2013. MAbs 5: 838–841.

13. Domnowski M, Jaehrling J, Frieß W. Assessment of Antibody Self-Interaction by Bio-Layer-Interferometry as a Tool for Early Stage Formulation Development. 2020. Pharm Res 37: 29.

14. Masson GR, Jenkins ML, Burke JE. An overview of hydrogen deuterium exchange mass spectrometry (HDX-MS) in drug discovery. 2017. Expert Opin Drug Discov 12: 981–994.

15. Dobson CL, Devine PWA, Phillips JJ, et al. Engineering the surface properties of a human monoclonal antibody prevents self-association and rapid clearance in vivo. 2016. Sci Rep 6: 38644.

16. Lerch TF, Sharpe P, Mayclin SJ, et al. Infliximab crystal structures reveal insights into self-association. 2017. MAbs 9: 874–883.

17. Hageman TS, Weis DD. Reliable Identification of Significant Differences in Differential Hydrogen Exchange-Mass Spectrometry Measurements Using a Hybrid Significance Testing Approach. 2019. Anal Chem 91: 8008–8016.

18. Chaturvedi SK, Ma J, Brown PH, et al. Measuring macromolecular size distributions and interactions at high concentrations by sedimentation velocity. 2018. Nat Commun 9: 4415.

19. Schuck P. Size-distribution analysis of macromolecules by sedimentation velocity ultracentrifugation and lamm equation modeling. 2000. Biophys J 78: 1606–1619.

20. Vistica J, Dam J, Balbo A, et al. Sedimentation equilibrium analysis of protein interactions with global implicit mass conservation constraints and systematic noise decomposition. 2004. Anal Biochem 326: 234–256.

21. Franke D, Petoukhov MV, Konarev PV, et al. ATSAS 2.8: a comprehensive data analysis suite for small-angle scattering from macromolecular solutions. 2017. J Appl Crystallogr 50: 1212–1225.

22. Petoukhov MV, Franke D, Shkumatov AV, et al. New developments in the ATSAS program package for small-angle scattering data analysis. 2012. J Appl Crystallogr 45: 342–350.

23. Tian X, Langkilde AE, Thorolfsson M, et al. Small-angle x-ray scattering screening complements conventional biophysical analysis: comparative structural and biophysical analysis of monoclonal antibodies IgG1, IgG2, and IgG4. 2014. J Pharm Sci 103: 1701–1710.

24. Lilyestrom WG, Shire SJ, Scherer TM. Influence of the cosolute environment on IgG solution structure analyzed by small-angle X-ray scattering. 2012. J Phys Chem B 116: 9611–9618.

25. Uchiyama S, Noda M, Krayukhina E. Sedimentation velocity analytical ultracentrifugation for characterization of therapeutic antibodies. 2018. Biophys Rev 10: 259–269.

26. Li L, Kumar S, Buck PM, et al. Concentration dependent viscosity of monoclonal antibody solutions: explaining experimental behavior in terms of molecular properties. 2014. Pharm Res 31: 3161–3178.

27. Binabaji E, Ma J, Zydney AL. Intermolecular Interactions and the Viscosity of Highly Concentrated Monoclonal Antibody Solutions. 2015. Pharm Res 32: 3102–3109.

28. Allmendinger A, Fischer S, Huwyler J, et al. Rheological characterization and injection forces of concentrated protein formulations: an alternative predictive model for non-Newtonian solutions. 2014. Eur J Pharm Biopharm 87: 318–328.

29. Hung JJ, Dear BJ, Dinin AK, et al. Improving Viscosity and Stability of a Highly Concentrated Monoclonal Antibody Solution with Concentrated Proline. 2018. Pharm Res 35: 133.

30. Plath F, Ringler P, Graff-Meyer A, et al. Characterization of mAb dimers reveals predominant dimer forms common in therapeutic mAbs. 2016. MAbs 8: 928–940.

31. Fukuda M, Moriyama C, Yamazaki T, et al. Quantitative Correlation between Viscosity of Concentrated MAb Solutions and Particle Size Parameters Obtained from Small-Angle X-ray Scattering. 2015. Pharm Res 32: 3803–3812.

32. Corbett D, Bye JW, Curtis RA. Measuring Nonspecific Protein-Protein Interactions by Dynamic Light Scattering. 2019. Methods Mol Biol 2039: 3–21.

33. Minton AP. Recent applications of light scattering measurement in the biological and biopharmaceutical sciences. 2016. Anal Biochem 501: 4–22.

34. Liu J, Yadav S, Andya J, et al. Analytical Ultracentrifugation and Its Role in Development and Research of Therapeutical Proteins. 2015. Meth Enzymol 562: 441–476.

35. Saito S, Uchiyama S. 2016. Biopharmaceutical Evaluation of Intermolecular Interactions by AUC-SE. In Uchiyama S, Arisaka F, Stafford WF, Laue T, editors. Analytical Ultracentrifugation, Tokyo: Springer Japan. p 419–440.

36. Liu J, Nguyen MDH, Andya JD, Shire SJ. Reversible self-association increases the viscosity of a concentrated monoclonal antibody in aqueous solution. 2005. J Pharm Sci 94: 1928–1940.

37. Nishi H, Miyajima M, Nakagami H, et al. Phase separation of an IgG1 antibody solution under a low ionic strength condition. 2010. Pharm Res 27: 1348–1360.

38. Houde D, Nazari ZE, Bou-Assaf GM, et al. Conformational Analysis of Proteins in Highly Concentrated Solutions by Dialysis-Coupled Hydrogen/Deuterium Exchange Mass Spectrometry. 2016. J Am Soc Mass Spectrom 27: 669–676.

39. Zhang A, Hu P, MacGregor P, et al. Understanding the conformational impact of chemical modifications on monoclonal antibodies with diverse sequence variation using hydrogen/deuterium exchange mass spectrometry and structural modeling. 2014. Anal Chem 86: 3468–3475.

40. Hao G, Wesolowski JS, Jiang X, et al. Epitope characterization of an anti-PD-L1 antibody using orthogonal approaches. 2015. J Mol Recognit 28: 269–276.

41. Geoghegan JC, Fleming R, Damschroder M, et al. Mitigation of reversible self-association and viscosity in a human IgG1 monoclonal antibody by rational, structure-guided Fv engineering. 2016. MAbs 8: 941–950.

Supplementary data

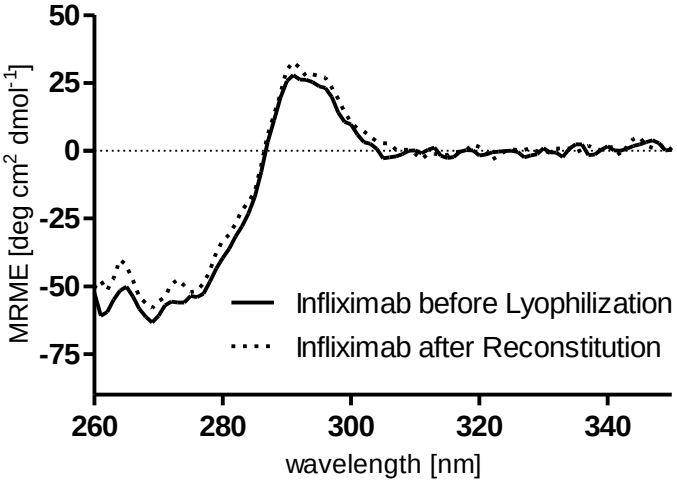

Figure S1 *CD spectra of Infliximab formulations before lyophilization in 2 mM sodium phosphate pH 6.2, 30 mM trehalose and after reconstitution in 6 mM sodium phosphate pH 6.2, 90 mM trehalose.*

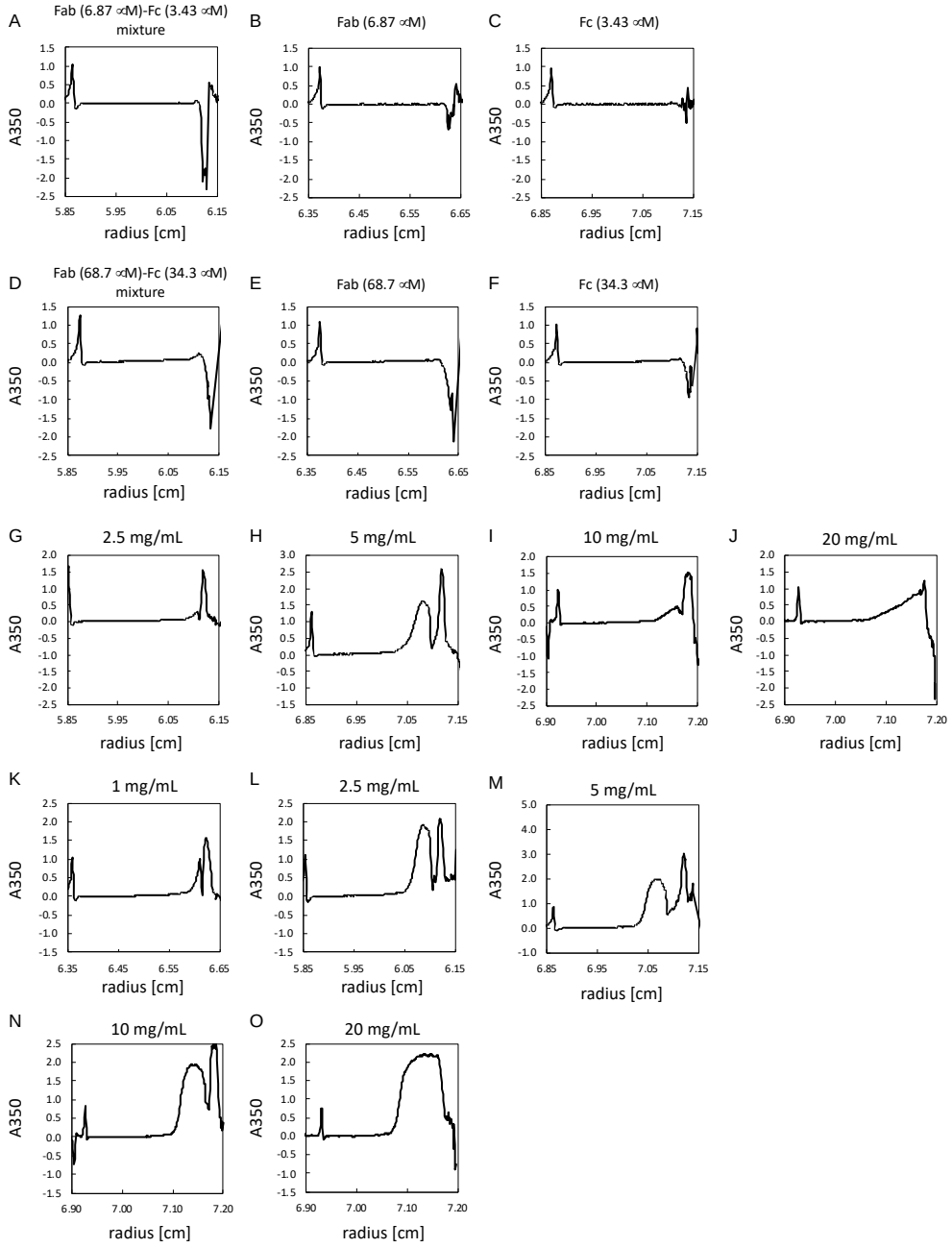

Figure S2: *Observation of turbidity in sedimentation equilibrium by A350 measurement; (A-F) Infliximab Fab, Fc and Fab-Fc mixture (sedimentation equilibrium at 5,000 rpm). (A) Fab (6.87 µM)-Fc (3.43 µM) mixture, (B) Fab (6.87 µM), (C) Fc (3.43 µM), (D) Fab (68.7 µM)-Fc (34.3 µM) mixture, (E) Fab (68.7 µM), (F) Fc (34.3 µM).*

(G-J) Full-length Infliximab (sedimentation equilibrium at 9,000 rpm). (G) 2.5 mg/mL, (H) 5 mg/mL, (I) 10 mg/mL, and (J) 20 mg/ml. (K-O) Full-length Infliximab (sedimentation equilibrium at 13,000 rpm). (K) 1 mg/mL, (L) 2.5 mg/mL, (M) 5 mg/mL, (N) 10 mg/mL, and (O) 20 mg/ml.

Data for (I), (J), (O) and (N) were obtained in 3mm path centerpiece, and the rest were obtained in 12 mm path centerpiece.

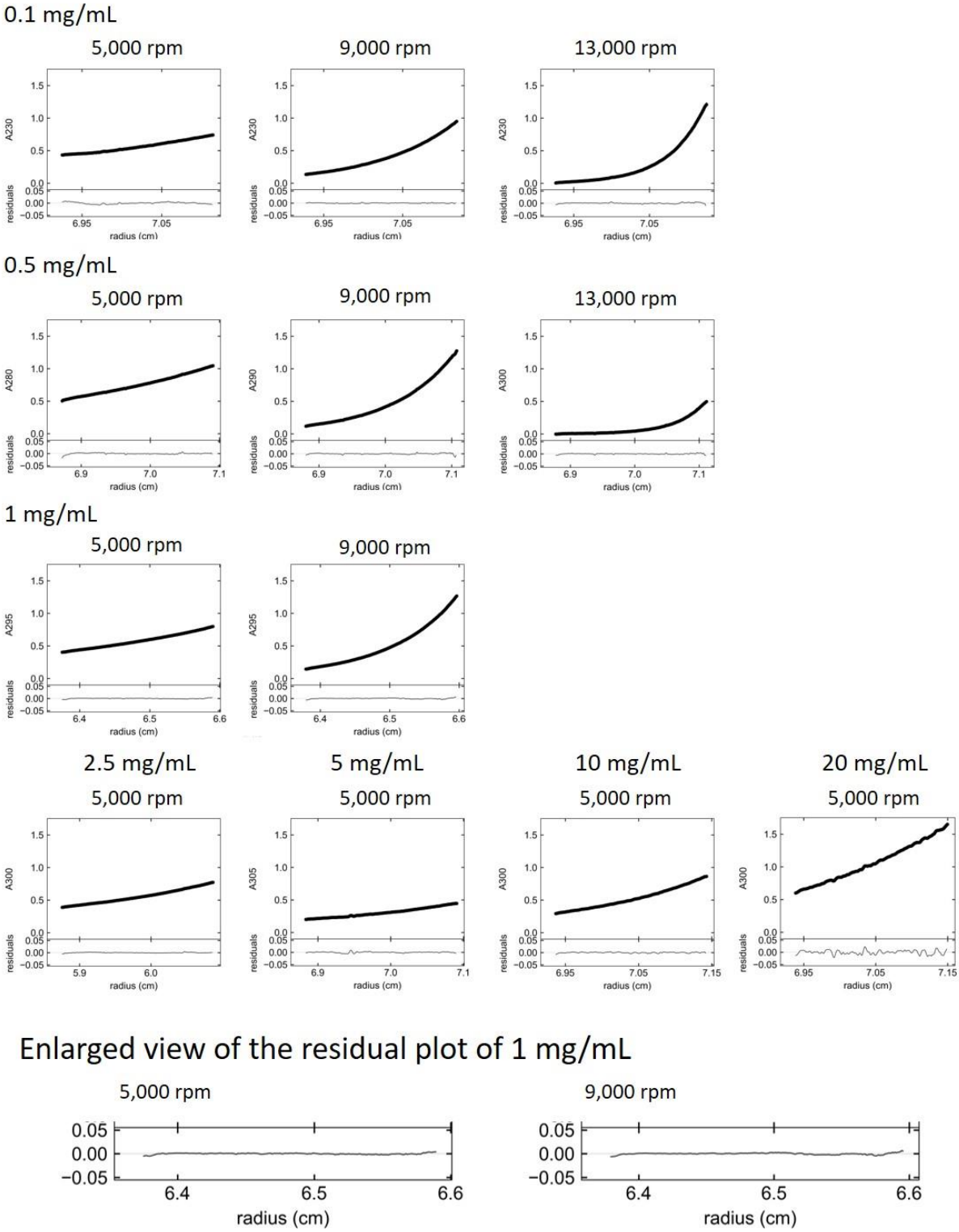

Figure S3 *Sedimentation equilibrium profiles of Infliximab with non-linear fitting analysis and residual plots.*

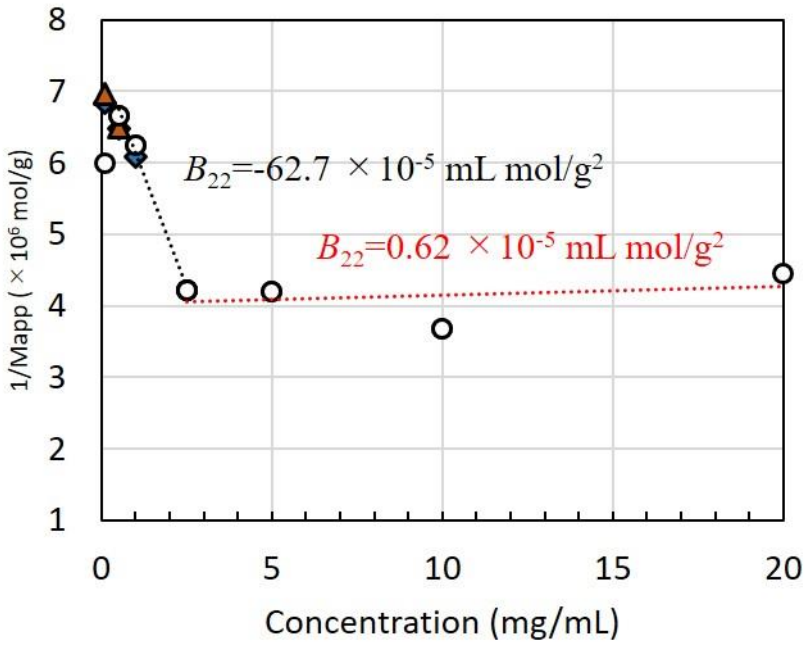

Figure S4 *Inverse plot of molecular weight at each sample concentration*

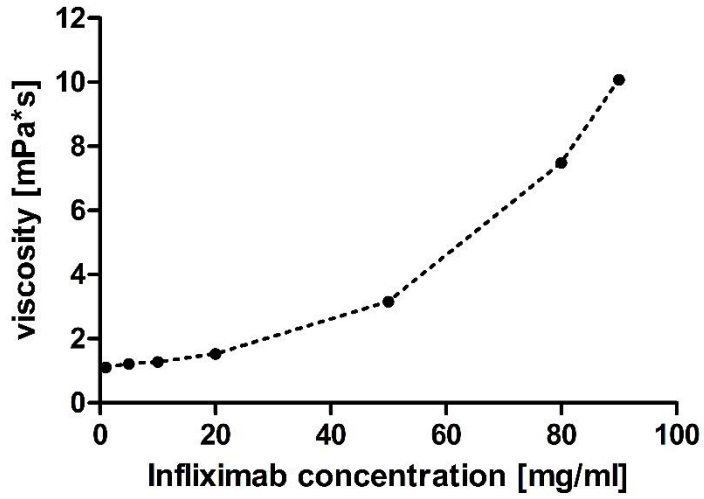

Figure S5 *Viscosity as a function of protein concentration. Infliximab was analyzed in 6 mM sodium phosphate pH 6.2, 90 mM trehalose.*

Table S1 *List of peptides with significant decrease in H/D uptake at 20 mg/ml compared to 0.5 mg/ml Infliximab*

	Protein	Start	End	Sequence	Exposure time [min]	ΔHX [Da]	p-value
Laboratory 1	Heavy chain	48	64	VAEIRSKSINSATHYAE	10	-0,32	0,002
		50	70	EIRSKSINSATHYAESVKGRF	10	-0,33	0,005
		51	62	IRSKSINSATHY	10	-0,31	0,003
		51	64	IRSKSINSATHYAE	10	-0,38	0,001
		51	64	IRSKSINSATHYAE	60	-0,37	0,001
		238	255	LGGPSVFLFPPKPKDTLM	1	-0,32	<0,001
		329	351	KALPAPIEKTISKAKGQPREPQV	10	-0,52	<0,001
		430	449	VMHEALHNHYTQKSLSLSPG	10	-0,46	0,006
		430	449	VMHEALHNHYTQKSLSLSPG	60	-0,37	0,006
	Light chain	149	172	KVDNALQSGNSQESVTEQDSKDST	60	-0,31	<0,001
		155	161	QSGNSQE	1	-0,45	0,003
Laboratory 2	Heavy chain	60	70	THYAESVKGRF	10	-0,32	0,003
		60	70	THYAESVKGRF	60	-0,40	0,005
		427	449	SCSVMHEALHNHYTQKSLSLSPG	10	-0,36	0,002
		427	449	SCSVMHEALHNHYTQKSLSLSPG	60	-0,43	0,001
	Light chain	136	161	LNNFYPREAKVQWKVDNALQSGNSQE	3	-0,29	<0,001
		136	161	LNNFYPREAKVQWKVDNALQSGNSQE	10	-0,29	0,003
		144	161	AKVQWKVDNALQSGNSQE	10	-0,28	<0,001
		162	172	SVTEQDSKDST	3	-0,28	0,001
		162	179	SVTEQDSKDSTYSLSSTL	1	-0,27	<0,001
		162	179	SVTEQDSKDSTYSLSSTL	60	-0,29	0,002

Table S2 *SAXS - experimental details*

Instrument	**P12 BioSAXS beamline (PETRAIII)**
Date	12th July 2019
Detector	Pilatus6m
Wavelength (nm)	1.23981
Beam size (mm^2)	0.2 × 0.12
Detector distance (m)	4.0
***q*-measurement range (nm^{-1})**	0.017- 5.506
Absolute scaling method	Comparison with scattering from BSA
Normalization	To transmitted intensity by beam-stop counter
Monitoring for radiation damage	Frame-by-frame comparison
Exposure time (s)	20 x 0.195
Sample configuration	Quartz glass capillary
Sample temperature (ºC)	20
c) Software employed for SAXS data reduction, analysis and interpretation	
SAS data reduction	*PRIMUSqt*[29] from *ATSAS* 2.8.3[30]
Basic analyses: Guinier, *p*(*r*), V_P	*PRIMUSqt*[29]

Chapter 5 Generation of mAb variants with less attractive self-interaction but preserved target binding by well-directed mutation

M. Domnowski[1,2], K. L. Presti[1], J. Binder[1], J. Reindl[2], L. Lehmann[2], F. Kummer[2], M. Wolber[2], M. Satzger[2], M. Dehling[2], J. Jaehrling[2], W. Frieß[1 *]

[1]Department of Pharmacy: Pharmaceutical Technology and Biopharmaceutics; Ludwig-Maximilians-Universitaet Muenchen, Butenandtstrasse 5, 81377 Munich, Germany

[2]MorphoSys AG, Semmelweisstraße 7, 82152 Planegg

Author contributions:

M.D., J.J. and W.F. conceived and designed the study. M.D. conducted and analyzed homology modelling, SI-BLI, HDX-MS, viscosimetry, mAb production, K.L.P. conducted BLI, SI-BLI and HDX-MS experiments, J.B. conducted homology modelling, F.K. and L.L. conducted mAb production, J.R. performed mAb cloning, M.S. performed and analyzed 3P measurements, M.W. conducted and analyzed BLI. M.D., K.L.P., J.J. and W.F. analyzed and interpreted the data. M.D., J.J. and W.F. contributed to the writing of the manuscript.

Keywords: Self-interaction, Self-association, Protein engineering, HDX-MS, viscosity, Unspecificity

Abbreviations: HCDR – Complementary determining region of the heavy chain, LCDR – Complementary determining region of the light chain, HDX-MS – Hydrogen-Deuterium-exchange mass spectrometry, BLI – bio-layer interferometry

5.1 Abstract

Strongly attractive self-interaction of therapeutic protein candidates can impose challenges for manufacturing, filling, stability and administration due to elevated viscosity or aggregation propensity. Suitable formulations can mitigate these issues to a certain extent. Understanding the self-interaction mechanism on a molecular basis and rational protein engineering provides a more fundamental approach, and it can save costs and efforts as well as alleviate risks at later stages of development. In this study, we used computational methods for identification of aggregation prone regions in a mAb and generated mutants based on these findings. We applied hydrogen-deuterium exchange mass spectrometry to identify distinct self-interaction hotspots. Ultimately, we generated mAb variants based on a combination of both approaches and identified mutants with low attractive self-interaction propensity, minimal off-target binding and even improved target binding. Our data show that the introduction of arginine in spatial proximity to hydrophobic patches is highly beneficial on all these levels. For our mAb, variants which contain more than one aspartate residue flanking to the hydrophobic HCDR3 show decreased attractive self-interaction at unaffected off-target and target binding. The combined engineering strategy described here underlines the high potential of understanding self-interaction in early stages of development to predict and reduce risk of failure in subsequent development.

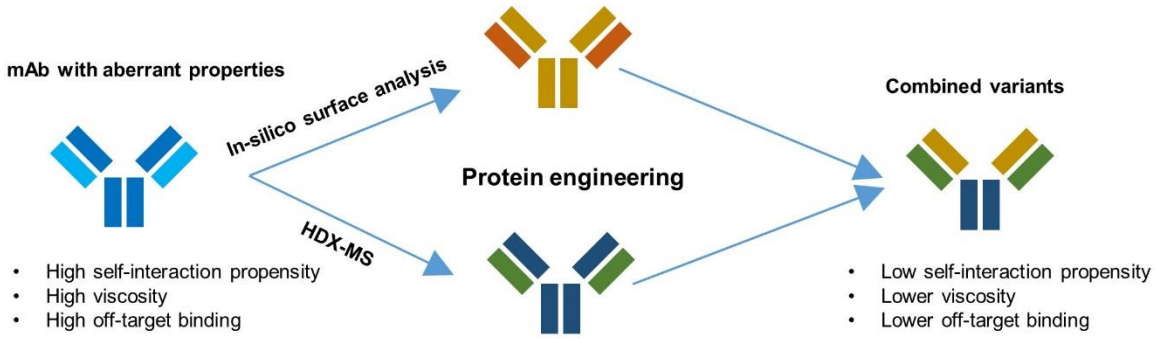

Graphical abstract *Generation of mAb variants with less attractive self-interaction but preserved target binding by well-directed mutation*

5.2 Introduction

By the end of 2019, more than 80 antibody therapeutics reached the biopharmaceutical market in US or EU.[1] The design of suitable candidate molecules and their formulation play a pivotal role in every stage of discovery and development. In general, a formulation must ensure chemical, conformational and colloidal protein stability. The latter objective is strongly influenced by the self-interaction of the protein molecules. This challenge is enhanced in case of high concentration protein, specifically monoclonal antibody (mAb) formulations which are increasingly demanded for subcutaneous self-application by patients and for other convenience and safety reasons. Protein aggregation can arise from native oligomers as a result of strong attractive self-interaction.[2] Self-interaction of mAbs can be associated with an extreme increase in viscosity at higher concentration[3–5], a higher tendency for aggregation due to increased frequency of intermolecular collisions[6] and filter clogging and fouling.[7]

Several studies showed that self-interaction processes of mAbs are diverse and can be triggered by Fab-Fab, Fab-Fc or Fc-Fc interactions.[4, 8–15] These interactions can be driven by both electrostatic and hydrophobic forces.[12, 16, 17] Thus, formulation strategies can be applied to reduce the self-interaction propensity of a mAb. Ionic excipients like sodium chloride and arginine hydrochloride disrupt the self-interaction processes by either charge shielding or hydrophobic interactions and therefore reduce solutions viscosity.[18–22] Additionally, the solutions pH has a strong impact on the solvent accessible charges of a mAb and thus on self-interaction.[10, 22-24]

Another approach to influence the propensity of a mAb to self-interact reversibly is rational mutagenesis. Data from *in silico* modeling or *in vitro* experiments can help to identify critical sites or residues in the protein, and thus set the basis for planning a rational engineering strategy.[9,17,25,26] Applying computational methodologies for calculation of aggregation prone regions led to antibody variants with high solubility and lowered viscosity at high protein concentrations. However, these tools address the aggregation prone regions and not discrete sites for reversible self-interaction. Additionally, mutations addressing unequal charge distributions on the mAb surface improved the physicochemical properties of a less soluble mAb.[17]

Besides computational tools, emerging techniques for studying mAb self-interaction such as HDX-MS have driven rational engineering.[9] Geoghegan et al. introduced mutations in protein regions, which were identified as self-interaction sites by HDX-MS.[27] Some of the mAb variants showed improved solution properties, whereas others showed a decrease in target binding or conformational stability. The prediction of self-interaction sites based on crystal structures was also used for rational mutagenesis of mAbs.[26, 28] The mAb CNTO607 is a model mAb with low solubility and high self-interaction propensity.[25, 29, 30] For this mAb, a hydrophobic triad within the HCDR3 was shown to mediate self-interaction. But mutations within this region compromised target binding affinity.[25, 29, 30]

In addition to mAb low self-interaction propensity and high target affinity, minimized off-target binding plays an important role for characterization and selection of drug candidates and needs to be considered upon mutation. As recently reviewed by Starr and Tessier, antibody specificity is a key property to optimize mAb therapeutics.[30] In a study of 137 antibodies, specificity measurements identified advantages of approved mAbs compared to mAbs currently under clinical investigations.[31]

Here, we present a study on a mAb directed against Estradiol-decorated BSA as a model IgG protein which was derived from a fully human phage library.[32] This mAb exhibits only one of the three desired features, namely high affine target binding, but shows several unwanted properties like precipitation in PBS during downstream processes, significantly higher retention time in SEC analysis compared to other mAbs and strong off-target binding.[33] Goal of this study was to understand the mAbs aberrant behavior and to find solutions based on rational mutagenesis. To maintain the paratope and thus, the antigen binding capacity of the mAb, we first determined the target binding site by HDX-MS. We analyzed the self-interaction propensity of the mAb by self-interaction bio-layer interferometry (SI-BLI) and found significant effects for pH and ionic strength. We used this knowledge for protein surface analysis to identify hydrophobic patches and aggregation prone regions, which could be potentially involved in reversible self-interaction. HDX-MS was additionally applied to identify distinct self-interaction sites. After identification of potential self-interaction hot spots by *in silico* and *in vitro* experiments, mutations were introduced to experimentally verify these predictions and resolve the described issues. In total, 39 mAb variants were generated and subsequently characterized regarding self-interaction, target binding and off-target binding. Thus we could gain a deeper

understanding of the self-interaction process of our model mAb and identify variants with improved specificity by combining both, *in silico* and in-vitro based rational engineering.

5.3 Experimental section

5.3.1 Materials

Phosphate buffered saline (Thermo Fisher Scientific, MA), L-histidine (Merck KGaA, Germany), sodium chloride (Carl Roth GmbH + Co. KG, Germany), hydrochlorid acid (Merck KGaA, Germany), L-Arginine (Merck KGaA, Germany), trehalose dihydrate (Pfanstiehl Technologies, Waukegan, IL) were all of analytical grade.

5.3.2 mAb Cloning

DNA of variants containing mutations in the CH and VH variants with mutations next to restriction sites (HCDR1 or 3) were prepared via mutagenesis PCR. Other DNA strings were purchased (Thermo Fisher Scientific, MA). For Gibson assembly®, DNA strings were designed with a 21bp overlap next to restriction sites.

The vectors were prepared via restriction digest followed by dephosphorylation with shrimp alkaline phosphatase and agarose gel purification prior to the Gibson cloning. After Gibson cloning, the DNA constructs were transformed in chemically competent DH5alpha competent E. coli cells and then checked via colony PCR sequencing. From the correct clones, Miniprep Plasmid DNA was prepared and sequenced. After consolidation via 50 pg retransformation, the final Plasmid Maxi prep DNA was transferred for transfection and expression of the constructs in HEK293 cells.

5.3.3 mAb Production

For large scale production, the wildtype mAb was expressed in HKB11 stable pool expression system for 6 days. Cell culture supernatant was applied to a MabSelect SuRe column with a column volume (CV) of 32 ml (Cytiva, MA) equilibrated with 0.1 M sodium phosphate pH 6.0 (NaPhos pH 6). Three washing steps were performed (wash 1: 5 CV NaPhos pH 6, wash 2: 5 CV NaPhos pH 6 + 1.5 M sodium chloride, wash 3: 5 CV NaPhos pH 6). Product was eluted with 0.1 M sodium acetate pH 3.0. Protein containing fractions

were pooled and adjusted to pH 5 with 2 M sodium acetate. The concentration was determined by UV absorbance at 280 nm (molar extinction coefficient 211580 M^{-1} cm^{-1}, 146.6 kDa) using Nanodrop 2000 (Thermo Fischer Scientific, MA).

The protein containing pool was subjected to buffer exchange using Sephadex G-25 in PD-10 desalting columns (Cytiva, MA) to the final formulation buffer (15 mM histidine hydrochloride pH 6.0). The concentration was determined by UV absorbance and adjusted to 20 mg/mL utilizing Amicon Ultra 15 centrifugal filter units (50 kDa cut-off, Merck KGaA, Germany). The final product was sterile filtered using a 50 mL Steriflip (Merck KGaA, Germany).

The protein variants were expressed in small scale in HEK293 cells for 6 days after transfection. Cell culture supernatants were applied to HiTrap MabSelect SuRe columns (Cytiva, MA) installed on an Äkta Xpress system equilibrated with NaPhos pH 6. Three washing steps were performed (wash 1: 5 CV NaPhos pH 6, wash 2: 5 CV NaPhos pH 6 + 1.5 M NaCl, wash 3: 5 CV NaPhos pH 6). Product was eluted with 0.1 M sodium acetate buffer pH 3 and protein containing fractions were pooled without pH adjustment. The protein containing pools were subjected to buffer exchange using Sephadex G-25 in PD-10 desalting columns (Cytiva, MA) to the final formulation buffer (15 mM histidine hydrochloride pH 6.0). The concentration was determined by UV absorbance at 280 nm using an average molar extinction coefficient of 208356 M^{-1} cm^{-1} and an average molecular weight of 146.6 kDa using Nanodrop 2000 (Thermo Fischer Scientific, MA). The final products were sterile filtered using Microsep Advance Centrifugal Devices (PALL, NY).

5.3.4 SI-BLI

The SI-BLI method was performed as previously described.[34] Anti-hIgG Fc capture (AHC) biosensors (FortèBio, CA) were used to assess antibody self-interaction on an Octet QK384 or HTX system (FortéBio, CA). In the first assay step, a baseline was established in 15 mM histidine hydrochloride pH 6.0 for at least 60 s, followed by capture of the mAb of interest at 25 nM in 15 mM histidine hydrochloride until the BLI signal increased by approximately 1 nm. Remaining binding capacity of the capture sensors was saturated for 300 s with 1 μM of human Fc in PBS. Subsequently, a second baseline was acquired in the formulation composition of interest for 500 s, followed by an association step with 2 μM mAb in the

same formulation of interest for at least 1200 s. The response at equilibrium was used for further calculations. To compensate for differences in the amount of captured mAb, the equilibrium binding signal obtained during self-interaction was normalized to the amount of captured mAb (R_{rel}, equation 1).

$$R_{rel} = \frac{Response_{Association\ equilibrium}\ [nm]}{Response_{capture\ step}[nm]} \quad (1)$$

5.3.5 HDX-MS

HDX-MS experiments were performed on a fully automated system equipped with a Leap robot (HTS PAL, Leap Technologies, NC), a Waters Acquity NanoUPLC, a HDX manager and the Synapt G2-Si mass spectrometer (Waters, MA).[35] For ionization in positive mode (300-2000 m/z) a capillary voltage of 3.0 kV, a desolvation gas flow of 500 L/hr, a source temperature of 80°C and a desolvation temperature of 250°C was applied. Sampling cone and offset was set to 40.0 and 50.0, respectively. Peptide elution occurred using a gradient from 10-60% (B) within 8.5 min followed by a 1.5 min gradient from 60-95% (B) prior a reconditioning-step. Peptides were identified via MS^E using a collision energy ramp from 10-45 eV.

5.3.6 Paratope mapping

For determination of the antigen binding site of the mAb, HDX-MS analysis was performed for the antigen-antibody complex and for mAb only. 1:10 dilutions of complex (3.7 µM antigen and 6.8 µM mAb) and mAb only (6.8 µM) in 15 mM histidine DCl pH 5.0 were incubated for 1, 10, 60 and 240 min at 25°C. After incubation in D_2O containing buffer, the labeling reaction was quenched by 1:1 dilution with quenching buffer (0.1 M potassium phosphate pH 2.6, 0.2 M TCEP, 4 M guanidine hydrochloride). For proper denaturation, the solution was incubated under quenching conditions for 1 min at 2.0 °C. Afterwards, 50 µl of the solution were directed to a pepsin column for online digestion at 15°°C (Waters Enzymate 300 Å, 5 µm; 3 min, 0.1 ml/min 0.1 % formic acid in H_2O). Peptides were trapped (Waters VanGuard C18) and subsequently separated on a Waters UPLC column at 0 °C (Waters Acquity UPLC, BEH C18, 130 Å, 1.7 µm).[36] Eluting peptides were directed

into a Synapt G2-Si TOF mass spectrometer by electrospray ionization (Waters, MA). Before fragmentation by MSE and mass detection in resolution mode, the peptide ions were additionally separated by drift time within the mobility cell. Data processing was performed using the Waters Protein Lynx Global Server PLGS (version 2.5.3) and DynamX (version 3.0). Each incubation time point was measured in triplicates. Statistical analysis of significant differences was performed using Hybrid Significance Testing as described.[37]

5.3.7 Self-interaction sites mapping

For determination of self-interaction sites, the protein stock solutions (180 mg/ml) were diluted 1:3 with 15 mM Histidine-DCl pH 7.0 to 60 mg/ml for high concentration condition and to 0.5 mg/ml for low concentration condition. After incubation for 0, 2 and 10 min, samples were analyzed and processed as described above. As control experiment, labeling was performed in 15 mM Histidine-DCl pH 5.0 because self-interaction propensity was low under these conditions.

5.3.8 Protein surface analysis

Homology models of the wildtype mAb were generated by using BioLuminate (Schrödinger Release 2018-2, Schrödinger LLC, NY, 2015). As template structure, an already published crystal structure derived from a HuCAL phage display library was used.[38] The knowledge based approach was used for model building. A further preparation of the structure was carried out by checking for missing side chains, overlapping H-bonds and false molecule geometry. A restrained minimization using the OPLS3e force field was performed. The Protein Surface Analyzer Tool in combination with AggScore calculation was used to identify aggregation prone regions and hydrophobic patches.[39]

5.3.9 Protein panel profiling

The method was essentially performed as described before.[33] Briefly, off-target binding of IgG samples was assessed in a plate-based assay, using electrochemiluminescence readout. A panel of 32 proteins and controls was coated onto two MSD standard 384-well plates per assay, each row coated with one protein or control. Subsequently, the plate was blocked with 3 % (w/v) BSA in PBS. The coated proteins and samples included highly abundant

serum proteins, different cytokines and cell-surface receptors, proteins bearing different post-translational modifications (phosphorylation, glycosylation), representatives for different pI values (ranging from 2.8 to 10.7), and vesicles prepared from HKB11 cells and Baculovirus particles[40]. Additionally, Protein A, anti-human Fc and anti-human Fab antibodies, lysozyme and target proteins of the sample IgGs, as well as blank rows were included as controls. Each IgG sample was assessed at 10 and 100 nM. For referencing purposes, an anti-lysozyme antibody was included known to show negligible non-specific binding. ECL-labeled anti-human Fab antibody was added for detection, and ECL-signals detected using a Sector Imager S 600 instrument (Meso Scale Discovery, MD). Binding signals were divided by the signal of the reference mAb on the same protein. The sum of binding ratios on all off-target probes (i.e. excluding specific antigens and controls) were used as a metric for off-target binding of the respective IgG.

5.3.10 BLI for target binding

BLI assays were performed on an Octet HTX system (FortéBio, CA) using Streptavidin sensors (Fortébio, CA) loaded with 3 µg/ml biotinylated MabSelect SuRe Ligand (Cytiva, MA) for 600 s followed by quenching for 5 min with 20 µg/ml biocytin (Merck KGaA, Germany) in PBS. PBS containing 0.05 % polysorbate 20 and 1 % (w/v) BSA was used as assay buffer. 5 µg/mL IgG was captured on several sensors in parallel, until a capture level of 0.8 nm was achieved. Subsequently, association of a 3-fold serial dilution series of estradiol-BSA (0.2 – 150 nM) was monitored for 300 s; dissociation was recorded for 300 s. After each interaction, captured IgG including bound estradiol-BSA was removed from the sensor with an acidic regeneration (Glycine-HCl pH 1.5; 3 steps à 30 s). Signals recorded on sensors with captured IgG but without estradiol-BSA were used for reference subtraction.

Each assay was performed in triplicates. Raw data were preprocessed using the Octet Data Analysis HT 10.0 software (FortéBio, CA), and evaluated using Xlfit software (IDBS, MA). Binding signals at the end of the association were plotted against analyte concentrations, and fitted to a steady state model. Due to the multivalent and unknown coupling ratio of estradiol-BSA, i.e. unknown valency of binding sites per molecule, only an apparent K_D value could be obtained, i.e. an apparent affinity including avidity.

5.3.11 Viscosity determination

Viscosity measurements were performed on a ViscoSizer TD system (Malvern, UK). The sample is automatically pumped through a capillary under constant pressure. Viscosity is calculated relative to a caffeine standard (1 mg/l in H_2O) depending on the time needed to pass a set capillary length. Protein samples were detected by UV absorbance at 280 nm.

5.4 Results and Discussion

5.4.1 Characterization of the self-interaction behavior of the wildtype mAb

SI-BLI was performed to analyze the formulation dependent self-interaction propensity of the wildtype mAb, using a histidine buffered formulation covering the typical pH range of mAb formulation 5 and 7. An increase in pH from 5 to 7 led to a higher R_{rel} and thus, to an increase in attractive self-interaction propensity (Figure 1 A). This effect was further intensified by addition of the ionic excipients sodium chloride and arginine hydrochloride. We further evaluated the effect of buffer concentration (Figure 1 B). At pH 5.0 the SI-BLI response clearly increased with higher buffer concentration. This effect was also observed at pH 6.0 and pH 7.0 but less pronounced at neutral pH. These results underlined the strong pH effect on the self-interaction of the wildtype mAb and may explain the aberrant precipitation and poor recovery during downstream processing, where typically buffers are applied which contain e.g. sodium chloride and are close to neutral pH.

Strong attractive self-interaction of mAbs can lead to a disproportionately high increase in viscosity at higher protein concentration. As shown in Figure 1 C, the viscosity increased extremely, starting at 50 mg/ml protein. At 100 mg/mL wildtype mAb the viscosities reached 300 mPa*s at pH 7.0, and 130 mPa*s at pH 5.0, respectively. We therefore decided to use formulations at pH 7.0 for in-depth characterization of the mAb self-interaction and at pH 5.0 as low self-interaction control condition for HDX-MS experiments.

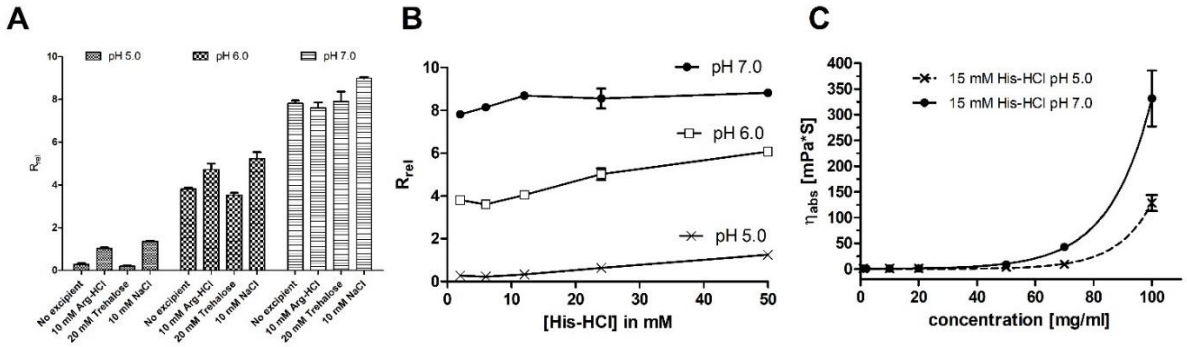

Figure 1 *Self-interaction analysis of the wildtype mAb. A) SI-BLI in 15 mM His HCl at pH 5.0, 6.0 and 7.0 with different excipients added; B) SI-BLI in dependence of buffer concentration and pH; C) Increase in solutions viscosity in 15 mM His-HCl at pH 5.0 and pH 7.0.*

5.4.2 Paratope mapping of the wildtype mAb by HDX-MS

HDX-MS was performed to detect the antibody-antigen interaction site comparing the deuterium uptake of the antibody-antigen complex to antibody alone by hybrid significance testing. For evaluation of significance, we calculated a ΔHX threshold of 0.41 Da (Table S1). Regions of the mAb that showed less uptake in the complex state were interpreted as antigen binding sites. In total, we analyzed 113 peptides of the heavy chain and 45 peptides of the light chain, which reflects a coverage of 85 % and 92 % respectively. In the Fc domain, peptides in proximity to the N-glycosylation region were not covered. However, antigen binding was expected to be mediated by the CDR regions of the mAb. We identified several peptides in the HCDR2 (W_{47}MGGIIPIYGTAYYAQKFQG_{65}) and the HCDR3 (S_{95}PRSYVTYRRYWFDY$_{102}$) of the Fab domain as being involved in antigen binding (Figure 2). The H/D exchange of the CDRs of the light chain did not depend significantly on the presence of antigen, indicating that these segments did not contribute to the antigen binding. Thus, the introduction of mutations in only one of the two identified regions could weaken target binding but may not abolish it.

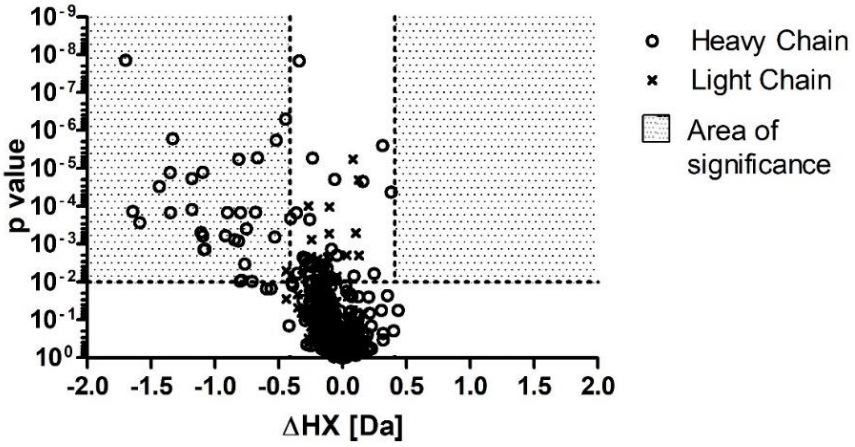

Figure 2 *Volcano plot of HDX-MS results of the paratope mapping of the wildtype mAb. Data points within the area of significance showed decreased uptake in the complex state compared to mAb alone. A peptide list and the calculation of ΔHX threshold can be found in the supplemental material in table S1. As ΔHX, the difference in uptake between mAb-antigen complex and mAb alone is shown.*

5.4.3 Identification of self-interaction sites by *in silico* surface analysis

We prepared a homology model of the wildtype Fab fragment to perform protein surface analysis at pH 7.0. Hydrophobic patches were identified in the HCDR2 and the HCDR3 (Figure 3). The hydrophobic patch of the HCDR2 consisted of I_{52}, I_{53}, Y_{54} and Y_{58}. The non-hydrophobic residues G_{55} and T_{56} were also located within the paratope region, and in close proximity to the hydrophobic patch In the HCDR3 the hydrophobicity was prominently driven by a surface exposed W_{100c}. In addition to visual analysis of the hydrophobicity, aggregation scores were calculated for individual HCDR2 residues[39]. For rational mutagenesis, we introduced residues into the identified regions by in-silico mutagenesis to change the extent of hydrophobicity or to insert negative or positive charges (Table 1). Additionally, we mutated HCDR1 (G_{27}) based on its spatial proximity to HCDR2 and HCDR3.

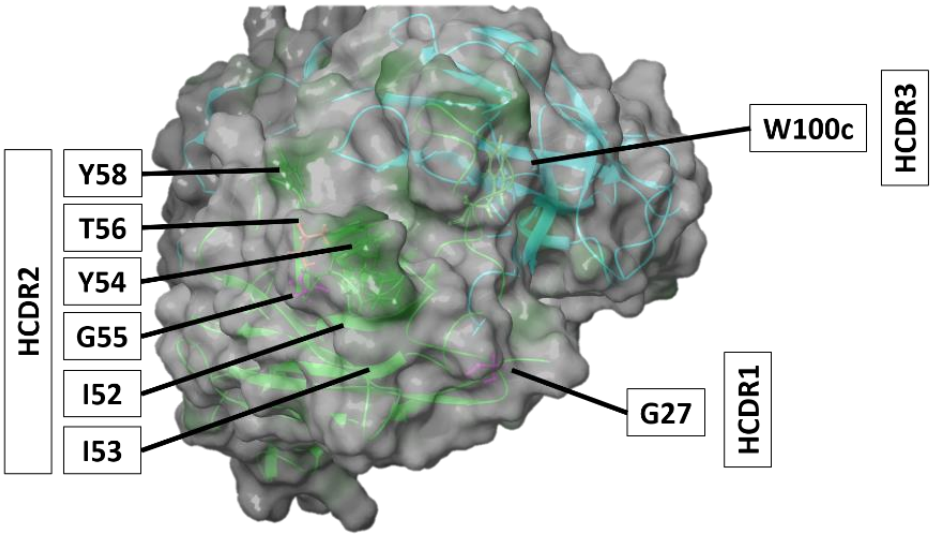

Figure 3 *Homology model of the wildtype Fab fragment on crystal structure 5D7S (Light Green: Heavy chain, Blue: Light chain, Dark green: Surface exposed hydrophobic patches).*

Table 1 *Characterization of mAb variants based on in silico surface analysis: Experimental parameters were compared to wildtype (Self-interaction, Target binding: ↓↓ decreased >2SD, ↓ decreased >1SD, ≈ comparable, ↑ increased >1SD, ↑↑ increased >2SD; Off-target binding: ↓↓ < 50 %, ↓ < 75 %, ↑ > 125 %). Absolute values can be found in the supplemental material in table S2.*

mAb variant	Region	Cumulative AggScore of HCDR2	Self-interaction	Off-target binding	Target binding
wildtype		43			
I52R	HCDR2	12	↓		↑
I53R		16	↓↓		↑
Y54R		13	↓↓		≈
Y58R		30	↓↓		≈
G55R		34	↓↓	↑	↑
G55D		25	↓↓		≈
T56R		23	↓		↑↑
T56D		29	↓↓	↓↓	↑
I52A I53A Y54A Y58A		7	↑	↓↓	↓↓
I52A I53A Y54S Y58S		2	≈	↓↓	↓↓
I52V I53V Y54A Y58A		12	≈	↓↓	↓↓
I52V I53V Y54S Y58S		5	↓↓	↓↓	↓↓
W100cV	HCDR3	44	↑↑	↓	↑
W100cS		44	↑	↓	≈
G27R	HCDR1	43	↓↓	↑	↑↑
G27R T56D	HCDR1/HCDR2	29	↓	↓	↑

5.4.4 Characterization of mAb variants engineered based on *in silico* surface analysis

The mAb variants shown in Table 1 were characterized regarding the change in the cumulative Aggscore, self-interaction, target binding and off-target binding.

For comparison of mutants, the scores of each residue of the patch were added up to a total AggScore. The cumulative AggScore was reduced for variants with single mutations in the HCDR2 (e.g. $I_{52}R$, $T_{56}D$) and further minimized for variants with multiple mutations (e.g. $I_{52}A$ $I_{53}A$ $Y_{54}S$ $Y_{58}S$). Mutations introduced to HCDR3 or flanking to HCDR2 ($G_{27}R$) did not influence the calculated AggScore of HCDR2.

All variants containing single point mutations in the HCDR2, which also introduced additional negative or positive charges, showed decreased self-interaction propensity. In case the hydrophobic patch in HCDR2 was resolved by replacing all positions with either Ser or Val, but no Ala, attractive self-interaction was reduced as well. Additionally, the introduction of a charged residue flanking HCDR2 ($G_{27}R$) resulted in improved self-interaction behavior. Variants of the HCDR3 showed unaffected or slightly increased attraction of the mAb molecules. Regarding target binding, single mutations in HCDR2 influenced the behavior only slightly whereas multiple mutations reduced the apparent target binding affinity. This was expected as HCDR2 was shown to mediate target binding. Target binding of HCDR3 variants was not changed or slightly improved. Introduction of arginine in HCDR1 and HCDR2 improved target binding slightly but increased off-target binding. The most prominent decrease in off-target binding was observed for variants containing multiple mutations in HCDR2. Thus, this region was involved in target and off-target binding. In summary, the introduction of charged residues into the hydrophobic patch of HCDR2 or in spatial proximity of the patch in HCDR1 of our mAb reduced self-interaction significantly. A single mutation did not impair target binding behavior. Inserting a charged residue in proximity to hydrophobic hotspots, which were identified as target binding region, could reflect an approach to reduce the self-interaction propensity while maintaining the target binding properties.

Additionally, we evaluated the combined effect of the most promising single mutations in reducing self-interaction propensity, $T_{56}D$ and $G_{27}R$, by producing and characterizing a variant containing both mutations in HCDR1 and HCDR2 (Table 1). Interestingly, the effects of the single mutations contributed additively to the properties of the double mutation variant. We observed decreased self-interaction propensity, improved target binding and decreased off-target binding. As mentioned above, G_{27} was not located in a hydrophobic patch based on results from computational calculations. We hypothesize, that the reduction of attractive self-interaction is driven by electrostatic shielding of self-interaction sites in HCDR2 and flanking to HCDR3. The interplay of CDRs for self-interaction has also been reported for the mAb MEDI1912 with relevant motifs in HCDR1 and HCDR2.[11] Additionally, shielding of self-interaction sites by more hydrophilic moieties like N-glycans was described for CNT0607[26] with a reintroduced Fab-

glycosylation shielding the hydrophobic triad, increasing the solubility and maintained high affine target binding.

The calculation of AggScores was used to generate and evaluate variants *in silico*. The scores indicate that the aggregation propensity of the HCDR2 mutants might be reduced due to the reduction of overall hydrophobicity of the identified patches. Overall, the AggScore was not predictive for self-interaction. However, mutants with a lower AggScore showed reduced off-target binding, indicating that these hydrophobic patches contributed to non-specificity. Additionally, our results showed that the Fc region was also involved in self-interaction. The AggScore calculations do only include properties of the Fab domain. This may explain the limited predictive power for lowering self-interaction only by inserting mutations into the Fab.

In summary, rational engineering of hydrophobic patches based on homology modeling and protein surface analysis led to mAb variants with reduced attractive self-interaction propensity. As shown by the 4-fold mutants, molecular modeling revealed insights into structural regions involved in off-target binding. Thus, this approach guided to "unspecificity" hot spots of the mAb. Additionally, we observed that mutations flanking this hydrophobic patch influenced the self-interaction behavior positively.

5.4.5 Identification of self-interaction sites by HDX-MS

HDX-MS experiments followed by Hybrid Significance Testing were performed to determine self-interaction sites of the wildtype mAb. At pH 7.0, we analyzed 92 peptides of the heavy chain and 51 peptides of the light chain, which corresponds to a total sequence coverage of 90 %. At pH 5.0, we identified 80 peptides of the heavy chain and 45 peptides of the light chain, resulting in a sequence coverage of 85 %. As shown in Figure 4 A, several peptides showed significant differences in deuterium uptake when comparing high and low concentration condition. Analyzing the H/D exchange of overlapping peptides and surface exposure at pH 7.0, three major hot spots of attractive self-interaction were defined: Hot spot 1 was located in spatial proximity to HCDR3 ($W_{103} – L_{108}$), hot spot 2 was located in the Fc part of the mAb containing the PENNY loop ($V_{379} – N_{384}$) and hot spot 3 was located in C_L of the Fab fragment ($S_{155} – T_{163}$). At pH 5.0 no significant differences of H/D exchange between high and low protein concentration were observed, confirming the

decreased attractive self-interaction at low pH seen in SI-BLI and viscosimetry (Figure 4 B). We additionally studied the $G_{27}R$ mutant at pH 7.0 by HDX-MS and identified 96 heavy chain and 48 light chain peptides, which reflects 90 % sequence coverage. The deuterium uptake did not differ significantly between the low and high concentration conditions demonstrating decreased attractive self-interaction propensity compared to the wildtype mAb (Figure 4 C).

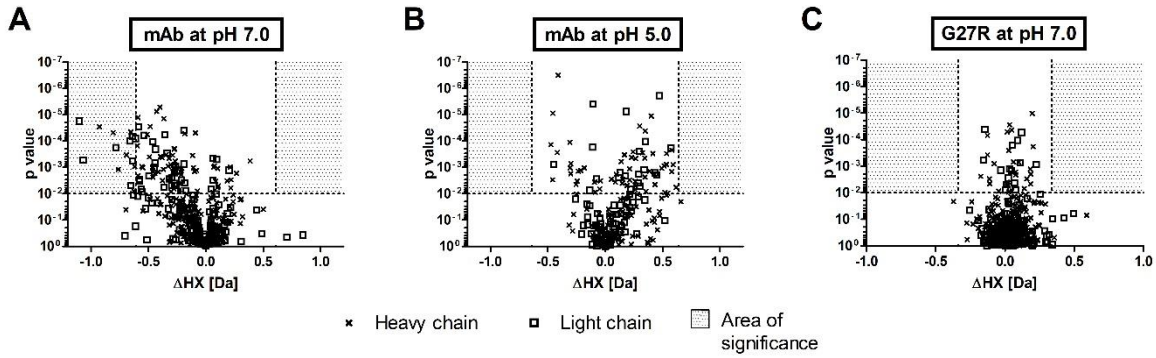

Figure 4 *Volcano plots of HDX-MS analysis of A) wildtype mAb at pH 7.0, ΔHX threshold = 0.61 Da; B) wildtype mAb at pH 5.0, ΔHX threshold = 0.64 Da; C) G27R variant at pH 7.0, ΔHX threshold = 0.34 Da. A peptide list and the calculation of ΔHX threshold can be found in the supplemental material in table S4. As ΔHX, the difference between the uptake at low protein concentration (0.5 mg/ml) and high protein concentration (60 mg/ml) is shown.*

5.4.6 Characterization of mAb variants engineered based on HDX-MS

Subsequently, we designed mAb variants with mutations in the identified hot spots introducing positive (R) or negative charges (D, E) or combinations thereof. The variants were analyzed regarding self-interaction, off-target binding and target binding (Table 2). Binding to the neonatal Fc receptor was not investigated, because the mutated regions were not in spatial proximity to the receptor binding site of our mAb.[41, 42] Introduction of arginine residues in hot spot 1 resulted in decreased self-interaction propensity ($Y_{102}R$, $Q_{105}R$ and $L_{108}R$) while target binding remained unaffected or was slightly improved. As already shown for the $G_{27}R$ variants, the presence of arginine residues increased off-target binding. Introducing aspartate did not affect the self-interaction behavior, improved target binding and only marginally impacted off-target binding ($Y_{102}D$, $Q_{105}D$ and $L_{108}D$). Introduction of more than one aspartate in hot spot 1 led to a decrease in self-interaction combined with improved target binding and decreased off-target binding ($Q_{105}D$-$L_{108}D$ and $Y_{102}D$-$Q_{105}D$-

$L_{108}D$). In addition, we identified residues R_{100} and R_{100a} as residues within HCDR3 contributing to target binding, which confirmed the results of the paratope mapping experiment ($R_{100a}D$, $R_{100a}D$-$Y_{102}D$ and $R_{100}D$-$R_{100a}D$).

We further analyzed the change in self-interaction by mutations of hot spot 2 located in the heavy chain of the Fc fragment. Contrary to hot spot 1, the introduction of one negatively charged aspartate residue decreased self-interaction while maintaining or improving target binding properties ($V_{379}D$). Mutations introducing arginine did not show significant changes in self-interaction ($E_{380}R$ and $E_{382}R$). Interestingly, off-target binding was increased for all the variants of hot spot 2, indicating that the engineering of the Fc region increased unspecific binding processes, presumably mediated via this domain.

Mutations introduced in the light chain of the mAb (hot spot 3) led to a reduction of self-interaction in variants containing arginine in position 155 or aspartate in position 157 or 159 ($S_{155}R$, $N_{157}D$ and $Q_{159}D$). As shown for hot spot 1, we saw a cumulative effect of more multiple negatively charged residues leading to a strongly reduced self-interaction propensity of the 4-fold mutant $S_{155}D$ $N_{157}D$ $Q_{159}D$ $T_{163}D$, resulting in 74 % of the self-interaction propensity of the wildtype (Table S3). Unexpectedly, all variants of the light chain showed an improved target binding behavior, indicating that not only the CDRs of a mAb contribute to target binding. Because this region did not light up in paratope mapping, we hypothesize that this segment of the light chain contributes to target binding by conformational effects. Similar effects were reported for the constant region of an immunoglobulin heavy chain.[43] Another hypothesis is based on the introduction of charged and polar residues, which could mediate additional interactions with the antigen. Additionally, the four fold light chain variant showed decreased off-target binding behavior which was not observed by the single mutations.

In summary, the variants which were engineered based on the HDX-MS results showed decreased self-interaction propensity if one positive charge was introduced in the hot spot 1 or 3. Additionally, self-interaction was reduced for variants in which more than one negatively charged residue was introduced in the region flanking the HCDR3. But a reduction in self-interaction was not necessarily accompanied by a reduction in off-target binding. Thus, HDX-MS results guided towards engineered mutants with reduced self-interaction, several of which additionally showed improved target binding or reduced off-

target binding. Contrary to that, changes in the hydrophobic patch identified by homology modeling reduced self-interaction by reducing the overall off-target binding behavior of the protein. Both approaches guided to mAb variants with decreased self-interaction propensity independent of the engineering approach. The lab-extensive approach including HDX-MS method development and refinement helped to identify specific self-interaction sites outside of the CDRs and thus led to variants with maintained affinity. For rapid identification of unspecificity hot spots, homology modeling followed by protein surface analysis was a valuable tool which can save cost and effort in the laboratory. But engineering may compromise the target binding properties because the paratope is not specified in silico. Further, homology modeling includes only the Fab region and cannot take Fab-Fc interactions or conformational effects into account.

Table 2 *Characterization of mAb variants engineered based on HDX-MS analysis: Experimental parameters were compared to wildtype: (Self-interaction, Target binding: ↓↓ decreased >2SD, ↓ decreased >1SD, ≈ comparable, ↑ increased >1SD, ↑↑ increased >2SD; Off-target binding: ↓↓ < 50 %, ↓ < 75 %, ≈ comparable, ↑ > 125 %; ↑↑ > 150 %). Absolute values can be found in the supplemental material in table S3.*

Hot spot	mAb variant	Domain / Chain	Self-interaction	Off-target binding	Target binding
1	Y102D	Fab/HC	≈	↓	↑↑
	Q105D		≈	≈	↑↑
	L108D		≈	≈	↑↑
	Q105D L108D		↓↓	≈	↑
	Y102D Q105D L108D		↓	↓↓	↑↑
	Y102R		↓	↑↑	↑
	Q105R		↓↓	≈	≈
	L108R		↓↓	↑↑	↑
	R100aD		↓	↓↓	↓
	R100aD Y102D		≈	↓↓	↓↓
	R100D R100aD		↓	↓↓	↓↓
2	V379D	Fc/HC	↓↓	↑	↑↑
	E380R		≈	↑↑	↑
	E382R		≈	↑↑	≈
	N384D		↓	↑	≈
3	S155D	Fab/LC	≈	↑	↑↑
	S155R		↓↓	↑	↑↑
	N157D		↓	↑↑	↑↑
	Q159D		↓	↑	↑↑
	Q159E		≈	↑	↑↑
	T163D		≈	↑	↑↑
	T163R		≈	↑↑	↑↑
	S155D N157D Q159D T163D		↓	≈	↑↑

5.4.7 Engineering of mAb variants based on results of HDX-MS and *in silico* surface analysis

Because both, the *in silico* approach and the *in vitro* HDX-MS approach resulted in mAb variants with improved properties regarding self-interaction, off-target binding and

apparent target binding affinity, we additionally generated and analyzed variants combining input from both methodologies. Based on the low self-interaction propensity, we selected the $G_{27}R$ and $T_{56}D$ variants from the in-silico approach and combined them with $Q_{105}D$, $L_{108}D$ and $N_{384}D$ from the HDX-MS approach, where these variants showed improved self-interaction behavior. Additionally, we chose $N_{384}D$ to generate a variant with mutations in both, Fab and Fc region. The analyzed combinations are shown in Figure 5. The pedigree visualizes how these new combined mAb mutants compare to the single mutants. All variants containing either $G_{27}R$ or $T_{56}D$ showed a decreased attractive self-interaction propensity. For $Q_{105}D$ and $L_{108}D$, a reduction of self-interaction was only observed if both mutations were introduced. The triple mutant $G_{27}R$ $Q_{105}D$ $L_{108}D$ showed the lowest self-interaction propensity. Additionally, target binding was improved. As shown for $G_{27}R$, introduction of arginine at this position increased off-target binding also for the triple mutant.

Based on the HDX-MS results a Fab-Fc interaction was hypothesized as a plausible self-interaction mechanism, because both sites were identified within Fab and Fc domain of the wildtype mAb. For further evaluation, a mutation in the Fab domain ($G_{27}R$) was combined with a mutation in the Fc domain ($N_{384}D$). Interestingly, self-interaction was not further improved compared to the wildtype mAb and the $G_{27}R$ mutant.

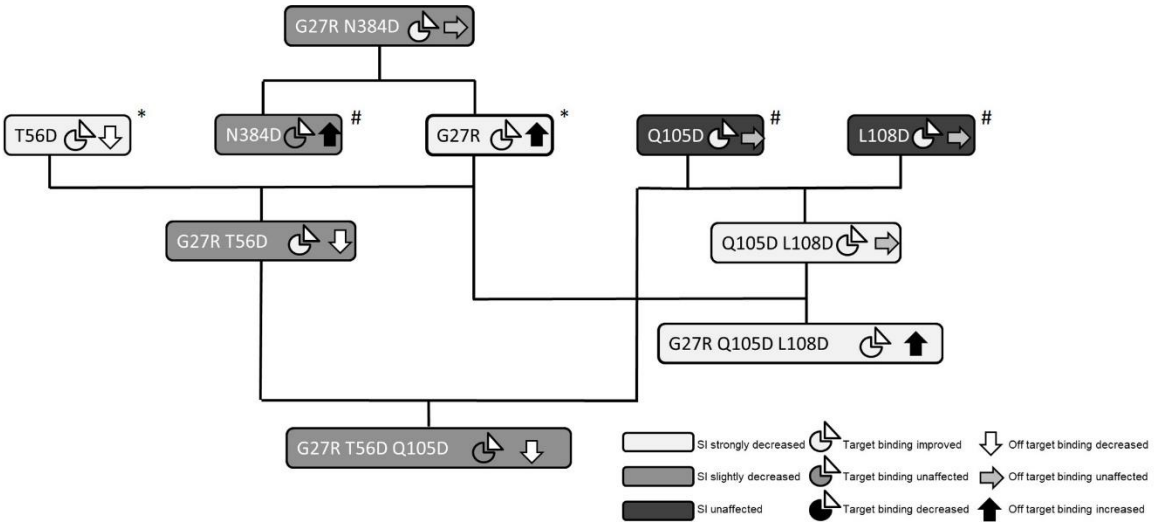

Figure 5 *Pedigree of combination mutants containing heavy chain mutations $G_{27}R$, $T_{56}D$, $Q_{105}D$, $L_{108}D$ and $N_{384}D$. * - variants originate from in-silico approach, # - variants originate from HDX-MS approach. Self-interaction, target binding and off-target binding are shown in relation to the wildtype properties.*

5.4.8 The effect of arginine and aspartate residues on mAb self-interaction

As shown in Tables 1 and 2, we generated variants containing either arginine or aspartate at distinct positions identified by surface analysis or HDX-MS. In total, we evaluated six pairs of this combination. Depending on the position, in 4 out of 6 cases the introduction of arginine decreased self-interaction more pronounced than the corresponding aspartate variant. In particular, this effect was observed for the region flanking HCDR3. Whereas the introduction of aspartate did not influence self-interaction at all, arginine drastically reduced attractive self-interaction. In two cases (G_{55} and T_{56}), both mutations showed the same extent in reduction of self-interaction indicating that the addition of a charged residue itself influenced interaction propensity. As both mutations affected the HCDR2 region of the mAb reflecting the hot spot of off-target binding, this effect could be associated with the overall decrease in off-target binding.

5.4.9 The effect of arginine residues on off-target binding

Within our set of mAb variants, the introduction of arginine residues in HCDR1, HCDR2 or in spatial proximity to HCDR3 increased off-target binding. Corresponding mutations to aspartate residues decreased this propensity. Thus our results confirmed former results by Tiller et al., who demonstrated that the enrichment of arginine residues in the CDRs of scF_v contributed to non-specificity while target binding affinity was improved for variants containing arginine in the CDR.[44] In particular, the introduction of arginine in HCDR1 ($G_{27}R$) led to more affine target binding but impaired off-target binding. However, self-interaction propensity of this variant was significantly reduced. This finding demonstrates that self-interaction propensity is not necessarily connected to non-specificity. The increased off-target binding coming with $G_{27}R$ was also observed for variants containing this mutation in combination. Whereas off-target binding was not affected by the combination of $Q_{105}D$ and $L_{105}D$, the addition of $G_{27}R$ increased off-target binding (Figure 5). Adding the $G_{27}R$ variation to the HCDR2 hydrophobic patch variant ($T_{56}D$), which show substantially reduced off-target binding, did not lead to an increase highlighting the impact of this mutation on off-target binding.

5.5 Conclusions

Here, we presented different, complementary approaches to study self-interaction of a mAb as input for a rational mutagenesis to reduce attractive self-interaction. We applied computational methods such as homology modeling and protein surface analysis of the Fab fragment to identify aggregation prone regions. This strategy enabled us to generate variants with decreased self-interaction by parallel maintaining target binding properties upon a single mutation. Additionally, we identified a hydrophobic patch in the HCDR2 responsible for the increased off-target binding. As an alternative approach, we determined self-interaction sites via HDX-MS by comparing the H/D exchange at high and low protein concentration. The introduction of mutations in the identified self-interaction hot spots reduced the self-interaction propensity of the variants compared to the wildtype mAb. Only for a subset of the generated variants the decrease in self-interaction was accompanied by a reduction in off-target binding. Except for variants with modifications in HCDR3, all variants showed comparable or improved target binding.

For our model system, *in silico* methodologies allowed us to identify residues within and close to the CDRs which could be addressed to reduce self-interaction. A hydrophobic patch in HCDR2 turned out to be additionally a hot spot for off-target binding. HDX-MS gave independent information on self-interaction sites even outside of the CDRs. This input helped to generate variants with in most cases reduced self-interaction, but concomitantly also affected target and off-target binding. For our mAb the introduction of one additional positive charge in form of an arginine in HCDR1 or HCDR2 reduced self-interaction, similar to the effect of introducing two negative charges (aspartates) flanking the HCDR3. In addition, the introduction of acidic residues also decreased off-target binding. If mutagenesis was guided by both, computational and in vitro experiments, we generated variants with properties improved in all investigated aspects, i.e. stronger target binding, lower attractive self-interaction propensity and reduced off-target binding, compared to the wildtype mAb. Thus, both approaches can be successfully applied to guide engineering with the aim to reduce self-interaction, and potentially influence additional parameters. *In silico* modeling provided information on CDR structures, exposed hydrophobic patches and suitable flanking residues amenable to engineering. Self-interaction sites were more specifically identified by HDX-MS experiments. As both approaches gave complementary

input for engineering, also combinatorial variants were generated, which mostly behaved as expected from the individual results obtained with the parental variants. Thus the most effective strategy for similar engineering campaigns should be to apply the combination of both approaches.

5.6 Acknowledgements

This study was part of the project “Self-Interaction and targeted Engineering of monoclonal antibodies (Self-I-E)” funded by the Bayerische Forschungsstiftung (Grant: AZ-1251-16).

References

1. Kaplon H, Muralidharan M, Schneider Z, Reichert JM. Antibodies to watch in 2020. 2020. MAbs 12: 1703531.

2. Roberts CJ. Therapeutic protein aggregation: mechanisms, design, and control. 2014. Trends Biotechnol 32: 372–380.

3. Binabaji E, Ma J, Zydney AL. Intermolecular Interactions and the Viscosity of Highly Concentrated Monoclonal Antibody Solutions. 2015. Pharm Res 32: 3102–3109.

4. Kanai S, Liu J, Patapoff TW, Shire SJ. Reversible self-association of a concentrated monoclonal antibody solution mediated by Fab-Fab interaction that impacts solution viscosity. 2008. J Pharm Sci 97: 4219–4227.

5. Li L, Kumar S, Buck PM, et al. Concentration dependent viscosity of monoclonal antibody solutions: explaining experimental behavior in terms of molecular properties. 2014. Pharm Res 31: 3161–3178.

6. Laue T. Proximity energies: a framework for understanding concentrated solutions. 2012. J Mol Recognit 25: 165–173.

7. Huisman IH, Prádanos P, Hernández A. The effect of protein–protein and protein–membrane interactions on membrane fouling in ultrafiltration. 2000. Journal of Membrane Science 179: 79–90.

8. Arora J, Hu Y, Esfandiary R, et al. Charge-mediated Fab-Fc interactions in an IgG1 antibody induce reversible self-association, cluster formation, and elevated viscosity. 2016. MAbs 8: 1561–1574.

9. Geoghegan JC, Fleming R, Damschroder M, et al. Mitigation of reversible self-association and viscosity in a human IgG1 monoclonal antibody by rational, structure-guided Fv engineering. 2016. MAbs 8: 941–950.

10. Gentiluomo L, Roessner D, Streicher W, et al. Characterization of Native Reversible Self-Association of a Monoclonal Antibody Mediated by Fab-Fab Interaction. 2020. J Pharm Sci 109: 443–451.

11. Dobson CL, Devine PWA, Phillips JJ, et al. Engineering the surface properties of a human monoclonal antibody prevents self-association and rapid clearance in vivo. 2016. Sci Rep 6: 38644.

12. Esfandiary R, Parupudi A, Casas-Finet J, et al. Mechanism of reversible self-association of a monoclonal antibody: role of electrostatic and hydrophobic interactions. 2015. J Pharm Sci 104: 577–586.

13. Lerch TF, Sharpe P, Mayclin SJ, et al. Infliximab crystal structures reveal insights into self-association. 2017. MAbs 9: 874–883.

14. Lilyestrom WG, Yadav S, Shire SJ, Scherer TM. Monoclonal antibody self-association, cluster formation, and rheology at high concentrations. 2013. J Phys Chem B 117: 6373–6384.

15. Nishi H, Miyajima M, Wakiyama N, et al. Fc domain mediated self-association of an IgG1 monoclonal antibody under a low ionic strength condition. 2011. J Biosci Bioeng 112: 326–332.

16. Yadav S, Shire SJ, Kalonia DS. Factors affecting the viscosity in high concentration solutions of different monoclonal antibodies. 2010. J Pharm Sci 99: 4812–4829.

17. Nichols P, Li L, Kumar S, et al. Rational design of viscosity reducing mutants of a monoclonal antibody: hydrophobic versus electrostatic inter-molecular interactions. 2015. MAbs 7: 212–230.

18. Liu J, Nguyen MDH, Andya JD, Shire SJ. Reversible self-association increases the viscosity of a concentrated monoclonal antibody in aqueous solution. 2005. J Pharm Sci 94: 1928–1940.

19. Neergaard MS, Kalonia DS, Parshad H, et al. Viscosity of high concentration protein formulations of monoclonal antibodies of the IgG1 and IgG4 subclass - prediction of viscosity through protein-protein interaction measurements. 2013. Eur J Pharm Sci 49: 400–410.

20. Pindrus MA, Shire SJ, Yadav S, Kalonia DS. The Effect of Low Ionic Strength on Diffusion and Viscosity of Monoclonal Antibodies. 2018. Mol Pharm 15: 3133–3142.

21. Luo H, Macapagal N, Newell K, et al. Effects of salt-induced reversible self-association on the elution behavior of a monoclonal antibody in cation exchange chromatography. 2014. J Chromatogr A 1362: 186–193.

22. Dear BJ, Hung JJ, Truskett TM, Johnston KP. Contrasting the Influence of Cationic Amino Acids on the Viscosity and Stability of a Highly Concentrated Monoclonal Antibody. 2017. Pharm Res 34: 193–207.

23. Sahin E, Grillo AO, Perkins MD, Roberts CJ. Comparative effects of pH and ionic strength on protein-protein interactions, unfolding, and aggregation for IgG1 antibodies. 2010. J Pharm Sci 99: 4830–4848.

24. Sarangapani PS, Weaver J, Parupudi A, et al. Both Reversible Self-Association and Structural Changes Underpin Molecular Viscoelasticity of mAb Solutions. 2016. J Pharm Sci 105: 3496–3506.

25. Bethea D, Wu S-J, Luo J, et al. Mechanisms of self-association of a human monoclonal antibody CNTO607. 2012. Protein Eng Des Sel 25: 531–537.

26. Wu S-J, Luo J, O'Neil KT, et al. Structure-based engineering of a monoclonal antibody for improved solubility. 2010. Protein Eng Des Sel 23: 643–651.

27. Arora J, Hickey JM, Majumdar R, et al. Hydrogen exchange mass spectrometry reveals protein interfaces and distant dynamic coupling effects during the reversible self-association of an IgG1 monoclonal antibody. 2015. MAbs 7: 525–539.

28. Teplyakov A, Obmolova G, Wu S-J, et al. Epitope mapping of anti-interleukin-13 neutralizing antibody CNTO607. 2009. J Mol Biol 389: 115–123.

29. Rabia LA, Desai AA, Jhajj HS, Tessier PM. Understanding and overcoming trade-offs between antibody affinity, specificity, stability and solubility. 2018. Biochem Eng J 137: 365–374.

30. Starr CG, Tessier PM. Selecting and engineering monoclonal antibodies with drug-like specificity. 2019. Curr Opin Biotechnol 60: 119–127.

31. Jain T, Sun T, Durand S, et al. Biophysical properties of the clinical-stage antibody landscape. 2017. Proc Natl Acad Sci U S A 114: 944–949.

32. Prassler J, Thiel S, Pracht C, et al. HuCAL PLATINUM, a synthetic Fab library optimized for sequence diversity and superior performance in mammalian expression systems. 2011. J Mol Biol 413: 261–278.

33. Frese K, Eisenmann M, Ostendorp R, et al. An automated immunoassay for early specificity profiling of antibodies. 2013. MAbs 5: 279–287.

34. Domnowski M, Jaehrling J, Frieß W. Assessment of Antibody Self-Interaction by Bio-Layer-Interferometry as a Tool for Early Stage Formulation Development. 2020. Pharm Res 37: 29.

35. Wei H, Ahn J, Yu YQ, et al. Using hydrogen/deuterium exchange mass spectrometry to study conformational changes in granulocyte colony stimulating factor upon PEGylation. 2012. J Am Soc Mass Spectrom 23: 498–504.

36. Wales TE, Fadgen KE, Gerhardt GC, Engen JR. High-speed and high-resolution UPLC separation at zero degrees Celsius. 2008. Anal Chem 80: 6815–6820.

37. Hageman TS, Weis DD. Reliable Identification of Significant Differences in Differential Hydrogen Exchange-Mass Spectrometry Measurements Using a Hybrid Significance Testing Approach. 2019. Anal Chem 91: 8008–8016.

38. Eylenstein R, Weinfurtner D, Härtle S, et al. Molecular basis of *in vitro* affinity maturation and functional evolution of a neutralizing anti-human GM-CSF antibody. 2016. MAbs 8: 176–186.

39. Sankar K, Krystek SR, Carl SM, et al. AggScore: Prediction of aggregation-prone regions in proteins based on the distribution of surface patches. 2018. Proteins 86: 1147–1156.

40. Hötzel I, Theil F-P, Bernstein LJ, et al. A strategy for risk mitigation of antibodies with fast clearance. 2012. MAbs 4: 753–760.

41. Ghetie, V.; Ward, E.S. Multiple roles for the major histocompatibility complex class I-related receptor FcRn. 2000. Annual Review of Immunology, 18, 739-766.

42. Jensen, P.F.; Larraillet, V; Schlothauer T et al. Investigating the interaction between the neonatal Fc receptor and monoclonal antibody variants by hydrogen/deuterium exchange mass spectrometry. 2014. Molecular & Cellular Proteomics 1: 148-161

43. Torres M, Casadevall A. The immunoglobulin constant region contributes to affinity and specificity. 2008. Trends Immunol 29: 91–97.

44. Tiller KE, Li L, Kumar S, et al. Arginine mutations in antibody complementarity-determining regions display context-dependent affinity/specificity trade-offs. 2017. J Biol Chem 292: 16638–16652.

Supplementary data

Table S1 *Peptide list of paratope mapping*

Chain	start	end	Sequence	time	ΔHX	p-value
Heavy Chain	46	58	EWMGGIIPIYGTA	1	-1.08	0.001
	46	58	EWMGGIIPIYGTA	10	-0.90	0.000
	46	58	EWMGGIIPIYGTA	60	-0.75	0.000
	46	58	EWMGGIIPIYGTA	240	-0.66	0.000
	48	59	MGGIIPIYGTAY	1	-1.08	0.001
	48	59	MGGIIPIYGTAY	10	-0.77	0.003
	48	59	MGGIIPIYGTAY	60	-0.81	0.000
	48	59	MGGIIPIYGTAY	240	-0.92	0.001
	50	59	GIIPIYGTAY	1	-1.09	0.001
	50	59	GIIPIYGTAY	60	-0.52	0.000
	50	59	GIIPIYGTAY	240	-0.53	0.001
	103	111	YVTYRRYWF	1	-0.85	0.001
	103	111	YVTYRRYWF	10	-0.80	0.009
	103	111	YVTYRRYWF	60	-1.18	0.000
	103	111	YVTYRRYWF	240	-1.33	0.000
	103	112	YVTYRRYWFD	1	-0.81	0.001
	103	112	YVTYRRYWFD	10	-0.79	0.009
	103	112	YVTYRRYWFD	60	-1.18	0.000
	103	112	YVTYRRYWFD	240	-1.43	0.000
	103	113	YVTYRRYWFDY	1	-1.11	0.000
	103	113	YVTYRRYWFDY	10	-0.68	0.000
	103	113	YVTYRRYWFDY	60	-1.59	0.000
	103	113	YVTYRRYWFDY	240	-1.70	0.000
	104	113	VTYRRYWFDY	1	-0.80	0.000
	104	113	VTYRRYWFDY	10	-0.71	0.010
	104	113	VTYRRYWFDY	60	-1.35	0.000
	104	113	VTYRRYWFDY	240	-1.64	0.000
	106	113	YRRYWFDY	1	-0.45	0.000
	106	113	YRRYWFDY	60	-1.09	0.000
	106	113	YRRYWFDY	240	-1.35	0.000

Criteria for significant differences of ΔHX:

Pooled standard deviation sp = 0.135, standard error of the mean SEM = 0.11, Confidence criteria for ΔHX values were calculated by following equation: $|\Delta HX| > k \times SEM$ using k = -3.75 according to Student's t-distribution (One-tailed, α = 0.01, df = 4)

Table S2 *Characterization of mAb variants generated based on in silico surface analysis - Absolute values*

mAb variant	Region	Self-interaction [%]		Off-target binding [%]	Target binding K_D^{app} [nM]	
		Average	SD		Average	SD
Wildtype	---	100.0	13.9	100	7.7	1.0
I52R	HCDR2	83.0	4.0		5.9	0.8
I53R		70.6	2.0		6.6	0.2
Y54R		67.6	2.0		7.4	0.4
Y58R		67.9	3.0		7.3	0.4
G55R		50.0	2.0	180	6.0	0.2
G55D		66.0	8.0		6.8	0.6
T56R		75.4	2.0		5.7	0.4
T56D		50.4	2.0	25	5.9	0.6
I52A I53A Y54A Y58A		127.8	3.0	8	9.7	0.5
I52A I53A Y54S Y58S		110.0	3.0	16	11.1	0.4
I52V I53V Y54A Y58A		86.2	3.0	18	9.8	0.6
I52V I53V Y54S Y58S		63.4	3.0	12	9.7	0.6
W100cV	HCDR3	135.5	2.0	67	5.8	0.2
W100cS		124.8	1.0	67	7.7	0.4
G27R	HCDR1	48.8	2.0	161	5.4	0.7
G27R T56D	HCDR1/HCDR2	85.7	7.4	61	6.3	0.8

Table S3 *Characterization of mAb variants engineered based on HDX-MS analysis – Absolute values*

Hot spot	mAb variant	Domain / Chain	Self-interaction [%]		Off-target binding [%]	Target binding [nM]	
			Average	SD		Average	SD
---	**Wildtype**	---	100.0	13.9	100	7.7	1.0
1	**Y102D**	Fab/HC	100.0	7.7	64	5.3	0.5
	Q105D		96.0	8.0	120	5.3	0.7
	L108D		88.0	5.0	118	5.3	0.5
	Q105D L108D		58.6	2.3	99	6.0	0.5
	Y102D Q105D L108D		81.4	1.9	38	5.6	0.6
	Y102R		73.2	2.0	180	5.8	0.8
	Q105R		65.7	2.5	119	7.0	0.9
	L108R		69.2	3.7	171	6.6	0.5
	R100aD		76.4	1.2	1	9.6	0.6
	R100aD Y102D		90.7	4.5	1	11.1	0.4
	R100aD R100		77.8	2.3	1	22.1	1.0
2	**V379D**	Fc/HC	53.5	0.8	140	4.5	0.9
	E380R		96.1	5.0	176	6.6	0.7
	E382R		90.9	4.4	183	7.2	0.8
	N384D		8.9	0.1	144	7.2	0.7
3	**S155D**	Fab/LC	95.2	8.8	144	4.0	0.7
	S155R		71.6	2.8	135	5.5	0.9
	N157D		82.4	1.5	160	4.7	0.8
	Q159D		85.3	3.7	139	4.7	0.6
	Q159E		95.8	1.5	140	4.7	0.6
	T163D		90.9	4.7	144	5.1	0.7
	T163R		93.0	3.9	151	4.7	0.6
	S155D N157D Q159D		74.1	1.8	119	5.4	0.8

Table S4. Peptide list of self-interaction sites mapping

Chain	start	end	Sequence	time	ΔHX	p-value
Heavy Chain	103	112	YVTYRRYWFD	10	-0.925	0.000
	103	113	YVTYRRYWFDY	10	-0.595	0.000
	104	119	VTYRRYWFDYWGQGTL	2	-0.761	0.001
	104	119	VTYRRYWFDYWGQGTL	10	-0.806	0.000
	106	119	YRRYWFDYWGQGTL	2	-0.589	0.002
	106	119	YRRYWFDYWGQGTL	10	-0.653	0.000
	107	119	RRYWFDYWGQGTL	10	-0.592	0.000
	363	387	EEMTKNQVSLTCLVKGFYPSDIAVE	10	-0.627	0.008
	387	405	EWESNGQPENNYKTTPPVL	2	-0.692	0.000
	388	405	WESNGQPENNYKTTPPVL	2	-0.620	0.001
Light Chain	150	173	KVDNALQSGNSQESVTEQDSKDST	2	-1.069	0.001
	150	173	KVDNALQSGNSQESVTEQDSKDST	10	-1.101	0.000
	156	173	QSGNSQESVTEQDSKDST	2	-0.560	0.007
	163	179	SVTEQDSKDSTYSLSST	2	-0.576	0.003
	163	179	SVTEQDSKDSTYSLSST	10	-0.580	0.003
	163	180	SVTEQDSKDSTYSLSSTL	2	-0.584	0.000
	163	180	SVTEQDSKDSTYSLSSTL	10	-0.637	0.000
	168	193	DSKDSTYSLSSTLTLSKADYEKHKVY	10	-0.652	0.005
	168	195	DSKDSTYSLSSTLTLSKADYEKHKVYAC	10	-0.782	0.000

Criteria for significant differences of ΔHX:

Wildtype mAb at pH 7.0

Pooled standard deviation sp = 0.183, standard error of the mean SEM = 0.15, Confidence criteria for ΔHX values were calculated by following equation: $|\Delta HX| > k \times SEM$ using k = -3.75 according to Student's t-distribution (One-tailed, α = 0.01, df = 4)

Wildtype mAb at pH 5.0

Pooled standard deviation sp = 0.208, standard error of the mean SEM = 0.17, Confidence criteria for ΔHX values were calculated by following equation: $|\Delta HX| > k \times SEM$ using k = -3.75 according to Student's t-distribution (One-tailed, α = 0.01, df = 4)

G_{27}R variant at pH 7.0

Pooled standard deviation sp = 0.107, standard error of the mean SEM = 0.09, Confidence criteria for ΔHX values were calculated by following equation: $|\Delta HX| > k \times SEM$ using k = -3.75 according to Student's t-distribution (One-tailed, α = 0.01, df = 4)

Chapter 6 Resolving high self-interaction propensity of therapeutic mAbs by *in silico* surface analysis and rational engineering

M. Domnowski[1,2], J. Binder[1], F. Kummer[2], J. Reindl[2], L. Lehmann[2], M. Satzger[2], J. Jaehrling[2], W. Frieß[1]

[1]Department of Pharmacy: Pharmaceutical Technology and Biopharmaceutics; Ludwig-Maximilians-Universitaet Muenchen, Butenandtstrasse 5, 81377 Munich, Germany

[2]MorphoSys AG, Semmelweisstraße 7, 82152 Planegg

Author contributions:

M.D., J.J. and W.F. conceived and designed the study. M.D. conducted and analyzed homology modelling, SI-BLI, mAb production and *protein-sol* calculations, J.B. conducted homology modelling, F.K. and L.L. conducted mAb production, J.R. performed mAb cloning, M.S. performed and analyzed 3P measurements, J.J. conducted and analyzed SPR experiments. M.D., J.J. and W.F. analyzed and interpreted the data and contributed to the writing of the manuscript.

Keywords: Antibody; Protein; Self-interaction; Self-association; Mutagenesis; AggScore; Protein-sol

Abbreviations: HIC – Hydrophobic Interaction Chromatography; CIC – Cross-Interaction Chromatography; CSI – Clone Self-Interaction; AC-SINS – Affinity-Capture Self-Interaction Nanoparticle Spectroscopy; SI-BLI – Self-Interaction Bio Layer Interferometry; CDR – Complementary Determining Region; DSF – Differential Scanning Fluorimetry; 3P – Protein Panel Profiling

6.1 Abstract

Strong attractive self-interaction of monoclonal antibodies (mAbs) poses the risk for limited solubility, increased aggregation propensity, and high viscosity at elevated protein concentration. We describe the improvement of two strongly self-interacting wildtype mAbs which are related, have the same target and show these adverse properties. Based on homology modeling and calculation of aggregation scores we designed and generated 26 variants. Self-interaction as well as target and off-target binding were characterized. Hydrophobic patches affected both self-interaction, as well as target binding. The LCDR3 hosts a self-interaction hot spot whereas a hydrophobic patch in the HCDR3 mediated target binding. Variants based on rational mutagenesis within the LCDR3 showed improved self-interaction behavior at a maintained highly affine target binding. The experimental results were compared to the mAbs' biophysical properties predicted by the algorithm of *protein-sol*. *Protein-sol* was able to distinguish between the model systems but showed limitations in its capability to predict the self-interaction behavior of the variants. Thus the approach of *in silico* identification of aggregation hot spots and subsequent generation and experimental characterization for mAb variants proved to be most suitable to achieve leads with low self-interaction and off-target binding as well as high target affinity during candidate selection.

6.2 Introduction

Attractive self-interaction processes of mAbs can be key driver for native oligomerization.[1] These oligomers can form clusters which entail a tremendous increase in viscosity[2–4], an enhanced tendency for aggregation[5] as well as downstream processing challenges.[6] Each domain of a mAb molecule can be involved in the self-interaction processes [3, 7–14] which are driven by both, electrostatic and hydrophobic forces.[11, 15, 16] Formulation factors such as pH and excipients influence the properties of the molecule and consequently impact aggregation propensity and solution viscosity.[9, 17–23] However, formulation development is usually initiated after lead candidate selection. At earlier project stages, during the selection process itself, changes within the protein sequence are still possible to address an enhanced self-interaction propensity.

Mutations can be introduced based on rationales derived from molecular modelling or experimental data.[8, 16, 24, 25] *In silico* methodologies have been developed to predict biophysical properties based on primary sequence alone, or in combination with structural information of homology models. Recently, Hebditch and Warwicker published a machine learning approach trained with the biophysical properties of 137 clinical stage or approved antibodies.[26, 27] This tool, called *protein-sol*, is available as web application and provides predictions based on the primary sequence of the variable fragment. Prediction of aggregation prone regions (APRs) is also possible with AggScore which is based on 3D homology models.[28] The input structure is used to calculate the energetic contribution of each residue to surface patches which can be hydrophobic or electrostatic in nature. Sankar et al. applied the AggScore algorithm on selected biophysical parameters of the dataset published by Jain et al. and observed correlations between hydrophobic interaction chromatography, cross interaction chromatography and standup monolayer adsorption chromatography with AggScore.[27, 28] Mutations based on computational methodologies were successfully applied to improve solubility and reduce viscosity at high concentration for mAbs. This can be achieved by disruption of a hydrophobic patch and neutralization of a negatively charged surface by single mutation[16] or by introduction of asparagine and positively charged residues such as arginine or lysine without negatively affecting target binding.[29]

The mAb CNTO607 has been used in various studies as an example for a mAb with low solubility and high self-interaction propensity.[24, 30, 31] A hydrophobic triad within the HCDR3 ($F_{99}H_{100}W_{100a}$) was shown to mediate aggregation of CNTO607.[25] Engineering of the hydrophobic patches increased solubility but diminished target binding, e.g. variants including $W_{100a}A$ [24] and $F_{99}A\ H_{100}AW_{100a}A$, also called mAbVI. [25] The precursor of CNTO607, a phage display derived mAb against hIL-13 from the Human Combinatory Antibody Library HuCAL GOLD[32] is used in the present study and is referred to as mAb1. The second mAb, mAb2, targets the same antigen.The two mAbs show a sequence similarity of 99.5 % and exhibited precipitation in typical platform formulations like PBS and phase separation after storage at 2-8°C during downstream processing.

Previous studies showed the generation of variants of CNTO607, which include mutations within the HCDR3 as the most striking hydrophobic patch of this mAb. By mutagenesis of this target binding region, the variants showed impaired antigen affinity. Therefore, in this

study we applied homology modelling and computational tools to understand the structure of the molecules and identify critical residues as a starting point for engineering. Variants of the two mAbs were generated with the aim of improving self-interaction behavior while maintaining the high affinity for the target, and the low off-target binding propensity. In addition to the hydrophobic patch of the HCDR3, we identified an additional hydrophobic patch in the LCDR3 which was not involved in target binding but in self-interaction processes. The aggregation propensity calculated based on AggScore corresponded with self-interaction determined by SI-BLI. The introduction of either positively or negatively charged residues in spatial proximity of the hydrophobic patches reduced self-interaction. By using computational techniques, lab and cost extensive techniques to identify self-interaction hot spots such as hydrogen deuterium exchange mass spectrometry were avoided, and distinct sequences for rational mutagenesis were defined faster. Our data extend the already published data set for CNTO607 and help to understand self-interaction processes for challenging mAbs based on structural analysis. Furthermore, we challenged our approach of experimentally generating and characterizing mAb variants by comparing our results with physico-chemical properties predicted by the machine learning tool protein-sol, which would have been a faster way to find superior variants.

6.3 Material and Methods

6.3.1 mAb cloning

Genestrings of mutated V_L and V_H were purchased from Thermo Fisher Scientific (MA). The DNA fragments were designed with a 21 bp overlap next to restriction enzyme sites. After Gibson cloning, the constructs were transformed in chemically competent DH5alpha cells. From resulting single colonies, Miniprep Plasmid DNA was prepared and sequenced. After consolidation via 50 pg retransformation the final plasmid Maxiprep DNA was used for transfection and expression of the constructs.

6.3.2 mAb production

The wildtype mAb was expressed in HKB11 stable pool expression system for 6 days. Cell culture supernatant was applied to a MabSelect SuRe column of 32 ml column volume (CV) (Cytiva, MA) equilibrated with 0.1 M sodium phosphate buffer pH 6.0 (NaPhos pH

6). After washing with 5 CV NaPhos pH 6, product was eluted with 0.1 M sodium acetate buffer pH 3.0. Protein containing fractions were pooled and adjusted to pH 5 with 2 M sodium acetate solution. The concentration was determined by UV absorbance at 280 nm (molar extinction coefficient 211580 M^{-1} cm^{-1}, 146.6 kDa) using Nanodrop 2000 (Thermo Fischer Scientific, MA).

The protein containing pool was subjected to buffer exchange using Sephadex G-25 in PD-10 desalting columns (Cytiva, MA) to the final formulation buffer (15 mM histidine hydrochloride pH 6.0). The concentration was determined by UV absorbance and adjusted to 20 mg/mL utilizing Amicon Ultra 15 centrifugal filter units (50 kDa cut-off, Merck KGaA, Germany). The final product was sterile filtered using a 50 mL Steriflip (Merck KGaA, Germany).

The protein variants were expressed in HEK293 cells for 6 days after transfection. Cell culture supernatants were applied to HiTrap MabSelect SuRe columns (Cytiva, MA) installed on an Äkta Xpress system equilibrated with NaPhos pH 6. Three washing steps were performed (wash 1: 5 CV NaPhos pH 6, wash 2: 5 CV NaPhos pH 6 + 1.5 M NaCl, wash 3: 5 CV NaPhos pH 6). Product was eluted with 0.1 M sodium acetate buffer pH 3 and protein containing fractions were pooled without pH adjustment. The protein containing pools were subjected to buffer exchange using Sephadex G-25 in PD-10 desalting columns (Cytiva, MA) to the final formulation buffer (15 mM histidine hydrochloride pH 6.0). The concentration was determined by UV absorbance at 280 nm using an average molar extinction coefficient of 208356 M^{-1} cm^{-1} and an average molecular weight of 146.6 kDa using Nanodrop 2000 (Thermo Fischer Scientific, MA). The final products were sterile filtered using Microsep Advance Centrifugal Devices (PALL, NY) and analyzed for monomer content by SEC-MALS. All variants contained a monomer portion of > 90 %.

6.3.3 Self-interaction Bio layer interferometry (SI-BLI)

SI-BLI was performed as described previously.[33] Briefly, anti-hIgG Fc capture biosensors were used on an Octet HTX system (Sartorius AG, FortéBio, CA) in a 384 well plate format. A baseline was established in PBS (Gibco), followed by capture of the mAb of interest at 25 nM in PBS until the BLI signal increased by approximately 1 nm followed

by saturation of the sensor with 1 μM human Fc in PBS. Subsequently, a second baseline was acquired in the formulation composition, followed by an association step with 2 μM mAb in the same formulation. The response at equilibrium normalized to the amount of captured mAb (R_{rel}) was used for further calculations. As control, sensors saturated with human Fc without IgG capture were used.

6.3.4 Homology Modelling and Protein Surface Analysis

Homology models of the wildtype mAb were generated with BioLuminate (Schrödinger Release 2019-4, Schrödinger LLC, NY). Homology modelling of the Fab fragment was based on the published crystal structure of CNTO607 (PDB: 3G6D) achieving a composite score of 0.99 for mAb1 and 0.97 for mAb2. A restrained minimization using the OPLS3e force field was performed. For both mAbs, loops of the LCDR1 to the HCDR2 were modelled by automated cluster selection and the HCDR3 by a built-in PRIME module for H3 prediction. The AggScore was calculated with the Protein Surface Analysis module. *In silico* mutations were generated with the residue-scanning module followed by backbone minimization and calculation of the solvent exposed surface area (SASA). Residue specific AggScores within the regions were added up for each model.

6.3.5 Protein-sol Analysis

Based on the *protein-sol* algorithm, regression values of 12 biophysical properties were calculated for our data set (https://protein-sol.manchester.ac.uk/abpred).[26] The variants were ranked regarding self-interaction, off-target binding and apparent temperature of unfolding. Afterwards, we ranked the mAbs of our data set based on our own experimental SI-BLI, protein panel profiling (3P) and nanoDSF results. Spearman correlation coefficients were calculated by PRISM 5 (GraphPad, CA). Raw data for apparent unfolding temperature and results from protein panel profiling can be found as supplemental material (Table S1).

6.3.6 Protein Panel Profiling (3P)

The method was performed as described before.[34] Briefly, off target binding of MAb samples was assessed in a plate-based assay, using electrochemiluminescence readout. A panel of 32 proteins and controls including highly abundant serum proteins, different cytokines and cell-surface receptors, proteins bearing different post-translational modifications (phosphorylation, glycosylation), representatives for different pI values (ranging from 2.8 to 10.7), and vesicles prepared from HKB11 cells and Baculovirus particles[35] as well as protein A, anti-human Fc and anti-human Fab antibodies, lysozyme and target proteins of the sample MAbs as controls was coated onto two MSD standard 384-well plates (Meso Scale Discovery, MD) per assay, each row coated with one protein or control. Subsequently, the plate was blocked with 3 % (w/v) BSA in PBS. Each mAb sample was assessed at 10 nM and 100 nM. For referencing purposes, an anti-lysozyme mAb was included known to show negligible non-specific binding. ECL-labeled anti-human Fab antibody was added for detection, and ECL-signals acquired using a Sector Imager S 600 instrument (Meso Scale Discovery, MD). For evaluation, binding signals of the mAb of interest were divided by the signal of the anti-lysozyme mAb on the same protein, resulting in a binding ratio. The sum of binding ratios on all off target probes (i.e. excluding specific antigens and controls) at 10 nM and 100 nM mAb were used as a metric for off target binding of the respective mAb.

6.3.7 Target Binding Analysis by SPR

Affinities were determined in kinetic experiments using a Biacore 8K+ instrument (Cytiva, MA). 0.01 M HEPES pH 7.4 with 0.15 M NaCl, 3 mM EDTA, and 0.05% (v/v) polysorbate 20 was used as assay buffer. Human IL-13 was produced and purified at MorphoSys and contained at 93% monomer by SEC-MALS. A high-capacity, high–affinity capture surface was prepared by covalently immobilizing MabSelect SuRe ligand (Cytiva, MA) at high density onto all flowcells and channels of a CM5 SPR chip (BR-1005-30; approx. 3700 RU). With each mAb (approx. 70 RU) captured onto one channel of the sensor, serial dilutions of hIL-13 (up to seven concentrations; highest concentration between 100 nM and 900 nM, depending on the K_D of the individual interaction) were analyzed in separate cycles for 240 s at 30 µL/min with subsequent 1200 s dissociation phase (multi-cycle

kinetics). At the end of each cycle, mAb and remaining bound antigen were completely removed from the sensor by two 30 s injections of Glycine / HCl pH 1.5. The sensorgrams were fitted to a monovalent binding model with both rate constants (k_{on}, k_{off}) fitted globally and bulk RI fixed at 0 RU. Sensorgrams not contributing to the kinetics (insignificant or no signal) were excluded from evaluation. All interactions were characterized at least in duplicate (n=2 to n=4).

6.3.8 Nano Differential Scanning Fluorimetry (nanoDSF)

1 mg/ml mAb samples were filled in standard nanoDSF glass capillaries and measurements were performed using a Prometheus NT.48 (NanoTemper Technologies, Germany). Intrinsic fluorescence at 330 nm and 350 nm was evaluated during a temperature ramp from 20 °C to 90 °C at 1 K/min. Transition onset and inflection points were determined from the first derivative using the PR.Control software (NanoTemper, Germany).

6.4 Results

6.4.1 Identification of self-interaction sites by *in silico* surface analysis

We generated homology models of mAb1 and mAb2 using the published crystal structure of CNTO607.[36] After model refinement, surface analysis was performed to calculate AggScores and SASA of residues in the CDRs (Table 1).

For mAb1, aggregation prone regions were identified in the LCDR3 and the HCDR3 (Figure 1A and B). The identification of the hydrophobic triad containing phenylalanine, histidine and tryptophan ($F_{99}HW_{100a}$) in the HCDR3 as aggregation hot spot confirmed previously published data for CNTO607.[24, 25] The SASA of W_{100a} was the highest in this patch pointing towards hydrophobic interactions mediated by this residue as the potential driver for aggregation. A patch consisting of methionine (M_{93}) and valine (V_{94}) in the LCDR3 was identified as second hydrophobic, aggregation prone region with M_{93} showing the highest solvent accessibility. Consequently, we selected M_{93} in the LCDR3 and the hydrophobic triad of the HCDR3 containing W_{100a} for structure guided engineering. Additionally, we generated the mAb formerly published as CNTO607 and its variants mAbVI and W_{100a}A in order to compare our data set to literature. The variants which

include alanine mutations in the HCDR3 were shown to have an improved solubility but diminished target binding. [24, 25]

For mAb2, two major aggregation prone regions were identified in the LCDR3 and the HCDR3 (Figure 1C and D). In the LCDR3, valine (V_{94}) and tyrosine (Y_{95}) showed the highest AggScores and highest surface accessibility. In the HCDR3, the patch $F_{99}VYLFF_{100d}$ contributed most to the surface exposed hydrophobicity. In addition to these two major hot spots, hydrophobic residues phenylalanine and tyrosine in the LCDR1 ($F_{31}Y_{32}$) contributed to an aggregation prone region but the AggScores were lower than in LCDR3 and HCDR3. To this end, $F_{99}VY_{100}$ in the HCDR3 and V_{94} and Y_{95} in the LCDR3 were mutated and additionally, aspartate (D_{27}) in the LCDR1, which is in spatial proximity to its hydrophobic residues. As shown by Teplyakov et al., the HCDR1 plays a subordinate role in IL-13 binding. Thus, we chose phenylalanine (F_{27}) as the most solvent accessible residue of the HCDR1 for further engineering to improve target binding affinity by introducing tryptophan as a more hydrophobic amino acid to enhance the interaction with IL-13. The generated and characterized mAb variants are shown in Table 2.

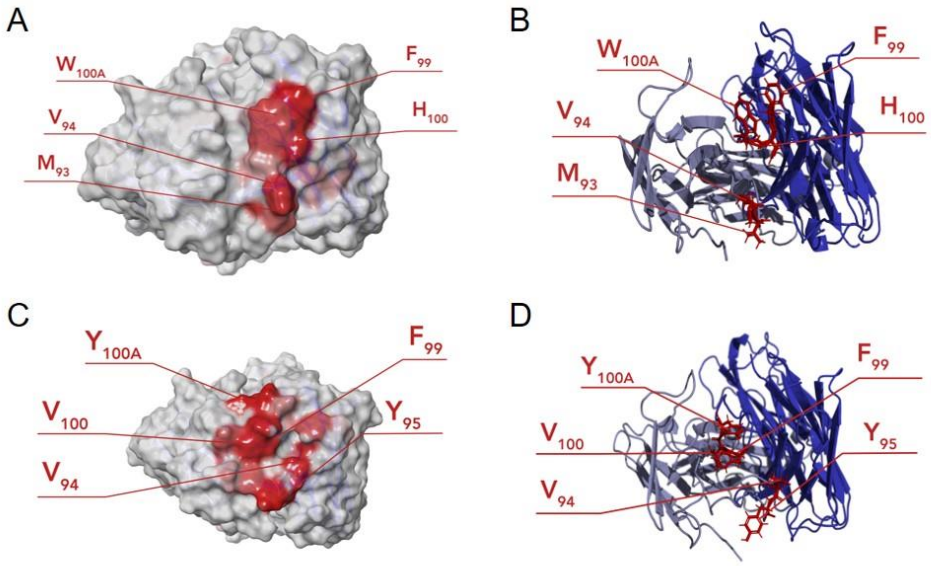

Figure 1 *Homology models of Fab fragments of mAb1 and mAb2. Grey: Light Chain; Blue: Heavy Chain; Red: Aggregation prone residues (high AggScore). A) Homology model and surface analysis of mAb1; B) Aggregation hot spot of mAb1 in HCDR3 ($F_{99}HW_{100a}$) and LCDR3 ($M_{93}V_{94}$); C) Homology model and surface analysis of mAb2; D) Aggregation hot spot of mAb2 in HCDR3 ($F_{99}VY_{100a}$) and LCDR3 ($V_{94}Y_{95}$).*

Table 1 *AggScores and SASA of residues located in hydrophobic patches of mAb1 and mAb2.*

Protein	Area	Residue	SASA [Å^2]	AggScore
mAb1	LCDR3	W91	50.5	4
		D92	20.5	8
		M93	165.5	9
		V94	91.0	6
		T95	45.6	0
		D95a	8.6	0
	HCDR3	A98	14.0	12
		F99	85.9	17
		H100	58.2	18
		W100a	146.5	7
		D100b	38.8	2
		M100c	0.0	0
		Q100d	7.7	0
		P100e	2.3	0
		D101	11.0	0
		Y102	112.1	0
mAb2	LCDR1	S24	40.7	0
		G25	17.6	0
		D26	116.3	0
		N27	7.9	0
		L28	1.1	0
		G29	56.8	0
		T30	117.7	6
		F31	47.8	8
		Y32	83.8	8
	LCDR3	S90	0.0	0
		F91	0.2	0
		D92	10.2	1
		T93	5.2	5
		V94	87.4	9
		Y95	173.1	10
	HCDR1	G26	45.3	0
		F27	109.8	0
		T28	82.3	0
		F29	7.6	0
		S30	56.6	0
		S31	57.2	0
		Y32	13.3	0
	HCDR3	F97	86.3	4
		G98	12.8	0
		F99	69.0	12
		V100	0.0	0
		Y100a	128.8	18
		L100b	49.1	21
		F100c	105.5	21
		F100d	45.2	17
		D101	3.6	0
		Y102	43.9	4

6.4.2 AggScore analysis of variants of mAb1 and mAb2

AggScores of mAb variants were calculated by surface analysis of homology models (Table 3). For mAb1, AggScores were decreased for the LCDR3 variants mAb1-6 ($M_{93}A$) and mAb1-7 ($M_{93}R$) as well as for the HCDR3 variants $W_{100a}A$, mAbVI ($A_{99}AA_{100a}$), mAb1-4 ($F_{99}HE_{100a}$) and mAb1-5 ($Y_{99}HH_{100a}$).

LCDR3 mutants of mAb2, $V_{94}Y_{95}$ to $A_{94}A_{95}$ (mAb2-5 and mAb2-12) and Y_{95} to T_{95} (mAb2-15) showed a markedly decreased AggScore compared to the wildtype and complete removal of hydrophobic residues as embodied by e.g. mAb2-6 ($V_{94}Y_{95}$ to $E_{94}S_{95}$) reduced the AggScore more than the introduction of a less hydrophobic residue e.g. in mAb2-7 ($V_{94}Y_{95}$ to $E_{94}L_{95}$). Also the HCDR3 mutation of mAb2 in case of mAb2-1 to mAb2-4, mAb2-8 to mAb2-10 and mAb2-15 led to lower AggScore. As observed for LCDR3, the complete removal of the hydrophobic residues in the HCDR3 represented by mAb2-1 ($A_{99}A_{100}A_{100a}$) had a more significant impact than a decrease in hydrophobicity by introducing less hydrophobic residues as reflected in mAb2-9 ($V_{99}A_{100}T_{100a}$).

6.4.3 Conformational properties of mAb1, mAb2 and variants thereof

To evaluate correlations of the change in AggScores with experimental data, we produced all variants of mAb1 and mAb2 and performed nanoDSF for determination of unfolding temperatures, protein panel profiling for off-target binding analysis, SI-BLI for the determination of self-interaction and SPR to evaluate target binding kinetics and affinity (Table S1 and Table 3). The wildtype proteins mAb2 and mAb3 differed in their unfolding temperatures by approximately 10 K. The T_m values of the mAb1 and mAb2 variants were in a range of ± 5 K and 3 K respectively of the wildtype T_m (see supplemental material Table S1). Thus, all variants showed a similar conformational stability as the wildtype proteins.

Table 2: Overview of the sequences of mAb1 and mAb2 as well as the generated variants thereof.

mAb Variant	LC 1-4	LCDR1	LC 76-81	LCDR3	HCDR1	HCDR2	HCDR3	Rationale
mAb1	DIEL	SGDNIGGTFVS	GTQAE	GTWDMVTNN	GFTFNSYWIN	WVSGIAYNSSNTLYADSVKG	GLGAFHWDMQPDY	
CNTO607	SYEL					…DSSN…		Wu et al. (2010)[25]
W100aA	SYEL					…DSSN…	AFHADM	Bethea et al. (2012)[24]
mAbVI	SYEL		RVEAG			…DSSN…	…AAAADM…	Wu et al. (2010)[25]
mAb1-1						…DSSN…		Removal of N-Glyc site
mAb1-2							…AFVYDM…	Change of hydrophobicity in HCDR3
mAb1-3						…DSSN…	…AFHLDM…	
mAb1-4						…DSSN…	…AFHEDM…	
mAb1-5						…DSSN…	…AYHHDM…	
mAb1-6				…DAVT…		…DSSN…		Change of hydrophobicity in LCDR3
mAb1-7				…DRVT…		…DSSN…		
mAb1-8		…TEVS				…DSSN…		Insertion of a charged residue
mAb2	DIEL	SGDNLGTFYVD	GTQAE	QSFDTVYPGI	GFTFSSYGLS	WVSSIVYSGSSTSYADSVGR	EKFGFVYLFFDY	
mAb2-1							…GAAALF…	Change in hydrophobicity in HCDR3
mAb2-2							…GAASLF…	
mAb2-3							…GVESLF…	
mAb2-4							…GFHWLF…	
mAb2-5				…DTAA…				Change in hydrophobicity in LCDR3
mAb2-6				…DTES…				
mAb2-7				…DTEL…				
mAb2-8				…DTAA…			…GAAALF…	Combination of HCDR3 and LCDR3 variants
mAb2-9				…DTAA…			…GVATLF…	
mAb2-10				…DTES…			…GVESLF…	
mAb2-11				…DTAA…	GWTF…			Change in hydrophobicity of HCDR1
mAb2-12		SGANL…		…DTAA…				Change in hydrophobicity in LCDR3 and removal of potential salt bridge in LCDR1
mAb2-13	DDEL							Insertion of a charged residue
mAb2-14	DDEL	SGLDL…						
mAb2-15	DDEL	SGLDL…		…DTVT…			…GAAALF…	Change in hydrophobicity of LCDR3 and HCDR3 and insertion of charges in LCDR1

Table 3: AggScore and experimental characteristics of mAb1, mAb2 and variants thereof.

	AggScore					Experimental data				
mAb Variant	**LCDR1**	**LCDR3**	**HCDR1**	**HCDR2**	**HCDR3**	**R_{rel}**	**k_{on} [1/M*s] (±SE)**	**k_{off} [1/s] (±SE)**	**K_D [nM] (±SE)**	**Off-target binding**
mAb1	0	28	0	0	57	3.4 ± 0.5	1.08E+6 (8.02E+4)	1.68E-4 (5.61E-5)	0.15 (0.06)	55
CNTO607	0	41	0	0	57	3.1 ± 0.2	1.34E+6 (1.79E+5)	8.95E-5 (9.23E-6)	0.07 (0.01)	68
W100aA	0	28	0	0	37	2.7 ± 0.2	1.31E+6 (2.22E+5)	8.70E-3 (1.50E-4)	6.9 (1.1)	59
mAbVI	0	43	0	0	0	1.8 ± 0.1	n.b.			70
mAb1-1	0	28	0	0	57	3.9 ± 0.2	1.27E+6 (1.11E+5)	1.11E-4 (2.01E-5)	0.09 (0.02)	54
mAb1-2	0	28	0	0	47	3.8 ± 0.2	1.10E+6 (1.11E+4)	3.85E-3 (2.73E-4)	3.5 (0.2)	59
mAb1-3	0	29	0	0	55	3.1 ± 0.1	4.74E+6 (9.92E+5)	4.98E-3 (5.26E-4)	1.1 (0.1)	64
mAb1-4	0	28	0	0	29	4.0 ± 0.1	5.46E+6 (7.76E+5)	3.43E-3 (1.56E-4)	0.65 (0.05)	55
mAb1-5	0	28	0	0	28	2.3 ± 0.1	2.28E+6 (3.79E+5)	8.65E-3 (3.86E-4)	3.9 (0.5)	67
mAb1-6	0	0	0	0	60	3.2 ± 0.1	1.54E+6 (9.57E+4)	1.39E-4 (4.57E-6)	0.09 (0.01)	57
mAb1-7	0	0	0	0	60	2.3 ± 0.2	1.08E+6 (9.23E+4)	1.16E-4 (1.63E-5)	0.11 (0.02)	60
mAb1-8	0	26	0	0	56	4.0 ± 0.1	1.71E+6 (1.73E+5)	6.43E-2 (9.13E-3)	37.2 (1.8) [HB]	56
mAb2	51	65	0	29	175	3.0 ± 0.6	3.54E+4 (3.47E+3)	1.05E-4 (8.84E-6)	3.0 (0.3)	102
mAb2-1	59	82	0	28	113	1.6 ± 0.1	n.b.			53
mAb2-2	59	82	0	28	103	1.7 ± 0.1	n.b.			53
mAb2-3	45	84	0	28	118	2.4 ± 0.2	n.b.			52
mAb2-4	52	78	0	29	221	1.5 ± 0.1	9.59E+3 (1.62E+3)	8.96E-3 (7.55E-4)	978 (110)	57
mAb2-5	64	1	0	28	181	1.5 ± 0.1	3.69E+4 (5.90E+3)	5.18E-4 (9.33E-6)	14.5 (2.5)	67
mAb2-6	62	1	0	21	169	2.2 ± 0.1	3.75E+4 (5.50E+3)	5.04E-4 (1.18E-5)	14.0 (2.7)	55
mAb2-7	65	10	0	26	169	1.6 ± 0.1	3.23E+4 (2.75E+3)	9.91E-4 (7.14E-5)	31.0 (2.7)	59
mAb2-8	66	1	0	28	113	1.6 ± 0.1	n.b.			57
mAb2-9	68	1	0	28	131	1.6 ± 0.2	n.b.			52
mAb2-10	48	1	0	23	112	2.5 ± 0.1	n.b.			56
mAb2-11	64	1	0	28	181	1.6 ± 0.1	2.64E+4 (7.63E+3)	4.59E-4 (2.32E-5)	13.5 (2.0)	61
mAb2-12	57	1	0	28	181	0.9 ± 0.1	2.54E+4 (3.23E+3)	5.14E-4 (6.15E-5)	21.0 (5.5)	59
mAb2-13	45	54	0	28	180	1.4 ± 0.1	2.09E+4 (2.01E+3)	2.58E-4 (1.01E-4)	11.8 (3.6)	n.d.
mAb2-14	49	54	0	28	180	1.8 ± 0.2	3.33E+4 (8.62E+3)	2.80E-4 (1.04E-4)	8.5 (2.7)	67
mAb2-15	60	7	0	28	111	2.1 ± 0.3	n.b.			52

n.b. – no binding observed; [HB] – heterogeneous binding, best approximation of monovalent model applied; n.d. – not determined

6.4.4 Evaluation of off-target binding by protein panel profiling (3P)

We determined the proteins propensity to interact with a variety of proteins which differ in size, charge and origin.[34] The sum of ratios of all variants were determined in a range of 52 to 102 (Table S1), which is well below the value of >5000 for the positive control. Thus, all variants were regarded as non-critical in terms of off-target binding.

6.4.5 Influence of the HCDR3 hydrophobic patch on self-interaction and target binding affinity of mAb1

In order to enable a comparison with previous publications on the behavior of CNTO607, we generated the mAb variants mAbVI and $W_{100a}A$ which had shown an increased solubility in these studies.[24, 25] Variant $W_{100a}A$ was shown to bind the target molecule with a 10-fold lower affinity.[24] Target binding of variant mAbVI, which contains a triple alanine mutant in the HCDR3 ($F_{99}A$ $H_{100}A$ $W_{100a}A$) was further reduced compared to CNTO607 and $W_{100a}A$.[25] We analyzed self-interaction by SI-BLI and observed a lower self-interaction propensity for both variants of CNTO607 which correlated with published solubility data.

We tried to maintain target binding by exchanging the hydrophobic residues phenylalanine and tryptophan by tyrosine, leucine, and histidine (mAb1-3, mAb1-5). Additionally, we added glutamic acid as negatively charged residue (mAb1-4). We observed slightly decreased target binding for all variants. The reduction in hydrophobicity of this patch led to less attractive self-interaction for mAb1-3 and mAb1-5. Because self-interaction propensity of mAb2 was less pronounced compared to mAb1, we generated variant mAb1-2 containing the hydrophobic triad $F_{99}VY_{100a}$ of mAb2 in the mAb1 backbone HCDR3. Self-interaction was not decreased for these variant but we observed a target affinity comparable to mAb2. Thus, we hypothesize that the HCDR3 is involved in target binding of both mAb1 and mAb2.

6.4.6 Influence of the LCDR1 and the LCDR3 hydrophobic patch on self-interaction and target binding affinity of mAb1

The LCDR1 showed a slightly hydrophobic surface element comprising phenylalanine (F_{31}) and valine. We generated a mutant containing glutamic acid instead of phenylalanine to switch from a hydrophobic to a negatively charged surface (mAb1-8). This variant showed no significant changes in self-interaction behavior but a drastically decreased target binding. To evaluate the impact of the LCDR3 hydrophobic patch, we introduced alanine and arginine at position 93 instead of methionine (mAb1-6. mAb1-7). Both variants showed comparable target affinity, indicating that M_{93} was not involved in target binding. Self-interaction was only slightly influenced for the alanine variant but decreased by the introduction of arginine. Based on these findings, a change in the hydrophobic patch in the LCDR3 reduces self-interaction of the mAb at maintained high target affinity.

6.4.7 Influence of the HCDR3 hydrophobic patch on self-interaction and target binding affinity of mAb2

mAb1 and mAb2 show a sequence similarity of 99.5 % but differ in their CDR composition. For mAb2, two major hydrophobic patches were determined *in silico*. Our targeted mutagenesis comprised the exchange of residues $F_{99}VY_{100a}$ in the HCDR3 to less hydrophobic amino acid such as alanine (mAb2-1, mAb2-2) or valine (mAb2-3). To maintain the polar hydroxyl group of Y_{100a}, serine containing mutants were generated (mAb2-2, mAb2-3). In addition, we introduced the hydrophobic triad of mAb1 in the mAb2 HCDR3 (mAb2-4).

With stronger depletion of the HCDR3 hydrophobicity the self-interaction propensity was significantly reduced for mAb2-1 and mAb2-2 whereas a less pronounced decrease of hydrophobicity (mAb2-3) led to little reduction of self-interaction (Table 3). All these variants with a reduced HCDR3 hydrophobicity lost affinity to the target molecule (exemplarily shown for mAb2-2 in Figure 2). Target binding of mAb2 appears to be mediated by the HCDR3, which indicates a comparable target binding mechanism to mAb1. Variant mAb2-4 contained the hydrophobic triad of mAb1 and CNTO607 and showed less self-interaction compared to the wildtype but reduced target binding affinity.

Based on AggScore calculation a higher self-interaction propensity could be expected. However, the lower target affinity of mAb2-4 may be due to conformational changes in the hydrophobic surface region which are not covered by AggScore calculations.

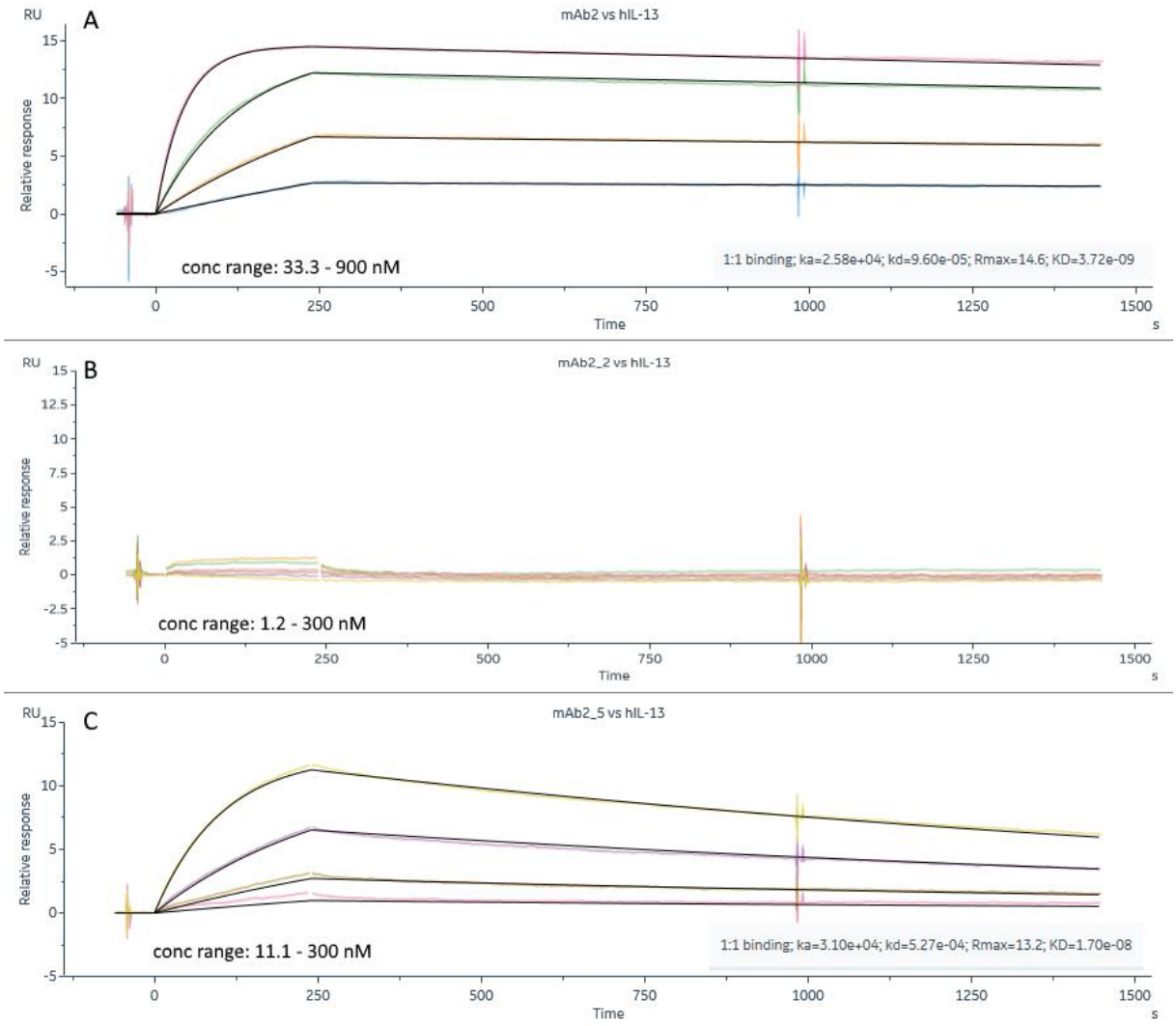

Figure 2 *SPR sensorgram overlays and applied monovalent fits of the interaction of human IL-13 with mAb2 (A), the HDCR3 variant mAb2-2 (B), and the LCDR3 variant mAb2-5 (C). SPR sensorgram overlays of all mAbs are depicted in figure S1 and S2 in the supplementary data.*

6.4.8 Influence of the LCDR3 hydrophobic patch on self-interaction and target binding affinity of mAb2

The variants mAb2-5, mAb2-6 and mAb2-7 were generated to illuminate the influence of the second hydrophobic patch identified for mAb2 in the LCDR3 on self-interaction propensity. The variants contained either alanine residues ($A_{94}A_{95}$, mAb2-5), charged and

polar residues glutamic acid and serine ($E_{94}S_{95}$, mAb2-6) or charged and hydrophobic residues glutamic acid and leucine ($E_{94}L_{95}$, mAb2-7) instead of the surface exposed hydrophobic residues $V_{94}Y_{95}$. All variants showed a decreased self-interaction propensity (Table 3). Target binding was reduced, especially for mAb2-7 (Figure 2C), but the effect was less drastic compared to mutations in the HCDR3. For further understanding, we generated a mAb2 variant that contained a double alanine mutation in the LCDR3 and a mutation to increase the HCDR1 hydrophobicity ($F_{27}W$ $V_{94}A$ $Y_{95}A$, mAb2-11). Compared to the variant mAb2-5, which only contains the double alanine mutation, self-interaction and target binding affinity were not further influenced by the introduction of the tryptophan residue (Table 3), indicating that the phenylalanine F_{27} as the most surface exposed hydrophobic residue of the HCDR1 was neither directly involved in self-interaction nor in target binding processes. Because changes in both, HCDR3 and LCDR3 influenced self-interaction propensity, we generated variants engineered in both hydrophobic patches (mAb2-8, mAb2-9 and mAb2-10). Self-interaction was not further reduced compared to single patch mutations, but all variants lost target binding affinity, which confirmed the involvement of the HCDR3 in hIL-13 binding.

Next, we engineered variants with modified hydrogen acceptor and modified potential for electrostatic interactions (mAb2-12 to mAb2-15). In mAb2-12, an aspartate to alanine mutation ($D_{27}A$) was introduced in addition to the LCDR3 mutations $V_{94}A$ $Y_{95}A$. Self-interaction was further reduced compared to mAb2-5, indicating that electrostatics are involved in self-interaction. Variants mAb2-13 to mAb2-15 contained a modified N-terminal sequence of the light chain. We determined a spatial proximity of this area to the hydrophobic patch in the LCDR3 *in silico* and hypothesized that the introduction of a negative charge may influence self-interaction. As shown for mAb2-13, self-interaction was drastically decreased compared to wildtype mAb2 and target affinity was slightly reduced. Adding further mutations did not decrease self-interaction, but affected hIL-13 binding, which was lost for mAb2-15.

6.4.9 Can machine learning approaches predict results of our engineering data set?

Protein-sol is a machine learning approach to predict the biophysical properties of antibodies based on the sequence of their variable fragments.[26, 27] Using tools for predicting the effect of distinct mutations can save costs and time compared to experimental mutagenesis. Thus, to challenge our approach, we compared our experimental results of the mAb variants generated based on homology modeling and AggScore evaluation with predictions of *protein-sol*. We focused on most similar methods and parameters with the highest impact in context of our engineering approach: i) self-interaction, the main focus of this engineering campaign, was experimentally determined by SI-BLI which is very similar to CSI included in *protein-sol;* additionally, we included AC-SINS (AC in *protein-sol*) in our analysis, ii) off-target binding experimentally evaluated by protein panel profiling (3P) was compared with CIC integrated in *protein-sol*. A major handicap of *protein-sol* is that it cannot predict target binding which was important aspect of the mAb optimization. Although we did not observe major effects of the mutations on T_m in our dataset by nanoDSF, we included comparison with T_m from DSF as included in *protein-sol* as indicator for conformational stability.

With regard to self-interaction, the correlation graph for CSI indicated a clustering of the two model systems (Figure 3A). We determined correlation coefficients cluster wise and found significant correlation for mAb2. In particular, the low measured self-interaction propensity of mAb2-12, where the LCDR3 hydrophobicity was depleted by a double alanine mutation, was predicted by *protein-sol* (Figure 3A). For mAb1, no significant correlation between the *protein-sol* prediction and the experimental results was obtained (Table 4). For the whole data set, we found a significant correlation between the predictions based on AC and the experimental results (Table 4). A low self-interaction propensity of mAb2-12 was also predicted based on AC (Figure 3B). The algorithm indicated clustering, predicting higher self-interaction propensity for the mAb1 variants compared to the mAb2 variants, which is opposite to the predicted self-interaction based on CSI. Therefore, cluster wise correlation analysis was performed, but no significant correlation was obtained.

Surprisingly, engineering of the mAbs did not influence the off-target binding as shown experimentally in the 3P assay. A similar outcome was predicted by *protein-sol* considering

CIC. Therefore, only a weak correlation could be found between experiment and prediction applying the whole data set (Table 4).

Finally, we looked for correlation between the T_m values measured and predicted as indicator for conformational stability. Using the whole data set, we found significant correlation indicating that the algorithm was able to predict the higher T_m^{app} of mAb2 and variants thereof. Clustering was observed for the two mAbs (Figure 3C and Table 4), but no significant correlations were given within the individual mAb clusters. Although the experimentally determined T_m^{app} values differed by 5 K for the mAb1 and 3 K for the mAb2 variants, the *in silico* approach was not able to predict the effect of the mutations. A detailed overview of the correlation matrices can be found in the supplemental material Table S2, S3 and S4.

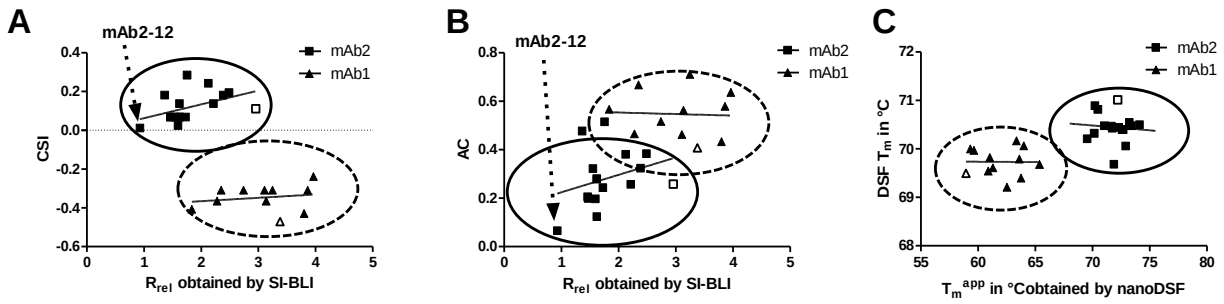

Figure 3 *Correlation plots of CSI (A) and AC-SINS (B) and R_{rel} obtained by SI-BLI; DSF and T_m^{app} obtained by nanoDSF (C). Circles indicate clustering of data prior to cluster wise correlation analyses. Open symbols reflect values of the wildtype proteins mAb1 and mAb2.*

Table 4 *Correlation matrix of experimental results and selected values from* protein-sol. *The complete correlation matrix can be found in the supplemental material Table S2 and S3.*

	SI-BLI Spearmans ρ (p-value)			**3P Spearmans ρ (p-value)**			**nanoDSF Spearmans ρ (p-value)**		
	Total (n=28)	**mAb1 (n=12)**	**mAb2 (n=16)**	**Total (n=28)**	**mAb1 (n=12)**	**mAb2 (n=16)**	**Total (n=28)**	**mAb1 (n=12)**	**mAb2 (n=16)**
CSI	-0.48 (<0.05)	0.40 (0.20)	0.61 (<0.05)						
AC-SINS	0.69 (<0.01)	0.24 (0.44)	0.40 (0.12)						
CIC				0.41 (<0.05)	0.39 (0.21)	0.41 (0.12			
DSF							0.70 (<0.01)	0.06 (0.86)	0.10 (0.71)

6.5 Discussion

6.5.1 The role of the HCDR3 in target binding and self-interaction

In our study, we focused on improving self-interaction while maintaining or as well improving other properties of our initial mAbs which are critical for developability and functionality: the T_m^{app} was included as an indicator for conformational integrity and stability, the 3P assay as a measure for off-target binding, SI-BLI for the determination of self-interaction, and ultimately affinity for the target molecule analyzed by SPR as a central factor for mAb functionality. Several algorithms are published to predict at least one part of developability such as spatial aggregation propensity and net charge[37] or hydrophobicity analyzed by HIC.[38] We used AggScore to identify regions with high aggregation propensity that trigger self-interaction.[28]

The HCDR3 of both wildtype proteins contain a hydrophobic region. By introducing more hydrophilic residues into these patches (e.g. triple alanine in mAbVI and mAb2-1), target binding was diminished. Thus, we identified the HCDR3 as paratope of both wildtype proteins. The target binding processes of mAb1 and mAb2 were comparable and showed

similarities to the published data for CNTO607.[36]Although self-interaction was decreased for many of the HCDR3 variants, a reduction in target binding affinity is not acceptable as trade off. Therefore, we focused on the second hydrophobic patch identified in the LCDR3.

6.5.2 The role of the LCDR3 in target binding and self-interaction

For mAb1 we focused on M_{93} as the most surface exposed residue of the patch. Mutations to alanine and arginine reduced the AggScore and the self-interaction propensity, especially for the arginine variant (mAb1-7) but did not affect binding to hIL-13. Despite slight differences in the primary sequence, mAb2 showed a similar hydrophobic patch in the LCDR3. Variants of mAb2 with LCDR3 mutations (mAb2-5 and mAb2-6) showed target affinities similar to the wildtype protein. However, self-interaction propensity was significantly reduced for these variants. To our knowledge, these are the first mAbs shown to undergo self-interaction mediated by the LCDR3. In previous studies, Fab-Fc interaction via the HCDR3, the LCDR2 and the Fc domain as well as Fab-Fab interaction between the HCDR2 and the LCDR2 were demonstrated.[7, 39] For Infliximab, a chimeric IgG1 from hybridoma, interacting regions outside of the CDRs were identified by X-ray crystallography.[12, 40] Furthermore, Fc-Fc-interactions were identified for a humanized IgG1.[14] mAbs derived from phage display, such as our model systems, show an overall increased prevalence of aliphatic residues which might have contributed to the generation of the hydrophobic LCDR3.[41] Our results show that rational mutagenesis of the CDRs of our model mAbs improved the physico-chemical behavior while maintaining a high affinity for the target hIL-13. Thus, CDRs can be addressed in engineering to resolve certain unwanted properties such as enhanced self-interaction, but knowledge of the paratope is a prerequisite for this approach.

Additionally, we introduced a shielding negatively charged aspartate at the N terminus of the light chain of mAb2 (mAb2-13) due to the spatial proximity to the hydrophobic patch in the LCDR3 and since positively charged residues are correlated to non-specific binding.[30] Compared to the wildtype, this variant showed a decreased self-interaction behavior and maintained high affinity to hIL-13. Thus, not directly mutating hydrophobic sites but changing the charge distribution in their vicinity appears another attractive

approach, especially in the context of the high conformational flexibility of the N terminal region.

For CNTO607, the reintroduction of the N-linked carbohydrate moiety in the HCDR2 increased the solubility, most probably due to shielding of the hydrophobic triad by the N-glycan.[25] Comparing mAb1 which contains the N-glycosylation consensus sequence and variant mAb1-1 containing $N_{53}D$ mutation shows that removal of the consensus sequence only slightly increases the self-interaction and that the carbohydrate attachment may simply increase solubility because of its hydrophilic nature.[42]

The conformational properties and stability was not influenced by the introduced mutations. With T_m^{app} values of 59 °C for mAb1 and 72 °C for mAb2, both mAbs can be regarded as conformationally stable. However, minor structural changes in secondary or tertiary structure of the mAbs cannot be resolved by nanoDSF experiments. Whereas self-interaction was significantly reduced for many variants, their off-target binding and unspecificity resp. were low compared to a non-specific positive control, and similar to the wildtype mAbs.

In summary, the CDRs of the model mAbs were shown to mediate both, target binding (HCDR3) and self-interaction processes (LCDR3). Engineering approaches of the LCDR3 led to variants with improved self-interaction behavior without negatively impacting target-binding. Additionally, negatively charged residues in the N-terminal region of the light chain decreased self-interaction, which reflects a new attractive approach to influence the physico-chemical behavior of a mAb. All variants showed comparable T_m^{app} and off-target binding behavior.

6.5.3 The use of *in silico* tools to predict the outcome of mutagenesis

Applying *protein-sol*, a machine learning approach to predict biophysical parameters of mAbs, followed by targeted mutagenesis of the predicted best variants has the potential to be a more efficient approach compared to lab and cost extensive engineering approaches. To challenge our combination of homology modeling, AggScore analysis and experimental engineering, we applied *protein-sol* to predict the properties of our mAb variants in terms of self-interaction, off-target binding and T_m and compared these predictions with the experimental data.

For self-interaction of mAb2, we found significant correlation of CSI and SI-BLI. Both methods highlighted mAb2-12 ($D_{27}AV_{94}AY_{95}A$) as the mAb with the lowest self-interaction propensity compared to other mAb2 variants. For this distinct variant, the prediction and the work extensive engineering approach led to similar results.

We did not observe correlations for mAb1. This may be due to the fact that SI-BLI was performed in 15 mM histidine hydrochloride pH 6.0 as formulation buffer, whereas the CSI data, which were used to train the algorithm, were acquired in PBS. Self-interaction strongly depends on formulation composition and pH-value.[15, 19, 22, 43–46] In addition, mAb1 contains unusual carbohydrate moieties and therefore its self-interaction behavior may differ from that of the mAbs used to train the machine learning tool.

Both the CIC predictions as well as the experimental 3P results indicated no remarkable effect of the mutations on off-target binding. This resulted in a weak correlation, but overall the *protein-sol* prediction was in agreement with the experimental results. Regarding the conformational stability, *protein-sol* predicted a higher T_m for mAb2, which was confirmed by our experimental data, but within the two groups, the mAb1 variants and the mAb2 variants, the algorithm could not predict the effects seen in the measurements.

In summary, for our data set, *in silico* predictions of *protein-sol* were not suitable to guide rational engineering by predicting residue specific effects to reduce self-interaction. Target binding affinity is an essential factor which is however not included in *protein-sol*. Applying homology modeling, AggScore evaluation to guide targeted mutagenesis, generating these mutants and analyzing self-interaction, target binding and off-target binding the mutagenesis was well directed and led to in-depth understanding of the contributions of the different CDRs, and effects of the individual mutations. The affinity measurements highlight which mutated regions are involved in the target binding process, in our case the HCDR3. Using the *in silico* approach based on *protein-sol* to design the variants, where target binding is not addressed, would have allowed to come up with mAb variants with reduced self-interaction propensity. But the scientist would be in the dark what the effect of the mutations on target binding would be and still needs to generate the variants and analyze their target affinity.

6.6 Conclusions

This study illustrates the application of structure guided engineering to reduce self-interaction of therapeutic mAbs. After homology modeling of wildtype proteins, the algorithm AggScore was used to identify aggregation prone surface patches. These were subsequently modified by targeted mutagenesis. In total, 26 variants of 2 wildtype proteins were generated and characterized. All variants showed comparable apparent T_m as indicator for conformational integrity, and unchanged off-target binding behavior. The results demonstrate the impact of mutations in hydrophobic patches on mAb self-interaction and target binding properties. For our model systems, HCDR3 mutations led to a decrease in self-interaction propensity but diminished target binding. Mutations in the LCDR3 resulted in reduced self-interaction but did not affect antigen affinity. In particular, a variant of mAb1 containing arginine in the LCDR3 showed improved self-interaction behavior. Comparable findings were shown for a double alanine variants of the LCDR3 of mAb2. Based on our observations, self-interaction of mAb1 and mAb2 are mediated by the LCDR3. In addition, introduction of a negatively charged residue at the N terminus of the light chain minimized self-interaction propensity indicating that a charge shielding of surface exposed hydrophobicity of the CDRs is a possibility to improve the developability of a mAb without compromising antigen affinity. Further, we used *protein-sol* as a machine learning approach to predict the effect of the mutations on the self-interaction, off-target binding and melting temperature for the variants. *Protein-sol* does not include the prediction of target affinity. The algorithm could be useful to come up with protein sequences which show reduced self-interaction, but its applicability for directing targeted engineering is limited.

Ultimately, deeper understanding of the self-interaction process as well as of the target binding is a prerequisite for successful engineering of therapeutic mAbs to improve their physico-chemical behavior while maintaining the antigen affinity. Homology modeling and identification of hydrophobic surface exposed region followed by generation and analysis of designed variants is well suited to resolve effects and ultimately find mAb variants with improved properties.

6.7 Acknowledgements

This study was part of the project “Self-Interaction and targeted Engineering of monoclonal antibodies (Self-I-E)” funded by the Bayerische Forschungsstiftung. The authors would like to thank the whole Department Protein Sciences of MorphoSys AG for their outstanding support and extend special gratitude to the Core Technology Team and PS Production teams for production of high quality DNA constructs and mAb variants, respectively. A special thanks is extended to Dr. Stefan Mitterreiter, who contributes to the project “Self-I-E” as a grant manager and did an excellent job outside of the scene.

References

1. Roberts CJ. Therapeutic protein aggregation: mechanisms, design, and control. 2014. Trends Biotechnol 32: 372–380.

2. Binabaji E, Ma J, Zydney AL. Intermolecular Interactions and the Viscosity of Highly Concentrated Monoclonal Antibody Solutions. 2015. Pharm Res 32: 3102–3109.

3. Kanai S, Liu J, Patapoff TW, Shire SJ. Reversible self-association of a concentrated monoclonal antibody solution mediated by Fab-Fab interaction that impacts solution viscosity. 2008. J Pharm Sci 97: 4219–4227.

4. Li L, Kumar S, Buck PM, et al. Concentration dependent viscosity of monoclonal antibody solutions: explaining experimental behavior in terms of molecular properties. 2014. Pharm Res 31: 3161–3178.

5. Laue T. Proximity energies: a framework for understanding concentrated solutions. 2012. J Mol Recognit 25: 165–173.

6. Huisman IH, Prádanos P, Hernández A. The effect of protein–protein and protein–membrane interactions on membrane fouling in ultrafiltration. 2000. Journal of Membrane Science 179: 79–90.

7. Arora J, Hu Y, Esfandiary R, et al. Charge-mediated Fab-Fc interactions in an IgG1 antibody induce reversible self-association, cluster formation, and elevated viscosity. 2016. MAbs 8: 1561–1574.

8. Geoghegan JC, Fleming R, Damschroder M, et al. Mitigation of reversible self-association and viscosity in a human IgG1 monoclonal antibody by rational, structure-guided Fv engineering. 2016. MAbs 8: 941–950.

9. Gentiluomo L, Roessner D, Streicher W, et al. Characterization of Native Reversible Self-Association of a Monoclonal Antibody Mediated by Fab-Fab Interaction. 2020. J Pharm Sci 109: 443–451.

10. Dobson CL, Devine PWA, Phillips JJ, et al. Engineering the surface properties of a human monoclonal antibody prevents self-association and rapid clearance in vivo. 2016. Sci Rep 6: 38644.

11. Esfandiary R, Parupudi A, Casas-Finet J, et al. Mechanism of reversible self-association of a monoclonal antibody: role of electrostatic and hydrophobic interactions. 2015. J Pharm Sci 104: 577–586.

12. Lerch TF, Sharpe P, Mayclin SJ, et al. Infliximab crystal structures reveal insights into self-association. 2017. MAbs 9: 874–883.

13. Lilyestrom WG, Yadav S, Shire SJ, Scherer TM. Monoclonal antibody self-association, cluster formation, and rheology at high concentrations. 2013. J Phys Chem B 117: 6373–6384.

14. Nishi H, Miyajima M, Wakiyama N, et al. Fc domain mediated self-association of an IgG1 monoclonal antibody under a low ionic strength condition. 2011. J Biosci Bioeng 112: 326–332.

15. Yadav S, Shire SJ, Kalonia DS. Factors affecting the viscosity in high concentration solutions of different monoclonal antibodies. 2010. J Pharm Sci 99: 4812–4829.

16. Nichols P, Li L, Kumar S, et al. Rational design of viscosity reducing mutants of a monoclonal antibody: hydrophobic versus electrostatic inter-molecular interactions. 2015. MAbs 7: 212–230.

17. Liu J, Nguyen MDH, Andya JD, Shire SJ. Reversible self-association increases the viscosity of a concentrated monoclonal antibody in aqueous solution. 2005. J Pharm Sci 94: 1928–1940.

18. Neergaard MS, Kalonia DS, Parshad H, et al. Viscosity of high concentration protein formulations of monoclonal antibodies of the IgG1 and IgG4 subclass - prediction of viscosity through protein-protein interaction measurements. 2013. Eur J Pharm Sci 49: 400–410.

19. Pindrus MA, Shire SJ, Yadav S, Kalonia DS. The Effect of Low Ionic Strength on Diffusion and Viscosity of Monoclonal Antibodies. 2018. Mol Pharm 15: 3133–3142.

20. Luo H, Macapagal N, Newell K, et al. Effects of salt-induced reversible self-association on the elution behavior of a monoclonal antibody in cation exchange chromatography. 2014. J Chromatogr A 1362: 186–193.

21. Dear BJ, Hung JJ, Truskett TM, Johnston KP. Contrasting the Influence of Cationic Amino Acids on the Viscosity and Stability of a Highly Concentrated Monoclonal Antibody. 2017. Pharm Res 34: 193–207.

22. Sahin E, Grillo AO, Perkins MD, Roberts CJ. Comparative effects of pH and ionic strength on protein-protein interactions, unfolding, and aggregation for IgG1 antibodies. 2010. J Pharm Sci 99: 4830–4848.

23. Sarangapani PS, Weaver J, Parupudi A, et al. Both Reversible Self-Association and Structural Changes Underpin Molecular Viscoelasticity of mAb Solutions. 2016. J Pharm Sci 105: 3496–3506.

24. Bethea D, Wu S-J, Luo J, et al. Mechanisms of self-association of a human monoclonal antibody CNTO607. 2012. Protein Eng Des Sel 25: 531–537.

25. Wu S-J, Luo J, O'Neil KT, et al. Structure-based engineering of a monoclonal antibody for improved solubility. 2010. Protein Eng Des Sel 23: 643–651.

26. Hebditch M, Warwicker J. Charge and hydrophobicity are key features in sequence-trained machine learning models for predicting the biophysical properties of clinical-stage antibodies. 2019. PeerJ 7: e8199.

27. Jain T, Sun T, Durand S, et al. Biophysical properties of the clinical-stage antibody landscape. 2017. Proc Natl Acad Sci U S A 114: 944–949.

28. Sankar K, Krystek SR, Carl SM, et al. AggScore: Prediction of aggregation-prone regions in proteins based on the distribution of surface patches. 2018. Proteins 86: 1147–1156.

29. Apgar JR, Tam ASP, Sorm R, et al. Modeling and mitigation of high-concentration antibody viscosity through structure-based computer-aided protein design. 2020. PLoS ONE 15: e0232713.

30. Rabia LA, Desai AA, Jhajj HS, Tessier PM. Understanding and overcoming trade-offs between antibody affinity, specificity, stability and solubility. 2018. Biochem Eng J 137: 365–374.

31. Starr CG, Tessier PM. Selecting and engineering monoclonal antibodies with drug-like specificity. 2019. Curr Opin Biotechnol 60: 119–127.

32. Rothe C, Urlinger S, Löhning C, et al. The human combinatorial antibody library HuCAL GOLD combines diversification of all six CDRs according to the natural immune system with a novel display method for efficient selection of high-affinity antibodies. 2008. J Mol Biol 376: 1182–1200.

33. Domnowski M, Jaehrling J, Frieß W. Assessment of Antibody Self-Interaction by Bio-Layer-Interferometry as a Tool for Early Stage Formulation Development. 2020. Pharm Res 37: 29.

34. Frese K, Eisenmann M, Ostendorp R, et al. An automated immunoassay for early specificity profiling of antibodies. 2013. MAbs 5: 279–287.

35. Hötzel I, Theil F-P, Bernstein LJ, et al. A strategy for risk mitigation of antibodies with fast clearance. 2012. MAbs 4: 753–760.

36. Teplyakov A, Obmolova G, Wu S-J, et al. Epitope mapping of anti-interleukin-13 neutralizing antibody CNTO607. 2009. J Mol Biol 389: 115–123.

37. Lauer TM, Agrawal NJ, Chennamsetty N, et al. Developability index: a rapid *in silico* tool for the screening of antibody aggregation propensity. 2012. J Pharm Sci 101: 102–115.

38. Jain T, Boland T, Lilov A, et al. Prediction of delayed retention of antibodies in hydrophobic interaction chromatography from sequence using machine learning. 2017. Bioinformatics 33: 3758–3766.

39. Arora J, Hickey JM, Majumdar R, et al. Hydrogen exchange mass spectrometry reveals protein interfaces and distant dynamic coupling effects during the reversible self-association of an IgG1 monoclonal antibody. 2015. MAbs 7: 525–539.

40. Strohl WR, Strohl LM. 2012. Therapeutic antibody engineering. Current and future advances driving the strongest growth area in the pharmaceutical industry / William R. Strohl and Lila M. Strohl, Sawston: Woodhead Pub.

41. Kaleli NE, Karadag M, Kalyoncu S. Phage display derived therapeutic antibodies have enriched aliphatic content: Insights for developability issues. 2019. Proteins 87: 607–618.

42. Sinclair AM, Elliott S. Glycoengineering: the effect of glycosylation on the properties of therapeutic proteins. 2005. J Pharm Sci 94: 1626–1635.

43. Shire SJ, Shahrokh Z, Liu J. Challenges in the development of high protein concentration formulations. 2004. J Pharm Sci 93: 1390–1402.

44. Sule SV, Cheung JK, Antochshuk V, et al. Solution pH that minimizes self-association of three monoclonal antibodies is strongly dependent on ionic strength. 2012. Mol Pharm 9: 744–751.

45. Tomar DS, Kumar S, Singh SK, et al. Molecular basis of high viscosity in concentrated antibody solutions: Strategies for high concentration drug product development. 2016. MAbs 8: 216–228.

46. Whitaker N, Xiong J, Pace SE, et al. A Formulation Development Approach to Identify and Select Stable Ultra-High-Concentration Monoclonal Antibody Formulations With Reduced Viscosities. 2017. J Pharm Sci 106: 3230–3241.

Supplementary data

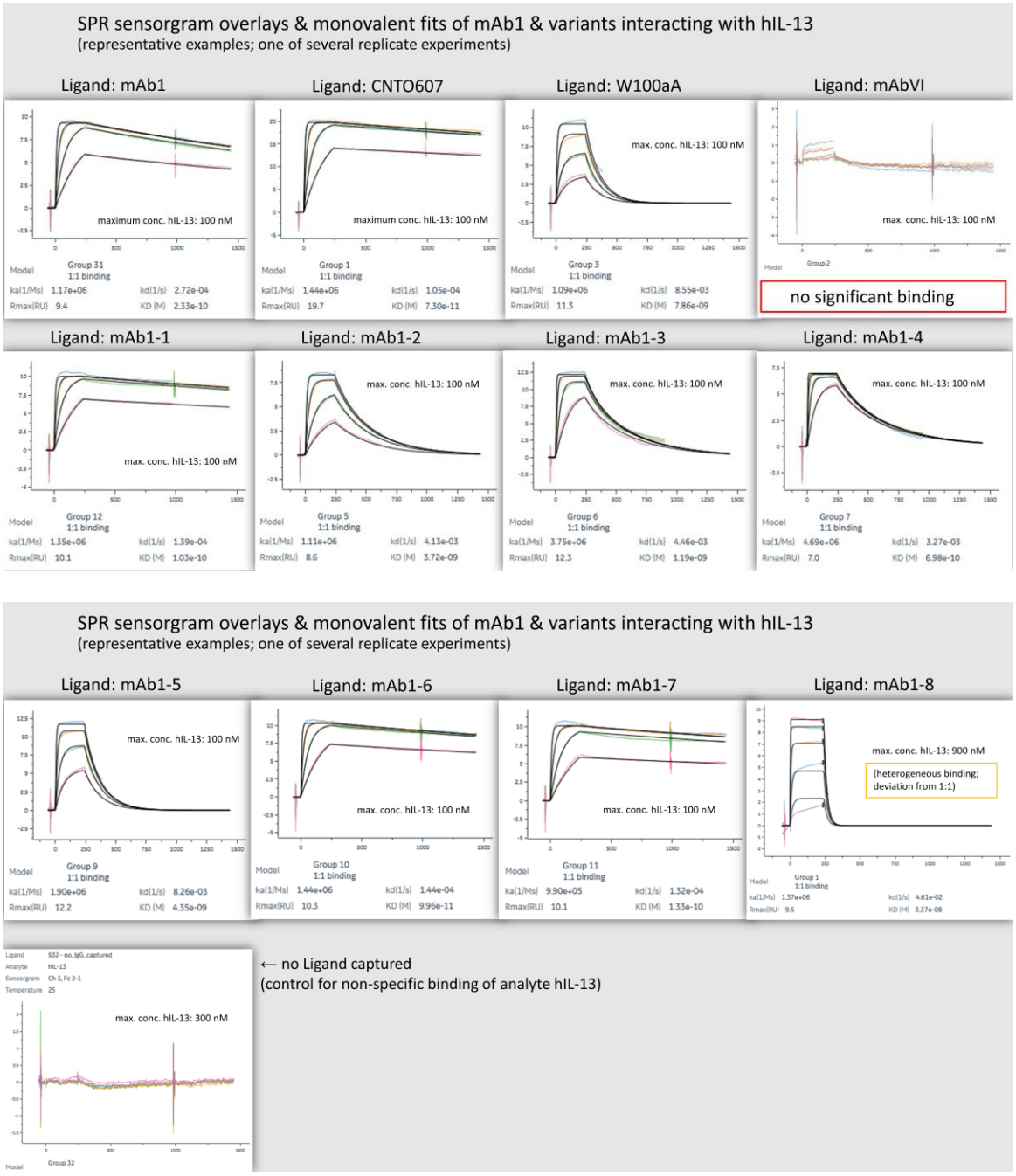

Figure S1 *SPR sensorgram overlays and applied monovalent fits of the interaction of human IL-13 with mAb1 and variants thereof*

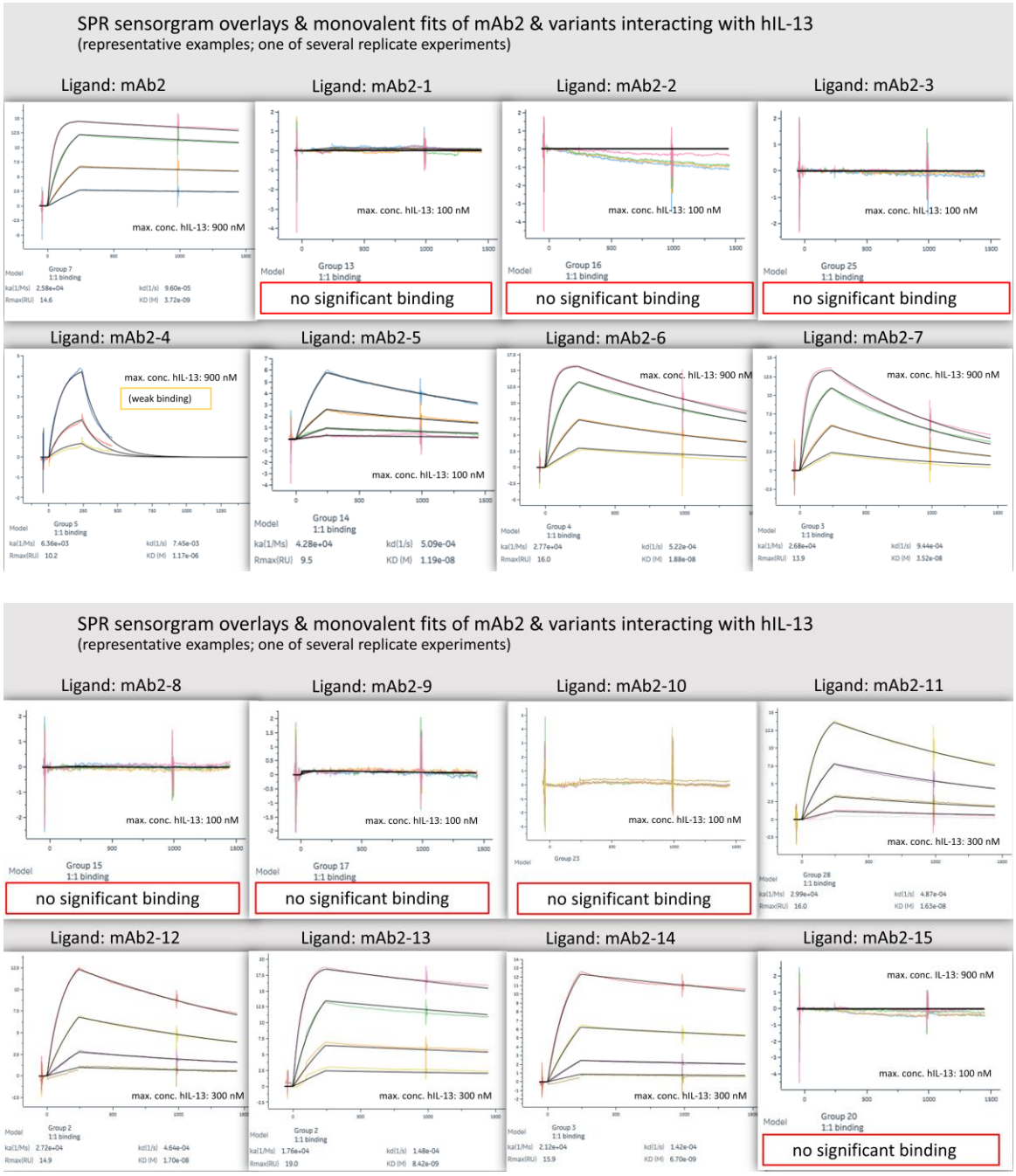

Figure S2 *SPR sensorgram overlays and applied monovalent fits of the interaction of human IL-13 with mAb2 and variants thereof*

Table S1 *Additional characterization of mAb2, mAb3 and variants thereof*

mAb Variant	T_m^{app} [°C]	Sum of off-target binding
mAb1	58.9	55
CNTO607	63.7	69
W100aA	61.0	59
mAbVI	65.4	70
mAb1-1	61.3	54
mAb1-2	59.3	59
mAb1-3	59.6	64
mAb1-4	60.9	55
mAb1-5	63.3	67
mAb1-6	63.6	57
mAb1-7	64.0	60
mAb1-8	62.5	56
mAb2	72.2	54
mAb2-1	71.7	53
mAb2-2	71.7	53
mAb2-3	71.0	52
mAb2-4	74.1	57
mAb2-5	73.2	67
mAb2-6	72.7	55
mAb2-7	72.6	59
mAb2-8	72.9	57
mAb2-9	72.3	52
mAb2-10	71.9	56
mAb2-11	69.5	61
mAb2-12	73.4	59
mAb2-13	70.5	n.d.
mAb2-14	70.2	67
mAb2-15	70.1	52
Positive control (3P)		5041 ± 1565

Table S2 *Spearman correlation matrix. The whole data set (n=28) was used for correlation analysis.*

n=28															
Spearman ρ	HIC	SMAC	SGAC	CIC	CSI	AC	HEK	PSR	ELISA	BVP	DSF	SI-BLI	Tm	3P	HEK
HIC	1.000	0.968	0.832	-0.145	0.602	-0.760	0.565	-0.932	-0.194	-0.841	0.837	-0.775	0.794	0.107	-0.527
SMAC	0.968	1.000	0.746	-0.031	0.444	-0.733	0.475	-0.919	-0.291	-0.791	0.774	-0.779	0.732	0.192	-0.456
SGAC	0.832	0.746	1.000	-0.176	0.565	-0.749	0.467	-0.796	-0.117	-0.776	0.848	-0.649	0.770	0.018	-0.430
CIC	-0.145	-0.031	-0.176	1.000	-0.626	0.430	-0.681	0.259	-0.430	0.248	-0.320	0.237	-0.405	0.418	-0.082
CSI	0.602	0.444	0.565	-0.626	1.000	-0.427	0.631	-0.533	0.438	-0.539	0.666	-0.476	0.637	-0.295	-0.238
AC	-0.760	-0.733	-0.749	0.430	-0.427	1.000	-0.729	0.880	0.303	0.881	-0.633	0.686	-0.794	0.179	0.199
HEK	0.565	0.475	0.467	-0.681	0.631	-0.729	1.000	-0.627	0.099	-0.678	0.529	-0.499	0.659	-0.422	-0.093
PSR	-0.932	-0.919	-0.796	0.259	-0.533	0.880	-0.627	1.000	0.285	0.913	-0.793	0.830	-0.864	-0.040	0.432
ELISA	-0.194	-0.291	-0.117	-0.430	0.438	0.303	0.099	0.285	1.000	0.413	0.051	0.212	-0.129	-0.298	0.273
BVP	-0.841	-0.791	-0.776	0.248	-0.539	0.881	-0.678	0.913	0.413	1.000	-0.660	0.758	-0.855	0.117	0.376
DSF	0.837	0.774	0.848	-0.320	0.666	-0.633	0.529	-0.793	0.051	-0.660	1.000	-0.717	0.696	0.046	-0.415
AS	0.827	0.699	0.783	-0.545	0.868	-0.781	0.788	-0.830	0.108	-0.842	0.781	-0.705	0.827	-0.269	-0.334
SI-BLI	-0.775	-0.779	-0.649	0.237	-0.476	0.686	-0.499	0.830	0.212	0.758	-0.717	1.000	-0.778	-0.067	0.427
Tm	0.794	0.732	0.770	-0.405	0.637	-0.794	0.659	-0.864	-0.129	-0.855	0.696	-0.778	1.000	-0.042	-0.304
3P	0.107	0.192	0.018	0.418	-0.295	0.179	-0.422	-0.040	-0.298	0.117	0.046	-0.067	-0.042	1.000	-0.279
HEK	-0.527	-0.456	-0.430	-0.082	-0.238	0.199	-0.093	0.432	0.273	0.376	-0.415	0.427	-0.304	-0.279	1.000
p-value	HIC	SMAC	SGAC	CIC	CSI	AC	HEK	PSR	ELISA	BVP	DSF	SI-BLI	Tm	3P	HEK
HIC	0.000	0.000	0.000	0.460	0.001	0.000	0.002	0.000	0.322	0.000	0.000	0.000	0.000	0.596	0.006
SMAC	0.000	0.000	0.000	0.875	0.018	0.000	0.011	0.000	0.133	0.000	0.000	0.000	0.000	0.336	0.019
SGAC	0.000	0.000	0.000	0.370	0.002	0.000	0.012	0.000	0.554	0.000	0.000	0.000	0.000	0.930	0.028
CIC	0.460	0.875	0.370	0.000	0.000	0.022	0.000	0.184	0.022	0.204	0.097	0.225	0.032	0.030	0.691
CSI	0.001	0.018	0.002	0.000	0.000	0.023	0.000	0.004	0.020	0.003	0.000	0.010	0.000	0.136	0.242
AC	0.000	0.000	0.000	0.022	0.023	0.000	0.000	0.000	0.117	0.000	0.000	0.000	0.000	0.370	0.330
HEK	0.002	0.011	0.012	0.000	0.000	0.000	0.000	0.000	0.618	0.000	0.004	0.007	0.000	0.028	0.651
PSR	0.000	0.000	0.000	0.184	0.004	0.000	0.000	0.000	0.141	0.000	0.000	0.000	0.000	0.842	0.027
ELISA	0.322	0.133	0.554	0.022	0.020	0.117	0.618	0.141	0.000	0.029	0.797	0.278	0.514	0.131	0.177
BVP	0.000	0.000	0.000	0.204	0.003	0.000	0.000	0.000	0.029	0.000	0.000	0.000	0.000	0.562	0.058
DSF	0.000	0.000	0.000	0.097	0.000	0.000	0.004	0.000	0.797	0.000	0.000	0.000	0.000	0.819	0.035
AS	0.000	0.000	0.000	0.003	0.000	0.000	0.000	0.000	0.585	0.000	0.000	0.000	0.000	0.176	0.095
SI-BLI	0.000	0.000	0.000	0.225	0.010	0.000	0.007	0.000	0.278	0.000	0.000	0.000	0.000	0.742	0.030
Tm	0.000	0.000	0.000	0.032	0.000	0.000	0.000	0.000	0.514	0.000	0.000	0.000	0.000	0.837	0.131
3P	0.596	0.336	0.930	0.030	0.136	0.370	0.028	0.842	0.131	0.562	0.819	0.742	0.837	0.000	0.176
HEK	0.006	0.019	0.028	0.691	0.242	0.330	0.651	0.027	0.177	0.058	0.035	0.030	0.131	0.176	0.000

Table S3 *Spearman correlation matrix. Cluster wise correlation analysis (mAb1. n=12)*

mAb1 (n=12)															
Spearman ρ	HIC	SMAC	SGAC	CIC	CSI	AC	HEK	PSR	ELISA	BVP	DSF	SI-BLI	Tm	3P	HEK
HIC	1.000	0.979	0.130	0.676	-0.780	-0.361	-0.515	-0.646	-0.742	-0.623	0.105	-0.340	0.088	0.497	-0.210
SMAC	0.979	1.000	0.165	0.613	-0.780	-0.452	-0.522	-0.646	-0.732	-0.587	0.147	-0.389	0.025	0.581	-0.155
SGAC	0.130	0.165	1.000	0.112	-0.338	-0.399	-0.455	-0.186	-0.172	-0.423	0.406	-0.308	-0.070	0.203	-0.273
CIC	0.676	0.613	0.112	1.000	-0.517	0.070	-0.706	-0.369	-0.525	-0.536	-0.343	-0.133	0.357	0.392	0.064
CSI	-0.780	-0.780	-0.338	-0.517	1.000	0.739	0.502	0.892	0.879	0.884	-0.160	0.397	0.022	-0.375	0.206
AC	-0.361	-0.452	-0.399	0.070	0.739	1.000	0.140	0.642	0.543	0.558	-0.238	0.245	0.469	-0.154	0.118
HEK	-0.515	-0.522	-0.455	-0.706	0.502	0.140	1.000	0.523	0.634	0.657	0.147	0.503	-0.483	-0.531	0.318
PSR	-0.646	-0.646	-0.186	-0.369	0.892	0.642	0.523	1.000	0.948	0.900	-0.183	0.574	-0.290	-0.484	0.368
ELISA	-0.742	-0.732	-0.172	-0.525	0.879	0.543	0.634	0.948	1.000	0.927	0.007	0.480	-0.305	-0.476	0.501
BVP	-0.623	-0.587	-0.423	-0.536	0.884	0.558	0.657	0.900	0.927	1.000	-0.021	0.401	-0.274	-0.341	0.516
DSF	0.105	0.147	0.406	-0.343	-0.160	-0.238	0.147	-0.183	0.007	-0.021	1.000	-0.594	0.056	0.385	0.136
AS	-0.481	-0.481	0.480	-0.393	0.318	-0.044	0.393	0.493	0.481	0.222	0.044	0.480	-0.480	-0.480	-0.100
SI-BLI	-0.340	-0.389	-0.308	-0.133	0.397	0.245	0.503	0.574	0.480	0.401	-0.594	1.000	-0.538	-0.783	-0.018
Tm	0.088	0.025	-0.070	0.357	0.022	0.469	-0.483	-0.290	-0.305	-0.274	0.056	-0.538	1.000	0.531	-0.245
3P	0.497	0.581	0.203	0.392	-0.375	-0.154	-0.531	-0.484	-0.476	-0.341	0.385	-0.783	0.531	1.000	0.055
HEK	-0.210	-0.155	-0.273	0.064	0.206	0.118	0.318	0.368	0.501	0.516	0.136	-0.018	-0.245	0.055	1.000
p-value	HIC	SMAC	SGAC	CIC	CSI	AC	HEK	PSR	ELISA	BVP	DSF	SI-BLI	Tm	3P	HEK
HIC	0.000	0.000	0.688	0.016	0.003	0.249	0.087	0.023	0.006	0.031	0.745	0.280	0.787	0.100	0.536
SMAC	0.000	0.000	0.609	0.034	0.003	0.140	0.082	0.023	0.007	0.045	0.648	0.212	0.940	0.047	0.649
SGAC	0.688	0.609	0.000	0.729	0.282	0.199	0.138	0.562	0.594	0.171	0.191	0.331	0.829	0.527	0.417
CIC	0.016	0.034	0.729	0.000	0.085	0.829	0.010	0.237	0.079	0.072	0.276	0.681	0.255	0.208	0.853
CSI	0.003	0.003	0.282	0.085	0.000	0.006	0.096	0.000	0.000	0.000	0.619	0.202	0.946	0.230	0.543
AC	0.249	0.140	0.199	0.829	0.006	0.000	0.665	0.024	0.068	0.059	0.457	0.443	0.124	0.633	0.729
HEK	0.087	0.082	0.138	0.010	0.096	0.665	0.000	0.081	0.027	0.020	0.649	0.095	0.112	0.075	0.340
PSR	0.023	0.023	0.562	0.237	0.000	0.024	0.081	0.000	0.000	0.000	0.569	0.051	0.360	0.111	0.265
ELISA	0.006	0.007	0.594	0.079	0.000	0.068	0.027	0.000	0.000	0.000	0.983	0.114	0.336	0.117	0.116
BVP	0.031	0.045	0.171	0.072	0.000	0.059	0.020	0.000	0.000	0.000	0.948	0.196	0.390	0.278	0.104
DSF	0.745	0.648	0.191	0.276	0.619	0.457	0.649	0.569	0.983	0.948	0.000	0.042	0.863	0.217	0.689
AS	0.113	0.113	0.114	0.206	0.313	0.893	0.206	0.104	0.113	0.488	0.893	0.114	0.114	0.114	0.770
SI-BLI	0.280	0.212	0.331	0.681	0.202	0.443	0.095	0.051	0.114	0.196	0.042	0.000	0.071	0.003	0.958
Tm	0.787	0.940	0.829	0.255	0.946	0.124	0.112	0.360	0.336	0.390	0.863	0.071	0.000	0.075	0.467
3P	0.100	0.047	0.527	0.208	0.230	0.633	0.075	0.111	0.117	0.278	0.217	0.003	0.075	0.000	0.873
HEK	0.536	0.649	0.417	0.853	0.543	0.729	0.340	0.265	0.116	0.104	0.689	0.958	0.467	0.873	0.000

Table S4 *Spearman correlation matrix. Cluster wise correlation analysis (mAb2. n=16)*

mAb2 (n=16)															
Spearman ρ	HIC	SMAC	SGAC	CIC	CSI	AC	HEK	PSR	ELISA	BVP	DSF	SI-BLI	Tm	3P	HEK
HIC	1.000	0.971	0.674	0.753	-0.442	-0.318	-0.212	-0.781	-0.419	-0.295	0.673	-0.453	0.276	0.689	-0.749
SMAC	0.971	1.000	0.629	0.738	-0.593	-0.444	-0.126	-0.879	-0.444	-0.358	0.612	-0.529	0.315	0.611	-0.627
SGAC	0.674	0.629	1.000	0.515	-0.322	-0.468	-0.124	-0.541	-0.374	-0.344	0.681	-0.144	0.559	0.314	-0.254
CIC	0.753	0.738	0.515	1.000	-0.364	-0.059	-0.338	-0.494	-0.484	-0.406	0.409	-0.379	-0.015	0.425	-0.552
CSI	-0.442	-0.593	-0.322	-0.364	1.000	0.876	-0.508	0.805	0.700	0.776	0.056	0.609	-0.584	-0.129	0.093
AC	-0.318	-0.444	-0.468	-0.059	0.876	1.000	-0.582	0.733	0.593	0.681	-0.010	0.403	-0.776	-0.021	-0.129
HEK	-0.212	-0.126	-0.124	-0.338	-0.508	-0.582	1.000	-0.129	-0.368	-0.452	-0.389	-0.059	0.338	-0.364	0.308
PSR	-0.781	-0.879	-0.541	-0.494	0.805	0.733	-0.129	1.000	0.572	0.562	-0.433	0.584	-0.558	-0.497	0.355
ELISA	-0.419	-0.444	-0.374	-0.484	0.700	0.593	-0.368	0.572	1.000	0.956	0.060	0.319	-0.456	-0.250	0.186
BVP	-0.295	-0.358	-0.344	-0.406	0.776	0.681	-0.452	0.562	0.956	1.000	0.130	0.370	-0.515	-0.106	0.083
DSF	0.673	0.612	0.681	0.409	0.056	-0.010	-0.389	-0.433	0.060	0.130	1.000	-0.159	0.096	0.418	-0.457
AS	1.000	1.000	1.000	1.000	1.000	1.000	1.000	1.000	1.000	1.000	1.000	1.000	1.000	1.000	1.000
SI-BLI	-0.453	-0.529	-0.144	-0.379	0.609	0.403	-0.059	0.584	0.319	0.370	-0.159	1.000	-0.326	-0.200	0.534
Tm	0.276	0.315	0.559	-0.015	-0.584	-0.776	0.338	-0.558	-0.456	-0.515	0.096	-0.326	1.000	0.221	0.054
3P	0.689	0.611	0.314	0.425	-0.129	-0.021	-0.364	-0.497	-0.250	-0.106	0.418	-0.200	0.221	1.000	-0.827
HEK	-0.749	-0.627	-0.254	-0.552	0.093	-0.129	0.308	0.355	0.186	0.083	-0.457	0.534	0.054	-0.827	1.000
p-value	HIC	SMAC	SGAC	CIC	CSI	AC	HEK	PSR	ELISA	BVP	DSF	SI-BLI	Tm	3P	HEK
HIC	0.000	0.000	0.004	0.001	0.087	0.231	0.431	0.000	0.106	0.267	0.004	0.078	0.300	0.004	0.001
SMAC	0.000	0.000	0.009	0.001	0.016	0.085	0.641	0.000	0.085	0.174	0.012	0.035	0.235	0.016	0.012
SGAC	0.004	0.009	0.000	0.041	0.224	0.068	0.649	0.030	0.154	0.192	0.004	0.594	0.024	0.254	0.360
CIC	0.001	0.001	0.041	0.000	0.165	0.829	0.200	0.052	0.057	0.119	0.116	0.147	0.957	0.114	0.033
CSI	0.087	0.016	0.224	0.165	0.000	0.000	0.044	0.000	0.003	0.000	0.837	0.012	0.018	0.646	0.742
AC	0.231	0.085	0.068	0.829	0.000	0.000	0.018	0.001	0.015	0.004	0.970	0.122	0.000	0.940	0.647
HEK	0.431	0.641	0.649	0.200	0.044	0.018	0.000	0.633	0.161	0.079	0.137	0.829	0.200	0.182	0.264
PSR	0.000	0.000	0.030	0.052	0.000	0.001	0.633	0.000	0.021	0.023	0.094	0.017	0.025	0.059	0.194
ELISA	0.106	0.085	0.154	0.057	0.003	0.015	0.161	0.021	0.000	0.000	0.824	0.228	0.076	0.368	0.506
BVP	0.267	0.174	0.192	0.119	0.000	0.004	0.079	0.023	0.000	0.000	0.630	0.159	0.041	0.708	0.767
DSF	0.004	0.012	0.004	0.116	0.837	0.970	0.137	0.094	0.824	0.630	0.000	0.557	0.725	0.121	0.086
AS	0.000	0.000	0.000	0.000	0.000	0.000	0.000	0.000	0.000	0.000	0.000	0.000	0.000	0.000	0.000
SI-BLI	0.078	0.035	0.594	0.147	0.012	0.122	0.829	0.017	0.228	0.159	0.557	0.000	0.217	0.475	0.040
Tm	0.300	0.235	0.024	0.957	0.018	0.000	0.200	0.025	0.076	0.041	0.725	0.217	0.000	0.428	0.849
3P	0.004	0.016	0.254	0.114	0.646	0.940	0.182	0.059	0.368	0.708	0.121	0.475	0.428	0.000	0.000
HEK	0.001	0.012	0.360	0.033	0.742	0.647	0.264	0.194	0.506	0.767	0.086	0.040	0.849	0.000	0.000

Chapter 7 Summary

Self-Interaction processes of monoclonal antibodies are linked to the intrinsic molecular properties as well as to the composition of the formulation environment. Considering both factors in combination helps the pharmaceutical scientist to understand the process itself and to master challenges arising from high self-interaction propensity during development, manufacturing and application.

Chapter 1 describes the current understanding of self-interaction of mAbs as a process as well as of the impact of protein structure and formulation. Additionally, the link between self-interaction and developability of mAbs is introduced. *In silico* approaches are highlighted which can be used to predict physicochemical parameters based on the proteins primary structure.

At first, a high-throughput assay was established for determining formulation dependent self-interaction based on bio layer interferometry (SI-BLI) **(Chapter 2)**. Due to minimal sample consumption and high throughput, this assay enables the differentiation between several candidate molecules in parallel to a formulation screening. The assay results correlated significantly with k_D from DLS, a parameter well-established for describing protein self-interaction. Whereas k_D analysis requires the preparation and measurement of various protein solutions at different protein concentration, SI-BLI requires only one low protein concentration (2 µM) and a single measurement of an association reaction. The assay can be implemented in early stages of developability assessments, when the available protein amount is low and the number of potential candidates is high. Subsequently the assay was utilized in a developability assessment for ranking potential lead candidates in combination with a preformulation screening **(Chapter 3)**. With SI-BLI, specific ion effects on mAb self-interaction were detected and further studied. In particular, bivalent magnesium ions reduce the self-interaction propensity of the mAbs more than sodium ions. Moreover, the SI-BLI results correlated with viscosimetry data. This case study confirmed the applicability of the assay for both, high-throughput studies and in-depth self-interaction characterization.

Chapter 4 describes a multi-method approach to analyze the self-interaction process of Infliximab as a model system. Within this study, established analytical techniques were combined with emerging techniques for analyzing self-interaction. Thus, AUC,

Viscosimetry, DLS, SAXS and SI-BLI were used for analysis on a protein resolution level. Additionally, SI-BLI and AUC investigations were carried out to describe the self-interaction process on a fragment level after digestion. Finally, HDX-MS, which comprises online pepsin digestion, led to high resolution results of peptides involved in the interaction. Based on the results, we hypothesize a self-interaction mechanism for Infliximab that differs from a previously published mechanism of Infliximab identified by X-ray crystallography of the Fab fragment. This study underlines the importance of a multi method approach on different level to analyze and understand mAb self-interaction in a pharmaceutically relevant formulation.

Ultimately we demonstrated the application of different approaches to modify mAb interactions by targeted mutation based on an understanding of loci involved in self-interaction **(Chapter 5 and 6)**.

At first, the self-interaction of a model mAb was analyzed, which showed striking disadvantageous properties, namely precipitation at low protein concentration during downstream processes, high retention time in size exclusion chromatography and strong off-target binding **(Chapter 5)**. The high self-interaction propensity of the mAb at neutral pH and high ionic strength was associated with an increase in viscosity at elevated protein concentration. Distinct self-interaction sites in the HCDR2, the HCDR3 as well as in the constant regions of the Fab and Fc domains were identified by HDX-MS and *in silico*. Based on the finding, 39 mAb variants were generated and characterized. The introduction of a positively charged residue in spatial proximity to the self-interaction hot spot in the HCDR2, which was identified *in silico* reduced self-interaction but increased off-target binding. Placing more than one negative charged residues in spatial proximity to the hydrophobic patch of the HCDR3, which was identified by HDX-MS, decreased self-interaction and off-target binding while maintaining high affine target binding.

Secondly, two closely related mAbs directed against the same target were mutated in hydrophobic hot spots in the HCDR3 and the LCDR3 regions identified based on homology modeling and calculation of the residue specific aggregation propensity **(Chapter 6)**. In total, 26 variants were generated and characterized. The HCDR3 was identified as essential paratope locus, whereas the introduction of alanine and aspartate residues in the LCDR3 decreased hydrophobicity and the self-interaction propensity without affecting target binding. The data set was used to challenge a recently published machine learning approach

(*protein-sol*). This approach was able to differentiate between the different parental mAbs and their variants, but the capability of rankings within the mAb family was limited.

In summary, the combination of *in silico* and experimental techniques is key to understand and improve the self-interaction propensity of mAbs. Fast screening methods with minimal material consumption and effort should be used in early stages of discovery, whereas methods with lower throughput but high resolution should be applied later. By that, the risk of failure due to developability issues arising from pronounced self-interaction propensity of a mAb can be reduced by engineering and formulation development. In particular, the use of HDX-MS to identify loci involved in self-interaction sites enables rational engineering without the loss of functionality.